

**SYNTHESIS AND CHARACTERIZATION OF
GRAPHITIC CARBON NITRIDE ($g\text{-C}_3\text{N}_4$)
NANOSTRUCTURES USING ALUMINA (Al_2O_3)
TEMPLATES**

Thesis

Submitted in partial fulfilment of the requirements for the degree of
DOCTOR OF PHILOSOPHY

By

Suchitra S.M



DEPARTMENT OF PHYSICS
NATIONAL INSTITUTE OF TECHNOLOGY KARNATAKA
SURATHKAL, MANGALORE – 575025
JULY, 2018

DECLARATION

(By Research scholar)

I hereby declare that the Research Thesis entitled “**Synthesis and characterization of graphitic carbon nitride (g-C₃N₄) nanostructures using Alumina (Al₂O₃) templates**” which is being submitted to the National Institute of Technology Karnataka, Surathkal in partial fulfillment of the requirements for the award of the Degree of **Doctor of Philosophy in Physics** is a *bonafide report of the research work carried out by me*. The material contained in this Research Thesis has not been submitted to any University or Institution for the award of any degree.

Suchitra S M.
(Reg. No. 145015PH14F03)
Department of Physics

Place: NITK, Surathkal

Date:

CERTIFICATE

This is to *certify* that the Research Thesis entitled “**Synthesis and characterization of graphitic carbon nitride (g-C₃N₄) nanostructures using Alumina (Al₂O₃) templates**” submitted by Suchitra S.M (Reg. No. **145015PH14F03**) as the record of the research work carried out by her, is *accepted as the Research Thesis submission* in partial fulfillment of the requirements for the award of degree of Doctor of Philosophy.

Prof. N.K Udayashankar
(Research Guide)

Chairman-DRPC

Date:

ACKNOWLEDGEMENT

Ph.D. has been a truly life-changing experience for me and it would not have been possible without support and guidance that I received from many people. First and foremost, I would like to express my sincere gratitude to respected supervisor Prof. N.K Udayashankar for considering me as his research student. It has been an honour to be his Ph.D. student. I heartily thank him for his kindness, valuable suggestions, and constant encouragement, which I received during tough times in the Ph.D. pursuit. His constant guidance, cooperation and moral support has always kept me going ahead. The research work presented here would have been impossible without support and guidance of my supervisor.

I knew that I am remembering people who grab me into this level in my life! I begin with my parents, Vishala G S & Maheswarappa S H for their affection, love and keenness towards my ambitions. Of course, I am grateful to my parents for their patience and *love*. Without them, this work would never have come into existence (literally). I rightly dedicate this work to them.

I sincerely thank the members of RPAC Dr. Shashikala H.D and Dr. Udayakumar D, for their valuable suggestions and excellent advice in accomplishing this research work. I am grateful to the Head of the Department, Dr. M.N. Satyanarayan for supporting me to attend various conferences and workshops, which in turn helped me to understand the current research trends. I offer my heartfelt gratitude to National Institute of Technology Karnataka, for providing financial assistance and wonderful work environment.

I heartily thank my research colleagues; Naveen kumar Reddy, Kiran Pedanaboyina, Dr. Ramana Reddy P, Brian jeevan Fernandies, Mahendra K and Jithin M, for their help, encouragement and best wishes. It was a great pleasure to work with them.

I am thankful to all faculty members, ex- and present research scholars and technical staffs of the department of Physics, NITK, Surathkal for their kind and sincere support throughout my work.

I owe special thanks to my sister and my brother in law (Sunitha S M & Arun kumar K M), who supported me and helped me throughout my life and during this study. Their constant encouragement and support enabled me to pursue my dreams.

A very special thanks to my dearest brother, Dr. Santhosh T.C.M., you are like father to me. Thank you for being there every time! I really feel blessed to have a brother like you. Thanks a lot. Special Thanks to my husband Mr. Basavaraj B A, Thank you for being best friend and for being caring husband.

I wish to thank the following: Achutha K, Karthik Hegde, Varadaraj, Amudha, Brijesh, Karthik Bhat, Sreejesh, Akila, Soumalya Bhattacharya, Manju, Sruthi and Surabhi. I remain thankful to all those who helped me directly/indirectly in carrying out this work.

I am greatly thankful to friends and family, who have supported me in many circumstances during the course of my work. I would like to thank, Siddesh K.P, Pallavi S.B Sowjanya V, Bindu, K, Komal Krishna, Sachin T.C.M, Prashanth and Shankamma. There are many more whom I must remember with gratitude. Their names, though I might have failed to mention here, shall never be forgotten.

Finally, I salute and thank the Almighty for always being with us giving us the required strength, energy, patience, knowledge, and resources which lead into *Success in Life*.

Suchitra S M

CONTENTS

CHAPTER 1 Introduction

1.1	Introduction	1-3
1.2	Types of nanomaterials	3
	(a) Zero dimensional nanostructures	3
	(b) One dimensional nanostructures	4
	(c) Two dimensional nanostructures	4
	(d) Three dimensional nanostructures	5
1.3	Synthesis of nanomaterials	6
	(a) Template based synthesis	6-7
1.4	Anodic aluminium oxide template (AAO)	7
	1.4.1 Basic mechanism of oxide formation in AAO template	8-9
	1.4.2 Fabrication and structure of AAO templates	9
	1.4.3 Anodization of aluminium	9-10
	1.4.4 Porous anodic aluminium oxide layer	10
1.5	Methods for the synthesis of nano materials using AAO templates	
	1.5.1 Electrodeposition	10-11
	1.5.2 Electroless deposition	11
	1.5.3 Chemical polymerization	10-11
	1.5.4 Sol-gel deposition	12
	1.5.5 Chemical vapour deposition	13
	1.5.6 Thermal condensation	14
1.6	Nanomaterials synthesized using AAO templates	
	1.6.1 Metal nanotubes	14
	1.6.2 Polymeric nanostructures	15
	1.6.3 Carbon nanotubes	15
	1.6.4 Ceramic nanostructures	15
	1.6.5 Graphitic carbon nitride nanostructures	15

1.7	Applications of graphitic carbon nitride	16
1.7.1	Organic Dyes	
	Classification of organic dyes	
	(i) Natural Dyes	17
	(ii) Synthetic Dyes	17-18
1.7.2	Methods for removal of pollution	
1.7.3	Photocatalysis	18
1.8	Literature Review	18-22
1.9	Scope and objectives of the work	
	(i) Scope	23
	(ii) Objectives	24
1.10	Organization of the thesis	25

CHAPTER 2 Experimental techniques

2.1	Preparation method	
	2.1.1 Experimental setup for AAO template preparation	26-27
	2.1.2 Experimental method to synthesize porous anodic alumina templates	27-28
	2.1.3 Experimental method to synthesize graphitic carbon nitride nanostructures	29-30
2.2	Characterization techniques	
2.3	Structural and morphological analysis	
	2.3.1 X-ray Diffraction	30-32
	2.3.2 Surface morphology analysis	
	(a) Field-Emission Scanning electron microscopy	32-33
	(b) Image processing	33-34
2.4	Optical analysis	
	2.4.1 Infrared spectroscopy	34-36
	2.4.2 UV-Vis Spectroscopy	36-37

2.4.3	Photoluminescence	37-38
2.5	Thermal analysis	
2.5.1	Thermo Gravimetric analysis	38-39
2.6	Photocatalysis	39-41
CHAPTER 3	Fabrication of porous anodic alumina templates: optimum conditions for self-ordered pores	
3.1	Optimum conditions for self-ordered pores	
3.1.1	Effect of voltage	42-43
3.1.2	Electrolyte concentration	43-44
3.1.3	Effect of bath temperature and different concentration of electrolyte	44-46
3.1.4	Effect of pore widening duration	46-61
3.2	Optimum conditions for template preparation	61-63
	Conclusions	63-64
CHAPTER 4	Synthesis and characterization of graphitic carbon nitride nanostructures using porous anodic alumina templates	
4.1	Results and discussion	
4.1.1	Structural analysis	67
4.1.2	Morphological analysis	68
4.1.3	Optical properties	
	(i) UV-Visible spectroscopy	68-69
	(ii) Photoluminescence spectroscopy	70
4.1.4	FTIR spectroscopy	70-71
4.1.5	Thermal analysis	71-72
	Conclusions	72-73

CHAPTER 5	Temperature dependent studies on tailored graphitic carbon nitride nanostructures	
5.1	Template assisted synthesis and characterization of nanostructures	75
5.2	Structural and morphological analysis	
5.3.1	X-ray diffraction studies	75-76
5.3.2	Morphological studies	76-77
5.3	Thermo gravimetric analysis	77-79
5.4	FTIR analysis	79-80
5.5	Absorption properties	80-82
5.6	Emission properties	82-84
	Conclusions	84-85
Chapter 6	Applications towards photocatalytic properties of GCN nanostructures	
6.1	Photocatalysis	
6.1.1	Principles of photocatalytic reactions	86-87
6.2	Photocatalytic properties of bulk and AAO assisted GCN nanostructures	
6.2.1	Photocatalytic activity of nanostructures for the degradation of methylene blue dye	87-90
6.2.2	Photocatalytic activity of nanostructures for the degradation of Rhodamine-B dye	90-92
6.2.3	Photocatalytic activity of nanostructures for the degradation of Methylene orange dye	92-93
6.3	Photocatalytic properties of GCN nanostructures synthesized at different temperatures	94-95
	Conclusions	95
Chapter 7	Summary and Conclusions	
7.1	Summary and conclusions	96-97
7.2	Directions for future work	97

REFERENCES	98-103
PUBLICATIONS	104-105
CURRICULAM VITTE	

List of figures

Figure 1.1	(a) General structure of Porous Anodic Alumina. (b) Top view of Anodic alumina	9
Figure 1.2	Schematic diagram for applications of graphitic carbon nitride nanostructures	17
Figure 2.1	Schematic of the experimental setup used for anodization	26
Figure 2.2	Schematic diagram of the two-step anodization process	27
Figure 2.3	Schematic diagram of synthesis of GCN nanotubes using AAO templates.	29
Figure 2.4	X-ray diffractometer Rigaku (Model Miniflex600).	31
Figure 2.5	Field Emission Scanning Electron Microscopy (Carl Zeiss)	33
Figure 2.6	Fourier transform infrared spectrometer (<i>Bruker Alfa FTIR spectrometer</i>).	35
Figure 2.7	UV-Vis- Spectrophotometer (Model: Ocean optics USB4000-XRI-ES)	37
Figure 2.8	Spectrophotometer (FluoroMax-4).	38
Figure 2.9	Thermogravimetric analyzer (<i>Perkin-Elmer TGA 4000 instrument</i>)	39
Figure 2.10	Schematic diagram of photocatalytic setup.	40
Figure 2.11	The experimental setup used for photocatalysis.	41
Figure 3.1	Top view SEM images of AAO templates grown at five different voltages.	43
Figure 3.2	Top view SEM image of pore arrays grown using oxalic acid at 18 °C and anodized at different electrolyte concentration (a) 0.1 M, (b) 0.2 M, (c) 0.3 M, (d) 0.4 M, (e) 0.5 M and (f) 1 M	44

Figure 3.3	Top view SEM images of AAO templates grown at two different bath temperatures and different anodization durations.	45
Figure 3.4	XRD pattern of the AAO templates prepared using oxalic acid, sulphuric acid, phosphoric acid and chromic acid and pore widened for 60 min respectively.	47
Figure 3.5	Schematic diagram of pore widening process	49
Figure 3.6	FESEM micrographs (a,d,g,j) together with FFT images (b,e,h,k) and radial average (c,f,I,l) of AAO templates prepared using Oxalic, Sulphuric, Phosphoric and Chromic acids and without pore widening.	50
Figure 3.7	FESEM micrographs (a,d,g,j) together with FFT images (b,e,h,k) and radial average (c,f,I,l) of AAO templates prepared using Oxalic, Sulphuric, Phosphoric and Chromic acids and pore widened for 15 min respectively.	51
Figure 3.8	FESEM micrographs (a,d,g,j) together with FFT images (b,e,h,k) and radial average (c,f,I,l) of AAO templates prepared using Oxalic, Sulphuric, Phosphoric and Chromic acids and pore widened for 30 min respectively.	52
Figure 3.9	FESEM micrographs (a,d,g,j) together with FFT images (b,e,h,k) and radial average (c,f,I,l) of AAO templates prepared using Oxalic, Sulphuric, Phosphoric and Chromic acids and pore widened for 45 min respectively.	53
Figure 3.10	FESEM micrographs (a,d,g,j) together with FFT images (b,e,h,k) and radial average (c,f,I,l) of AAO templates prepared using Oxalic, Sulphuric, Phosphoric and Chromic acids and pore widened for 60 min respectively	54
Figure 3.11	Regularity ratio vs. pore widening time for of AAO templates prepared using Oxalic, Sulphuric, phosphoric and Chromic acids and pore widened for 0 min, 15 min, 30 min, 45 min and 60 min.	55

Figure3 .12	Variation of (a) pore diameter, (b) Inter pore distance, (c) Porosity and (d) Pore density with respect to different pore widening time of AAO templates prepared using Oxalic, Sulphuric, phosphoric and Chromic acids.	59
Figure 3.13	Circularity vs. pore widening time for of AAO templates prepared using Oxalic, Sulphuric, phosphoric and Chromic acids and pore widened for 0 min, 15 min, 30 min, 45 min and 60 min.	61
Figure 3.14	XRD pattern of the AAO template prepared using 0.3 M oxalic acid.	61
Figure 3.15	SEM images of AAO templates fabricated using 0.3 M oxalic acid	62
Figure 3.16	Cross sectional view of AAO templates fabricated using 0.3 M oxalic acid	62
Figure 4.1	XRD pattern of (a) Bulk GCN and (b) GCN nanofibers	67
Figure 4.2	FESEM images of (a) Bulk GCN and (b) GCN nanofibers	68
Figure 4.3	UV-Visible spectrs of (a) Bulk GCN and (b) GCN nanofibers	69
Figure 4.4	Tauc's plot of (a) Bulk GCN and (b) GCN nanofibers	69
Figure 4.5	Photoluminescence spectra of (a) Bulk GCN and (b) GCN nanofibers	70
Figure 4.6	FTIR spectra of (a) Bulk GCN and (b) GCN nanofibers	71
Figure 4.7	TGA curve of (a) Bulk GCN and (b) GCN nanofibers	72
Figure5.1	The XRD spectra of the GCN nanostructures obtained at different temperatures.	76
Figure5.2	The FESEM images of GCN nanostructures obtained at different temperatures (a) 400 °C, (b) 450 °C, (c) 500 °C, (d) 550 °C, (e) 600 °C.	77

Figure 5.3	TGA results of the GCN nanostructures synthesized at different temperatures.	78
Figure 5.4	DTG plots of the GCN nanostructures synthesized at different temperatures.	79
Figure 5.5	The FTIR spectra of the GCN nanostructures obtained at different temperatures.	80
Figure 5.6	The UV-Vis spectra of the GCN nanostructures obtained at different temperatures.	81
Figure: 5.7	The Tauc's plot of the UV-Visible spectra of GCN nanostructures obtained at different temperatures.	82
Figure: 5.8	(a)The normalized PL emission spectra of the GCN nanostructures prepared at different temperatures. (b),(c),(d),(e) and (f) the Gaussian fitting of PL emission spectra of the 400,450,500,550 and 600 °C samples respectively, which indicate 3 major PL peaks (R1, R2 and R3).	83
Figure: 5.9	The peak position of R1, R2 and R3 of the GCN nanostructures obtained at different temperatures.	84
Figure 6.1	Photodegradation of MB solution for (a) bulk GCN and (b) GCN nanofibers	88
Figure: 6.2	(a) Dye relative concentration (b) Dye kinetics (c) Dye rate constant and (d) Dye stability of bulk and GCN nanofibers for MB dye.	89
Figure 6.3	Photodegradation of Rh-B dye solution for (a) bulk GCN and (b) GCN nanofibers	90
Figure: 6.4	(a) Dye relative concentration (b) Dye kinetics (c) Dye rate constant and of bulk and GCN nanofibers for photodegradation of RhB dye.	91

- Figure: 6.5 Photodegradation of MO dye solution for (a) bulk GCN and 92
(b) GCN nanofibers.
- Figure 6.6 (a) Dye relative concentration (b) Dye kinetics (c) Dye rate 93
constant and of bulk and GCN nanofibers for photodegradation
of MO dye.
- Figure: 6.7 (a) Dye relative concentration (b) Dye kinetics (c) Dye rate 94
constant of GCN nanostructures obtained at different
temperatures.

List of tables

Table 3.1	Structural parameters of AAO templates prepared by Oxalic acid with respect to different pore widening durations	57
Table 3.2	Structural parameters of AAO templates prepared by Sulphuric acid with respect to different pore widening durations	57
Table 3.3	Structural parameters of AAO templates prepared by Phosphoric acid with respect to different pore widening durations	58
Table 3.4	Structural parameters of AAO templates prepared by Chromic acid with respect to different pore widening durations	58
Table 3.5	Optimum conditions for self-ordered AAO template	63

CHAPTER 1
INTRODUCTION

CHAPTER 1

INTRODUCTION

Overview

This chapter provides a preface to the field of nanoporous anodic aluminium oxide templates, porous alumina nanostructures, basics of anodic alumina formation, fundamental properties and practical applications of graphitic carbon nitride (GCN) nanostructures. This chapter also provides information regarding the up-to-date account of research activities pertaining to the field of GCN nanostructures synthesized using porous anodic alumina templates. Further, the chapter ends with the research objectives and organization of the thesis.

1.1 INTRODUCTION

In the modern era of scientific research, the potential of nanotechnology is immense and encompasses literally all branches of science. Nanotechnology is the understanding and control of matter at dimensions of roughly 1–100 nm, where unique phenomena exhibited by nanomaterials and nanostructures enable them for novel applications [Sanguansri and Augustin 2006]. The physical and chemical properties of nanomaterials are uniquely dependent on their size, shape and morphology [Li et al. 2006]. As a result, materials scientists are focusing their efforts on developing simple and effective methods for fabricating nanomaterials with controlled size and morphology and hence, tailoring their properties. An important aspect of the nanoscale is that the smaller a nanoparticle gets, the larger its surface to volume ratio [Heath 1999]. At the nanoscale, electrical, magnetic, optical, catalytic and mechanical properties are different from their bulk form [Smith et al. 2006].

Some nanomaterials occur naturally, but of particular interest are engineered nanomaterials, which are already being used in many commercial products and processes. They can be found in such things as sunscreens, cosmetics, sporting goods, stain-resistant clothing, tires, electronics, as well as many other everyday items, and are used in medicine for purposes of diagnosis [Xie et al. 2006], imaging and drug delivery [Yang et al. 2010]. Engineered nanomaterials are resources designed at the molecular (nanometre) level to take advantage of their small size and novel properties

which are generally not seen in their conventional, bulk counterparts. The two main reasons why materials at the nano scale can have different properties are increased relative surface area and new quantum effects [Takei et al. 2011]. Nanomaterials have a much greater surface area to volume ratio than their conventional forms, which can lead to greater chemical reactivity and affect their strength [Wang et al. 2008]. Also at the nano scale, quantum effects can become much more important in determining the material properties and characteristics, leading to novel optical, electrical and magnetic behaviour [Sun et al. 2005].

Nanomaterials have the structural features in between those of atoms/molecules and the bulk materials. While most micro structured materials have similar properties as the corresponding bulk materials, the properties of materials with nanometer dimensions are significantly modified from those of atoms and bulks materials [Šepelák et al. 2003]. This is mainly due to the nanometer size of the materials which render them: (i) Large fraction of surface atoms [Arico et al. 2011], (ii) High surface energy [Simon and Gogotsi 2010], (iii) Spatial confinement [Bell 2003], (iv) Reduced imperfections [Wang 2006b], which do not exist in the corresponding bulk materials.

Due to their small dimensions, nanomaterials have extremely large surface area to volume ratio. Especially when the sizes of nanomaterials are comparable to length, the entire material will be affected by the surface properties of nanomaterials. This in turn may enhance or modify the properties of the bulk materials [Zhang et al. 2005].

Nanomaterials can be prepared from a wide range of solid materials such as metals, ceramics, polymers, organic materials and composites. They can come in a wide range of morphologies, namely porous materials, spheres, rods, tubes and plates [Schäfer et al. 2014]. In recent years, a lot of research has been focused on the production of novel nono porous materials and their applications. Anodic aluminium oxide (AAO) is a self-ordered nanoporous template that consists of a hexagonal array of cells with uniform and parallel straight cylindrical nanopores perpendicular to the template surface.

AAO templates prepared by anodization of aluminum foil, possesses outstanding chemical, optical, and mechanical properties such as chemical resistance, thermal stability, hardness, biocompatibility and large surface area. Particularly, its

high surface area to volume ratio is widely useful to enhance optical signals when target molecules (analytes) are attached inside the nanopores. Therefore, anodic aluminium oxide is an excellent platform to develop sophisticated devices and systems such as selective molecular separation, chemical/biological sensing, catalysis, cell adhesion and culture, data storage, energy generation, drug delivery and template synthesis [Kumeria et al. 2014]. Nanorods/wires can be fabricated onto these AAO templates because of controlled pore diameter, cylindrical shape, periodicity and their density distribution [Gorisse et al., 2013]. Nanostructures can be fabricated onto AAO templates by pressure injection, physical vapour deposition, electrodeposition, polymerization, sol-gel and chemical vapour deposition (CVD), thermal condensation, etc.

1.2 TYPES OF NANOMATERIALS

By reducing the one, two and three dimensions of bulk materials to the nanometer scale, three dimensional (3D), two dimensional(2D), one dimensional(1D), zero dimensional nanostructure can be produced [Tiwari et al. 2012]. The dimensions of nanostructures play an important role in shaping their properties.

(a) Zero-dimensional nanostructures

Zero dimensional nanostructures like fullerenes, quantum dots and nanoparticles, having all three quantum confined dimensions, have been widely studied. The various chemical and physical methods have been used and developed to synthesize nanodots or quantum dots with controlled shape and size to form a rich variety of materials [Cao and Wang 2004]. These methods include both the top-down and bottom-up approaches. The nanoparticles may be amorphous, polycrystalline or single crystals in nature. This gives rise to nanostructures with different morphologies such as the sphere, cubes. For practical purposes, the methods need to be controlled in such a way that the resulting particles have an identical size and shape. In addition nanoparticles should also readily dispersible with no agglomeration [Bryant 1989]. Significant progress has also been made not only in the size dependent physical and chemical properties A rich variety of physical and chemical methods have been developed for fabricating 0D nanostructures with well-controlled dimensions [Marsal

et al. 2002]. Recently, 0D nanostructures such as uniform particles arrays (quantum dots), heterogeneous particles arrays, core shell quantum dots, onions, hollow spheres and nanolenses have been synthesized by several research groups.

(b) One- dimensional nanostructures

One-dimensional (1D) nanostructure can be considered as a structure with lateral dimensions falling within the range of 1-100 nm. These nanostructures include nanowires/rods, nanobelts and fibers [Xia et al. 2003]. Nanorods are usually shorter than nanowires and have a smaller aspect ratio. The unique feature of 1D nanomaterials that makes them different from other low dimensional systems is that they have two quantum confined directions while still leaving one unconfined direction for electrical conduction. The growth of 1D material requires that two dimensions are kept in scale of nanometer while the third dimension can be extended to any macroscopic dimensions. This overall requirement is significantly more difficult than corresponding constraints needed for zero and two dimension structures [Huang et al. 2001]. To achieve 1D growth in systems where atomic bonding is relatively isotropic requires that the growth symmetry must be broken rather than simply isotropic growth at an early stage. They are ideal systems for investigating the dependence of electrical transport, optical and mechanical properties on size and dimensionality and expected to play important roles as both interconnection and functional components in the fabrication of nanoscale electronic and optoelectronic devices [Li et al. 2013]. Up to now, 1D nanomaterials such as nanotube, nanorods, nanowires, nanobelts or nanoribbons, nanocables have been successfully synthesized with a variety of methods. However the growth of such nanostructures by controllable means is still a difficult problem needed to be resolved [Tian et al. 2014]. Many methods have been used to synthesize these nanostructures include spontaneous growth, electro spinning, template based synthesis and lithography [Kuchibhatla et al. 2007].

(c) Two dimensional nanostructures

In recent years, a synthesis 2D nanostructured materials have become a important area in nanoscale research, because of their low dimensional characteristics which are different from the bulk properties. 2D nano materials with certain geometries exhibit

unique shape-dependent characteristics and subsequent utilization as building blocks for the key components of nano devices [Muller et al. 2015]. In addition, 2D nanomaterials are particularly interesting not only for basic understanding of the mechanism of nanostructure growth, but also for investigation and development of novel applications in sensors, photocatalysis, nanoreactors, and templates for 2D structures of other materials

It is well known that the characteristics of nanostructured materials strongly depend on the sizes, shapes, dimensionality and morphologies, which are thus the key factors to their ultimate performance and applications [Zhang 2015]. Two dimensional materials such as graphene and quantum wells and thin films have been thoroughly fabricated and studied for use in fields of electronic devices and photovoltaic applications in the past two decades. They can be easily synthesized by commercially available techniques such as metal- organic chemical vapour deposition, molecular beam epitaxy, ultra high chemical vapour deposition etc [Khan et al. 2017].

(d) Three dimensional nanostructures

Due to the large specific surface area and other greater properties over their bulk equivalents arising from quantum size effect, 3D nanomaterials have attracted considerable research interest and many 3D nanomaterials have been synthesized in the recent years. Therefore it is of great interest to synthesize 3D nanomaterials with a controlled structure and morphology [Aruna and Mukasyan 2008]. In addition, 3D nanostructures are technically important materials due to their wide range of applications in the areas of catalysis, magnetic and electrode materials for batteries, solar fuel cells and chemical sensors. Moreover, the 3D nanomaterials have recently attracted intensive research interests because the nanostructures have higher surface area and supply enough absorption sites for all involved molecules in a small space [Holmes et al. 2003]. On the other hand, such materials with porosity in three dimensions could lead to a better transport of the molecules. Examples for 3D nanostructures are nanoballs, nanocoils, nanocones, nanopillars and nanoflowers etc .

1.3 SYNTHESIS OF NANOMATERIALS

There are two basic approaches used for the fabrication of nanostructures: top-down and bottom up. Top down approach refers to successive cutting of a bulk material to get nano sized pieces using mechanical, chemical or other form of energy. This fabrication approach reduces a large piece of a bulk material all the way down to the nanoscale. This approach requires larger amounts of materials and can lead to waste if excess material is subdivided. However an alternative and most promising strategy to exploit science and technology at nanometer scale is offered by the bottom-up approach. This starts from nano scale objects to build up nanostructures. This approach refers to the build-up of a material from the bottom: atom by atom, molecule by molecule or cluster by cluster [Weintraub et al. 2010]. This is an opposite approach to top down used to synthesize the material from atomic or molecular species via chemical reactions, allowing the precursor particles to grow in size. The bottom up approach is to create desired nano size product by building them up from atomic and molecular scale components according to a natural physical principle or an externally applied driving force, which can be time consuming [Chen and Mao 2007].

Bottom up approach leads to the bulk production of nano material. This approach plays an important role in the fabrication and processing of nanostructures. Because this approach provides a better chance to obtain nanostructures with less defects, more homogeneous chemical composition and better short and long range ordering [Wiesner et al. 2006]. The bottom-up approach has the potential to overcome the limitations of the conventional top-down approach by providing the methodology having control over lattice compositions, scaling of devices to the molecular scale, and minimal surface roughness.

(a) Template based synthesis

The template based synthesis of nanostructures is a conceptually simple, cost effective and suitable technique to fabricate nanowires, nanotubes, nanorods and nanofibers. Template based synthesis is a bottom-up approach based on principles similar to those of producing components through the use of replication. These templates contain very small nanoporous channels within the host material and their

empty spaces are filled with the required material, which adopts the morphology of pores to form nanostructures [Wang 2006a]. In template assisted synthesis of nanostructures the chemical stability, mechanical properties of the template, pore diameter, uniformity and density of the pores are the important characteristics to consider.

Template based synthesis is very fascinating method for the fabrication of one-dimensional nanostructured materials with controlled morphology [Ye et al. 2010]. It can be used in fabrication of nanorods, nanowires, nanoneedles and nanotubes of polymers, metals, semiconductors and oxides [Lakshmi et al. 1997]. Number of templates with nanosized channels has been explored for the template growth of nanostructures [Rossinyol et al. 2005]. The most commonly used and commercially available templates are anodized alumina templates.

1.4 Anodic Aluminum oxide template (AAO)

Al is a reactive metal that reacts readily with the oxygen present in the atmosphere at ambient temperatures to create a thin amorphous nanometer (1–10 nm) oxide layer. This layer has the advantage of preventing further dissolution of the Al and thus provides an effective protective barrier. This is in direct contrast to the permeable oxide layer that is built up on ferrous metal surfaces; thus allowing further corrosion to continue. The protective oxide layer on the surface of Al has enabled this metal to be used in a variety of industrial applications.

This oxide layer is very important and the control of its morphology and surface features are critical to many applications. It was shown as early as 1935 by Verwey [Verwey 1935] and other researchers [Diggle et al. 1969] that the anodic film will react further with the environment, resulting in hydration of the outer surface of the barrier film. Thus, the oxide structure consists of two distinct layers, a hydrated porous layer growing on top of a thin inert dense layer, normally called the barrier layer.

To use Al effectively for a wide variety of applications means that the metal needs to be protected. Anodization of Al was first used on an industrial scale in the mid-1920s, since then the range of applications has steadily increased and accordingly the anodization process has been actively investigated and refined. It is known that during

the anodization process, Al produces a highly resistant protective layer on its surface. The anodic layer parameters such as barrier layer thickness, pore diameter and pore height are directly dependent upon the voltage used in the creation of the layer [Uchi et al. 2001].

1.4.1 Basic mechanism of oxide formation in AAO templates

The preparation and applications of AAO templates were studied over the last three decades, but the formation and growth mechanism of pores still remain quite controversial. Several theories have been proposed and developed. First research group reported that oxygen ions are generated on the bottom of the pores at the gas/electrolyte interface. Meanwhile, the dissolution of the oxide layer leads to the pore growth [Baumann, 1936]. Second research group developed a theory according to which a homogeneous barrier film is formed at the beginning of the anodizing process and the dissolution is caused by the current. Meanwhile the current raises the local temperature enhancing the dissolution of the oxide [Keller et al., 1953]. Another research group developed a different theory for the oxidation process (Murphy and Michelson, 1962). They reasoned that the outer side of the barrier layer was transformed into hydroxide and hydrate compounds because of the contact with the electrolyte. This layer could absorb or bond with anions from the electrolyte to create a gel-form matrix. The inner layer is a dense oxide layer. Transmission of oxygen anions towards the metal base leads to the oxidation between the inner and the outer layer, and initial pores are formed.

Four steps involved in the pore growth mechanism of AAO templates are (a) Formation of a barrier layer on the aluminum surface, (b) random formation of pore centres, (c) pores deepen and form a new barrier layer on the interface between the metal and the oxide and (d) stable growth of pores [Alkire et al., 2008] [Murphy and Michelson, 1962]. Where each step is related with a different growth pore regime. In the stage-a, a constant voltage is applied on the surface of the aluminum, the current decreases with time until the local minimum is reached. Simultaneously a barrier layer grows on the interface of the electrolyte and aluminum, which is non-porous with a homogeneous thickness. In the stage-b, the current increases gradually to a steady point, and pore precursors form on the oxide layer (barrier layer) surface, which can be dissolved in the electrolyte. In the stage-c, the formation of these pore precursors is random, and usually occurs around a defect. Further anodizing and etching results in

the growth of pores, and the aluminum is constantly anodized under an electric field, pores are widened, and at the same time the growth of the barrier layer is increasingly stable. In the stage-d, the growth and the dissolution of the oxide layer reach an equilibrium on the electrolyte-oxide interface and oxide-metal interface (O'sullivan and Wood, 1970), the current density is constant. Anodizing conditions determine the current parameters, such as the minimum current value, the rate of current decrease, and the time after which the steady state forms.

1.4.2 Fabrication and Structure of AAO templates

Electrochemical oxidation of aluminum forms hexagonally honey-comb arrays of pores, ideally aligned normal to the surface. To obtain this structure, aluminum has to be subjected to anodization under controlled experimental conditions [Jai Poinern et al., 2011]. An ideal honey-comb array of anodic aluminum oxide (AAO) is shown in Figure 1.1.

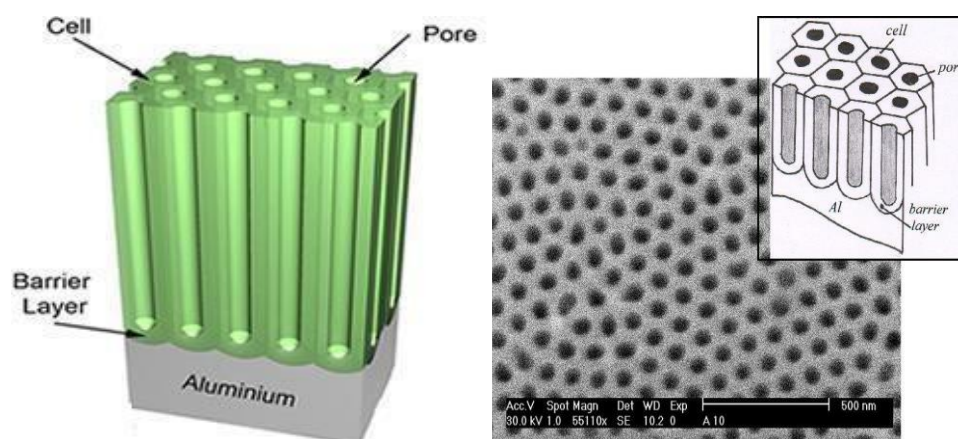


Figure 1.1 (a) General structure of Porous Anodic Alumina. (b) Top view of Anodic alumina.

1.4.3 Anodization of aluminium

Al metal is a substantial component of the earth's crust, (approximately 8%) but due to its reactivity with naturally occurring oxygen in the atmosphere, it is found in combination with other materials. Alumina (Al_2O_3) is the only known stable oxide of Al and contains 52.8% of the element by weight. Today, due to its wide applications,

Al is the most produced non-ferrous metal. Al is a reactive metal that reacts readily with the oxygen present in the atmosphere at ambient temperatures to create a thin amorphous oxide layer. The thickness of the oxide layer is temperature dependent and at temperatures above 700 °C, both amorphous and crystalline alumina's are present [Dignam 1962].

1.4.4 Porous anodic aluminium oxide layer

A regular self-organized porous nanostructure can be formed when Al is anodized in certain acidic media [Masuda et al. 1998]. This porous nanostructure is electrically insulating, optically transparent or semi-transparent, chemically stable, bio-inert and a biocompatible material. The nanostructure is well defined and has a highly ordered nano-design that enables these structures to be used as templates [Shingubara 2003]. The creation of this template is possible due to the well-developed and refined anodized techniques and electro-chemical parameters that are employed [Chik and Xu 2004]. The anodization technique and the electro-chemical parameters make it possible to control a number of surface parameters [Dignam 1962]. A barrier type of anodic film can be formed by anodizing aluminium in a neutral solution [Deepak et al., 2014]. The group of electrolyte used for this kind of thin film formation includes boric acid, ammonium borate, ammonium tartrate and aqueous phosphate solution, as well as tetra borate in ethylene glycol, and some organic electrolyte such as citric, malic, succinic and glycolic acid.

1.5 Methods for the synthesis of nano materials using AAO templates

1.5.1 Electrodeposition

The art of electrodeposition of metals and metallic alloys has been in practice for nearly a century. The possibility of using the electrodeposition technique as a tool of material technology is attracting great attention as a means of obtaining films of a wide variety of materials including semiconductors, superconductors, polymer films, specific electronic device application materials and others. Electrodeposition was originally used for the preparation of metallic mirrors and corrosion resistant surfaces. In its simplest form, electrodeposition consists of an electrolyte containing metal ions, an electrode or substrate on which the deposition is desired, and a counter electrode.

When a current flows through the electrolyte, the cations and anions move towards the cathode and anode, respectively, and may deposit on the electrode after undergoing a charge transfer reaction. Electrodeposition of a material within the template pores is preceded by coating one face of the membrane with a metal film and using this metal film as a cathode for electroplating [Huckzo et al . 2000]. The volume of the pore is continuously filled up beginning from the pore bottom. Thus, the length of the nanostructures can be controlled by varying the amount of material deposited. Both metal and conductive polymer nanotubes and nanowires have been synthesized using this method.

1.5.2 Electroless deposition

Electroless deposition, also known as chemical or auto-catalytic plating, is a method that involves several simultaneous reactions in an aqueous solution, which occur without the use of external electrical power. In contrast, an electroless deposition process uses only one electrode and no external source of electric current. However, the solution for the electroless process needs to contain a reducing agent. The reaction is accomplished when hydrogen is released by a reducing agent.

Metal nanotubes have been prepared by electroless deposition involving a chemical agent to plate a material from the surrounding phase onto a template surface [Brumlik et al. 1994] [Curulli et al. 2005]. This method differs from the previous one, since the surface that must be coated does not need to be electrochemically conductive. The material deposition in the pores starts from the pore walls. Two types of 1D nanostructure are provided. After short decomposition times, nanotubes are obtained within each pore, whereas long deposition times result in solid nanowires.

A major benefit of this approach over electroplating is that the power sources and plating baths are not needed, reducing the cost of production. This technique can also plate diverse shapes and types of surface. The downside is that the plating process is usually slower and cannot create thick plates of metal. As a consequence of these characteristics, electroless deposition is quite common in the decorative arts.

1.5.3 Chemical polymerization

Chemical polymerization is a process of reacting monomer molecules together in a chemical reaction to form polymer chains or three-dimensional networks. Different conductive polymers can be template-synthesized by the polymerization of the corresponding monomer to yield tubular nanostructures [De Vito and Martin 1998]. The process can be accomplished by simply immersing the template into a solution containing the desired monomer and a polymerization reagent. The polymer preferentially nucleates and grows on the pore walls, resulting in nanotubes at short deposition times and nanofibers at long times.

1.5.4 Sol-gel deposition

In sol gel process initially a stable colloidal solution called sol is formed. The sol is a liquid suspension of solid particles ranging in size from 1 nm to 1 micron. It can be obtained by hydrolysis and partial condensation of precursors such as inorganic salt or a metal oxide. The further condensation of sol particles into a three dimensional network produces a gel material. The gel is a diphasic material in which the solids encapsulate the solvent. The molecular weight of the oxide species produced continuously increases. The materials are referred to aqua sol or aqua gels when water is used as a solvent and aquosol or alcogel when alcohol is used. The encapsulated liquid can be removed from a gel by either evaporative drying or with supercritical drying /extraction. The resulting solid products are known as xerogel and aerogel respectively. When gels are dried by evaporation, the dried product is called xerogel. When the gels are dried by supercritical drying, the dried gel is called aerogels. The aerogel retains high porosity and has very high pore volume.

Sol-gel synthesis within the pores of a template involves preparation of a solution of a precursor molecule to obtain first a suspension of colloid particles (the sol) and then a gel composed of aggregated sol particles. The gel is then thermally treated to yield the desired nanostructures within the membrane pores [Hulteen and Martin 1997]. The process can be conducted to synthesize nanotubes and nanowires.

1.5.5 Chemical vapour Deposition (CVD)

CVD is a method of depositing gaseous reactants onto a substrate. The way CVD works is by combining gas molecules in a reaction chamber which is typically set at ambient temperature. When the combined gas molecules come into contact with the substrate within the heated reaction chamber, a reaction occurs that creates a material film on the substrate surface. The waste gases are then pumped from the reaction chamber. The temperature of the substrate is a primary condition that defines the type of reaction that will occur [Shah and Tali 2016].

During the CVD process, the substrate is usually coated a very small amount, at a very slow speed, often described in microns of thickness per hour. The process is similar to physical vapour deposition (PVD), the only difference being that the precursors are solid compounds, rather than gases, and therefore the process is slightly different. The solid compound is vaporized, and then deposited onto a substrate via condensation.

The benefits of using CVD to deposit materials onto a substrate are that the quality of the resulting materials is usually very high. Other common characteristics of CVD coatings include high purity, fine grained and increased hardness over other coating methods. It is a common solution for the deposition of films in the semiconductor industry, as well as in optoelectronics, due to the low costs involved compared to the high purity of films created [Mattevi et al. 2011].

Chemical vapour deposition has been extensively applied in the commercial production of solid thin films [Huczko 2000]. The technique entails surface solidification of desired reactants resulting from their gas-phase chemical transformations. The method has successfully been developed for the template synthesis of carbon nanotubes the starting reactants were thermally activated and decomposed to solid carbon within porous templates while traversing the length of the pore. Thermal decomposition of the gas occurred throughout the pores, resulting in the deposition of carbon films along the length of the pore walls and formation of carbon nanotubes within the pores.

1.5.6 Thermal condensation

This is a chemical approach for the synthesis of nanostructures inside the AAO templates [Li et al. 2011]. During thermal condensation some small molecules can join together to make very long molecules. Mainly thermal condensation relies on the presence of monomer and thus it is a continuous process during the entire course of polymerization as long as residual monomer molecules exist in the system. This is equivalent to an overall slow initiation stage in the presence of a chemical initiator.

This method involves filling of a rigid template with a precursor material, treatment of the precursor to form the desired material and finally removal of the template to create replica. This is one of the simple and cost effective methods for the synthesis of GCN nanostructures inside the AAO templates by heat treatment of nitrogen rich precursors in AAO templates.

1.6 Nanomaterials synthesized using AAO templates

Various 1D nanomaterials have been prepared using the membrane template method, including semiconductor, metal, polymeric, carbon and ceramics.

Nanostructures of various materials

- ◆ Nanostructures made of materials such as polymers, ceramic materials and carbon have been synthesized. Polymer nanotubes can be made by the electrochemical deposition method within the pores of a nanoporous membrane.

- ◆ The deposition and solidification of polymer inside the template pores starts at the surface and proceeds inwardly. The electrostatic attraction between the oppositely charged growing polymer and the sites along the pore walls of the membrane may be responsible for the inward growth.

- ◆ The diffusion of monomer molecules through the pores can become a limiting step and the monomer molecules within the pores can be depleted quickly causing the deposition of polymer inside the pores to stop.

1.6.1 Metal nanotubes

Metal nanotubes are of interest because they can have good electrical conductivity and low electron work functions. Vacuum deposition with an

electroplating method was used to prepare metal nanotubes in the pores of AAO templates [Brumlik et al. 1994].

1.6.2 Polymeric nanostructures

Conducting polymer nanotubes have been attracting considerable attention because of their potential applications as nanosized transistors, displays, sensors and molecular wires. They were prepared using template and electrochemical or oxide polymerization.

1.6.3 Carbon nanotubes

Carbon nanostructures are of tremendous interest, from both a fundamental and an applied perspective. Applications investigated include their use for the storage of hydrogen and other gases, as a catalyst support and as a tip for scanning probe microscopy. Templating methods have been successfully applied to produce ensembles of aligned and monodispersed nanotubes of graphitic carbon. CVD technique was applied and hydrocarbons were pyrolyzed in alumina templates yielding graphitic carbon nanofiber and nanotube ensembles (with diameters as small as 20 nm and lengths around 50 μm) [Parthasarathy et al. 1995; Kyotani et al. 1996; Che et al. 1998].

1.6.4 Ceramic nanostructures

Ceramic nanostructures, like silicon carbides SiC nanostructures, were obtained with carbosilane and polycarbosilane precursors by using a membrane templating method [Cheng et al. 2005].

1.6.5 Graphitic carbon nitride nanostructures

GCN is a layered material consisting of C and N atoms. GCN nanostructures are synthesized using AAO templates by simple thermal condensation of urea, thiourea, and melamine into the anodic alumina templates. The method of synthesizing GCN using AAO templates involves filling or casting of a template with a precursor material, treatment of the precursor to form the desired material and finally removal of AAO template to get pure GCN nanostructures with desired dimensions. The GCN structures are having high thermal stability up to 600 °C. These structures have high chemical stability when facing chemical attacks from acid, base and organic solvent. These

materials have the bandgap of about 2.7 eV [Yang et al. 2015]. These materials are the most promising materials for surface modification, light emitting devices, photocatalysis [Naseri et al. 2017]. Among various analogies, GCN constructed via thermal condensation of nitrogen rich precursors is one of the novel carbon materials used for potential applications [Liu et al. 2016].

1.7 Applications of Graphitic carbon nitride nanostructures

Graphitic carbon nitride (g-C₃N₄) nanostructures are becoming increasingly significant due to the theoretical prediction of their unusual properties and promising applications ranging from photocatalysis, heterogeneous catalysis, to fuel cells. In recent years, a variety of nanostructured and nanoporous GCN materials have been developed for a wide range of new applications. The present work gives an overview on the synthesis of GCN nanomaterials with controllable structure and morphology, and presents applications of GCN as catalyst for organic dye degradation.

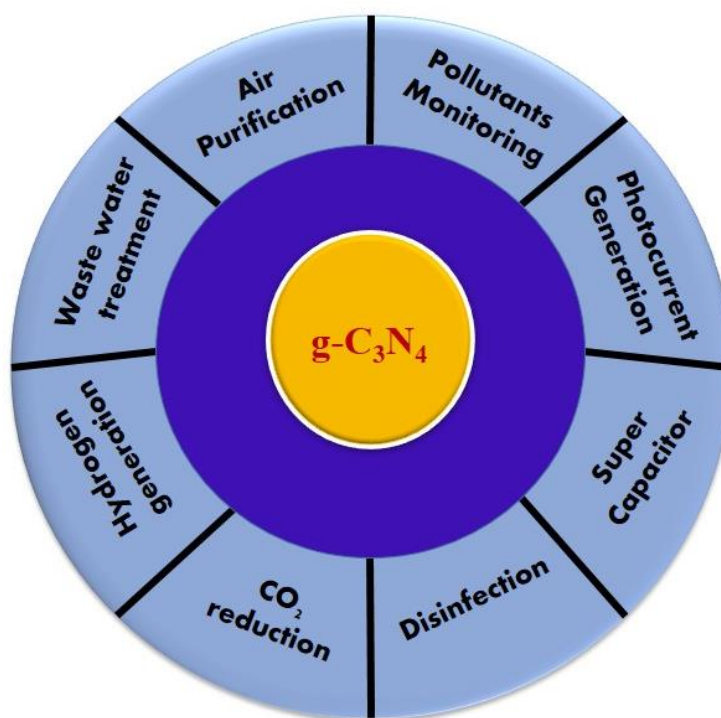


Figure 1.2 Schematic diagram for applications of graphitic carbon nitride nanostructures

A special emphasis is placed on the potential applications of nanostructured GCN in the areas of artificial photocatalysis for hydrogen production, oxygen reduction reaction (ORR) for fuel cells, and metal-free heterogeneous catalysis. Finally, this perspective highlights crucial issues that should be addressed in the future in the aforementioned exciting research areas.

1.7.1 Organic Dyes

Coloring materials have been used for many years for different purposes such as leather, cloth, food, pottery and housing. The largest consumption of dyes takes place in the textile industry. The residual dyes from different sources such as textile industries, paper and pulp industries, dye intermediates industries, pharmaceutical industries etc. are considered a wide variety of organic pollutants introduced into the natural water resources.

Classification of Organic Dyes

Organic dyes are classified into two types as discussed below:

(i) Natural Dyes

Natural dyes are derived from plants. The majority of natural dyes is vegetable dyes and obtained from plant parts such as roots, berries, bark, leaves and wood. Natural dyes are often negatively charged and positively charged dyes are rarely exist. Each dye has been named according to their specific color. The most commonly used natural dye is saffron (natural yellow 6) obtained from the stigmata of *Crocus sativus*. It is used as an acid dye for coloring and spice of food.

(ii) Synthetic Dyes

The dyes derived from organic or inorganic compound are known as synthetic dyes. Due to the presences of heavy metals and complexity in aromatic structure of the dyes, they enhance the mutagenic or carcinogenic toxicity. Some of the synthetic dyes are Methylene blue, Methyl orange, Rhodamine B, Malachite green etc. The carcinogenicity of azo dyes cause bladder cancer. Methyl orange exerts neurotoxic effects on the central nervous system. Malachite green dye not only affects the immune and reproductive systems but is a potential genotoxic and carcinogenic agent.

Methylene blue dye caused the bladder irritation, dizziness, headache, sweating, nausea/vomiting, diarrhoea, frequent urination, stomach cramps, high fever and fast or pounding heartbeats.

1.7.2 Methods for the Removal of Pollutants

Efficient techniques for the removal of highly toxic organic compounds from water have drawn significant interest. Using better purification technologies can reduce problems of water shortages, health, energy, and climate change. A considerable saving of potable water can be achieved through reuse of wastewater which requires the methods which are efficient, cost-effective, and reliable. Due to better solubility in water, the dyes are considered as the common water pollutants. If organic dyes present beyond a certain limit in water then they affect the quality of the water. So it is necessary to eliminate the dyes from wastewater before discharging to the environment. A number of methods have been used for the removal of organic and inorganic dyes from waste water, such as biological methods, chemical methods, physical methods and photocatalysis.

1.7.3 Photocatalysis

The word “photocatalytic” is of Greek origin and composed of two parts as the prefix “photo” (light) and the word “catalysis” (decompose). In photocatalysis process light is used to activate a substance without being involved itself in the chemical transformation. The photocatalytic activity depends on the ability of the catalyst to create electron hole pairs, which generate free radicals which are able to undergo secondary reactions. Photocatalysis result in mineralization of organic pollutants, disinfection of water and air, production of renewable fuels etc.

1.8 LITERATURE REVIEW

A large number of research reports are available on the synthesis of nanomaterials using AAO as template. Researchers studied preparation methods, structural, optical and many other properties and their applications in different fields. In this section, some of the important works on synthesis of AAO templates, synthesis of graphitic carbon nitride nanostructures, structural, optical, morphological and

thermal properties of prepared nanostructures are highlighted.

[Stępniewski and Bojar 2011] reported that Anodic aluminum oxide (AAO) could serve as a suitable template for nanofabrication. Structural features of AAO like pore diameter, interpore distance, porosity, pore density could be fully controlled. Self-organized two step anodization of aluminium in 0.3 M oxalic acid were investigated. Nanopores with relatively small diameters (below 30 nm) with simultaneous high pore density and porosity could serve as templates for production of close packed nanowires, nanotubes and nanodots with sub-30 nm diameters.

[Wang et al. 2010] reported the, production and characterization of the porous alumina, and other nanoporous structures. The nanoporous structures were used to prepare nanometer-sized fibrils, rods, and tubules of conductive polymers, metals, semiconductors, carbons, and other solid matter. Electrochemical and electroless depositions, chemical polymerization, sol-gel deposition, and chemical vapour deposition were considered as major template synthetic strategies. In particular, the template-based synthesis of carbon nanotubes were demonstrated as this is the most promising class of new carbon-based materials for electronic and optic nanodevices as well as reinforcement nanocomposites.

[Kwon et al. 2011] reported different methods to prepare nanostructured materials using highly ordered porous anodic alumina templates. They synthesized inorganic nanowires by paired cell method, platinum nanowires by electrochemical method and metal nanowires by using vacuum evaporation methods. They concluded that template based synthesis of nanomaterials using anodic alumina templates is a simple, low cost method to get ordered nanostructured arrays over a large area using wide range of materials.

[Stępniewski et al. 2014] et al. reported the detailed surface morphology control of porous anodic alumina templates fabricated in phosphoric acid. Second anodization can dramatically lessen the surface defects and improve cell arrangement. The electric field distribution is not regular due to different AAO pore shape and size at the beginning of second anodization, which leads to the simultaneous growth of vertical and horizontal holes, as well as surface distortion. One way to eliminate the surface distortion is to dissolve the spots under higher temperature and higher anodizing

voltage, and another way is to have well-ordered nanopore array in oxalic acid before anodizing in phosphoric acid.

[Stepniowski et al. 2014a] reported the Fast Fourier transform based quantitative arrangement analysis of poorly ordered nanopores of AAO templates prepared using chromic acid electrolyte. The fast fourier transform based analysis showed the distinct tendencies in the evolution of regularity with operating conditions. Moreover, this method was tested for AAO formed in chromic acid, which provided poorly arranged nanopores, where typical approach of quantitative arrangement analysis, dedicated or highly-ordered pores is useful. It was found that regularity ratio of the anodic alumina nanopores formed in chromic acid increases with anodizing voltage. The best nanopores arrangement was found for anodic aluminum oxide formed at the highest temperature (23°C).

[Belwalkar et al. 2008] reported the effect of processing parameters on the pore structure and thickness of anodic aluminium oxide templates. They reported that the voltage affected the pore size: the pore size increased with increase in the applied voltage and decreased with increase in acid concentration. Concentration of the acids also influenced the pore size in a way that higher acid concentration increased the rate of oxidation than dissolution thereby decreasing the pore size. The rate of oxide growth was found to be greater in higher acid concentrations. It was proposed that this was caused by the conductivity of the acid, as higher acid concentrations resulted in larger current densities.

The template thickness was found to be proportional to the concentration of acidic electrolyte. However, it was also observed that prolonged second anodization time eventually reduced template thickness. This suggests that the membrane thickness must be described by the dynamic equilibrium of the oxidation and dissolution rates. It was proposed that the attenuation of the oxidation rate and the resulting limiting thickness is due to depletion of oxygen ions in the acid electrolyte solution. As each acid concentration exhibited a different oxidation rate, it was proposed that each acid concentration also displayed a characteristic limiting thickness at a specific time.

[Stepniowski et al. 2014] reported the effect of time and temperature on the arrangement of anodic aluminium oxide nanopores. They explained the quantitative

arrangement of pores using FFT analysis. They observed that would be improvement in the nanopore ordering when the duration of anodization was sufficiently long. And also they showed that the longer first step of anodization leads to the better pre-texturing of the aluminum beneath the pore bottoms, at the metal–oxide interface and the better ordering of the final array.

[Choudhari et al. 2012] et al. reported the thermal stability of AAO membranes prepared at different anodization voltages. And also the membranes prepared in oxalic acid were pore-widened in 5 wt% phosphoric acid solution for different durations and the progress of the pore widening process was investigated. They showed that the as-prepared membranes are amorphous. Thermal stability studies of the AAO membranes indicated that there was no apparent change in the morphology of the AAO membranes when heated at temperatures of up to 600 C. However, there was a small amount of destruction of the nanostructures of PAA membranes when heated beyond 700 C. In accordance with the thermal analysis and X-ray diffractogram analysis it was evident that the as-prepared AAO membrane which was amorphous at room temperature could be transformed to crystalline Al_2O_3 phase by carrying out the heat treatment at the temperature above 700 C.

[Li et al. 2010] reported a simple method to self-assemble porous anodic aluminum oxide templates with nano channels by anodizing in phosphoric acid solution. Due to high field conduction and anionic incorporation an increase of anodizing voltage leads to an increase of the impurity levels and also the field strength across barrier layer. On the basis of both experiment and simulation results, the initiation and formation of nano porous channels were found to depend on the processing parameters.

[Zaraska et al. 2013] et al. reported the effect of anodizing temperature on structural features and hexagonal arrangement of nanopores in alumina synthesized by two-step anodizing in oxalic acid. It was found that increasing temperature of anodization increases the pore diameter and porosity of AAO and decreases both the cell wall and barrier layer thickness. This can be attributed to the enhanced field assisted dissolution of aluminium oxide at the oxide/electrolyte interface at higher temperatures.

On the other hand, the interpore distance was found to be independent on the temperature of anodization.

[Huang et al. 2001] et al. reported facile and direct synthesis of porous nanorod-type graphitic Carbon Nitride materials. The g-C₃N₄ nanocomposite demonstrated improved visible-light induced photocatalytic activities. The results indicate that metalmelamine supramolecular frameworks can be promising precursors for the preparation of efficient g-C₃N₄ nanocomposite photocatalysts.

[Cao et al. 2015] et al. reported that GCN has a flexible structure and is thus well suited to form different morphologies with the assistance of different templates. Indeed, several typical nanostructures of GCN have been obtained, such as porous GCN, hollow spheres and 1D nanostructures. GCN photocatalysts are extremely fascinating, because the porous structure can provide a large surface area and numerous channels to facilitate mass diffusion, as well as charge migration and separation. Hard and soft templating methods are often used because they allow tuning of the porous structure of GCN by choosing different templates.

[Mousavi et al. 2018] et al. reported the recent advances in fabrication, characterization, and applications of magnetic GCN based nanocomposites, as effective photocatalysts, to address separation challenges of the applied catalysts from the reaction systems. Herein, the combinations of GCN with magnetic nanoparticles were not only solved the separation problem, but also enhanced the photocatalytic activity by improving the visible-light absorption response, extending the charge separation duration, and facilitating the photogenerated electron- hole transportations. Moreover, the fabricated magnetic GCN based nanocomposites exhibited good stability to use in successive runs.

From the above literature, it may be inferred that, most of the researchers are interested in the synthesis of novel nanomaterials by using anodic alumina as templates. Recently the researchers concentrated on the growth of graphitic carbon nitride nanostructures and the synthesis of graphitic carbon nitride composite nanostructures and their applications.

1.9 SCOPE AND OBJECTIVES OF THE WORK

(i) Scope

Anodic aluminum oxide (AAO) membranes are used as templates in a variety of nanotechnology applications without the need for expensive lithographical techniques. AAO templates are excellent materials with unique properties and applications. The structure and properties of the nano porous anodic alumina templates depend on the preparation method, precursors of the electrochemical reaction, external parameters like reaction temperature, voltage, reaction time, etc. So templates can be prepared with different pore sizes by using simple electrochemical anodization method. Electrochemical anodization is a versatile method of AAO template synthesis.

A great amount of work has been done on almost all template based synthesis of nanomaterials except GCN nanostructures and graphitic carbon nitride composite nanostructures. GCN nanostructures can be synthesized by the pyrolysis of nitrogen rich precursors such as urea, thiourea, and melamine which results into 2D sheets of tri-s-triazine connected via ternary amines. This is symbolized as GCN and most stable allotrope of various carbon nitride structures. An extensive research has to be done on this material to understand its structural and optical properties. There is a scope to prepare GCN composites by simple template assisted thermal condensation method. Also the study of structural and optical properties of GCN nanostructures and GCN nano composites will give an opportunity to understand their applications in various fields including photocatalysis[Fujita et al. 2016].

Researchers are most interested in structural and optical properties of the GCN nanostructures. Further, electrochemical properties of GCN nanostructures are quite important due to their applications in electrochemical sensors and energy storage. From electrochemical studies, one can understand the reaction mechanism of the material at the electrode surface with electrolyte at applied potentials. So that, one can estimate the relation between the electrical and chemical properties of the material. GCN nanostructures are used for photocatalysis and GCN composites can catalyze water reduction and degradation of dye molecules with visible light.

(ii) Objectives

1. Preparation of porous anodic alumina templates using electrochemical anodization.
2. To study the structural, morphological and optical properties of prepared AAO templates.
3. Preparation of GCN nanostructures using AAO templates by thermal condensation method.
4. To study the structural, morphological optical and thermal properties of GCN nanostructures.
5. To study the temperature dependent synthesis and characterization of graphitic carbon nitride nanostructures.
6. To study the applications of prepared graphitic carbon nitride and nanostructures.

1.10 Organization of thesis

The thesis is organized as follows:

Chapter 1 presents the overview of aluminium oxide nanostructures, synthesis of different nanostructures using various methods. It includes synthesis of graphitic carbon nitride nanostructures and applications towards photocatalysis. The chapter contains the objectives and organization of the thesis.

Chapter 2 gives the brief description of two-step anodization process, which is employed to synthesize AAO and graphitic carbon nitride based nanostructures. This is followed by a concise description of different characterization techniques such as X-ray diffraction (XRD), field emission scanning electron microscopy (FESEM), FTIR spectroscopy (FTIR), UV-Vis spectroscopy, Photoluminescence spectroscopy(PL), Thermo gravimetric analysis (TGA) etc.

Chapter 3 begins with a discussion of fabrication of anodic Aluminum Oxide (AAO) templates using different electrolytes and also the influence of anodization conditions on the growth of AAO template. It contains the discussion on influence of pore widening duration on pore morphology of AAO templates prepared using different electrolytes such as oxalic acid, phosphoric acid, sulphuric acid and chromic acid.

Chapter 4 deals with the preparation of GCN nanostructures using porous anodic aluminium oxide as templates through thermal condensation process and studies on structural, morphological, thermal and optical properties of the prepared nanostructure.

Chapter 5 deals with the synthesis and characterization of a series of GCN nanostructures by varying the temperature during thermal condensation of cyanamide using porous anodic aluminium oxide (AAO) templates.

Chapter 6 gives some applications of GCN nanostructures towards photocatalytic degradation of various dyes such as Methylene blue (MB), Methylene orange (MO), Rhodamine B (RhB) dyes.

Chapter 7 gives the overall summary of the results described in the previous chapters. Moreover, the scope for future research work in this area is also highlighted.

CHAPTER 2
EXPERIMENTAL TECHNIQUES

CHAPTER 2

EXPERIMENTAL TECHNIQUES

Overview

This chapter gives detailed description of experimental techniques involved in two-step anodization process, which is employed to prepare AAO templates for the synthesis of GCN nanostructures using thermal condensation method in the present research work. This includes a description of experimental setup used for the synthesis and characterization of AAO templates and related nanostructures.

2.1 PREPARATION METHOD

2.1.1 Experimental setup for AAO template preparation

In the present anodization work, two electrode electrochemical cell was used. The schematic of the experimental setup is shown in the Figure 2.1. The main part of the setup was a laboratory scale two-electrode electrochemical cell. The cell consists of a two electrode stand, DC power supply, ice bath and a magnetic stirrer.

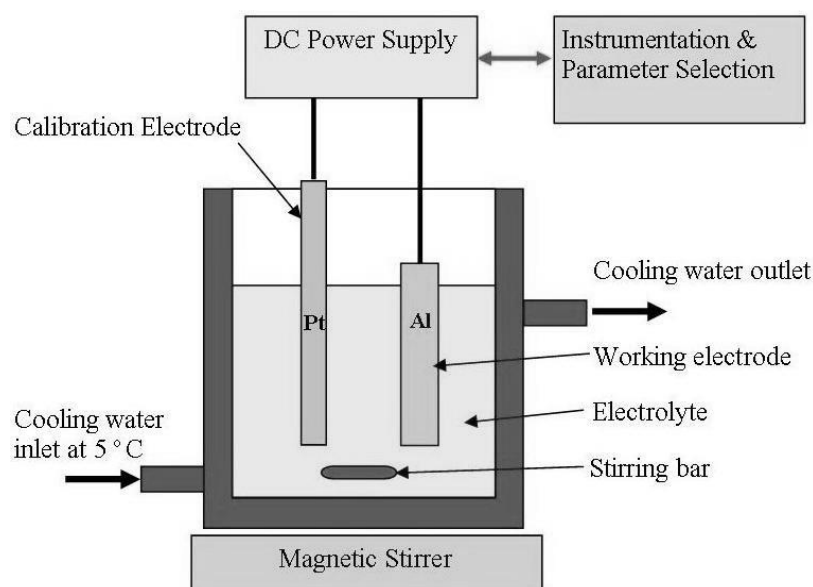


Figure 2.1: Schematic of the experimental setup used for anodization

The electrolyte was taken in a borosil beaker and placed on the magnetic stirrer. The typical volume of the electrolyte was 100 ml. The magnetic stirrer was used to stir the electrolyte continuously. This keeps the electrolyte at equilibrium temperature. The potentiostat used had a working range of 0 - 300 V and 0 - 5 A.

2.1.2 Experimental method to synthesize porous anodic alumina templates.

In the present study, AAO templates were prepared using two step self-organized anodization process. The purpose of this section is to describe the preparation conditions for self-assembled porous alumina with variable pore sizes. The preparation of porous alumina consists of three processes, pre-treatment, two step anodization and post-treatment as shown in the Figure 2.2. Firstly, the aluminum foil (high purity-99.99%, Merck-0.3 mm thickness) is cleaned with acetone in an ultrasonic bath for 30 min to remove contaminations. Then the aluminum foil is annealed in air at 500 °C for 5 h to reduce the mechanical stress in the material.

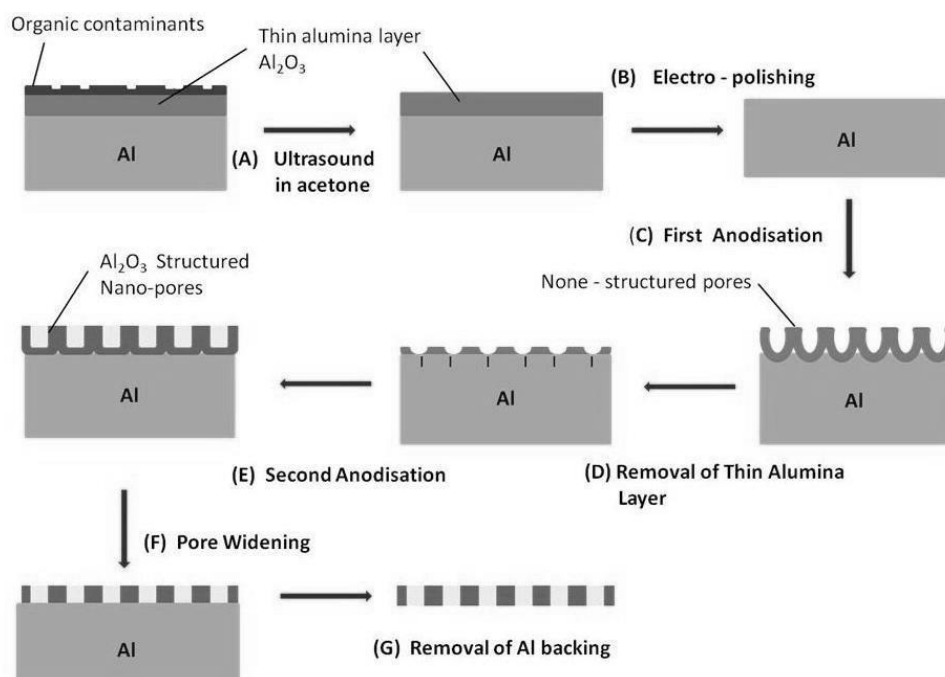


Figure 2.2: Schematic diagram of the two-step anodization process.

The electrochemical polishing of the aluminum foil is then carried out in a mixture of perchloric acid (HClO_4) (99.9% Alfa Aesar) and ethanol ($\text{C}_2\text{H}_6\text{O}$) (Lab grade) with a volume ratio of 1:4, with polishing parameters of current density (200 mA/cm^2) for 2 min at 10°C . After polishing, the aluminium surface becomes smooth

and shiny. In our experiments, oxalic acid ($C_2H_2O_4$) (99.9% Alfa Aesar), sulphuric acid (H_2SO_4) (99.9% Alfa Aesar), phosphoric acid (H_3PO_4) (99.9% Alfa Aesar) and chromic acid (H_2CrO_4) (99.9% Alfa Aesar) were used as the anodizing electrolytes.

For each electrolyte, there is a certain potential and concentration which can be applied without burning the oxide film. The self-organized growth of pores takes place perpendicular to the surface of the aluminium foil. In order to get a highly ordered arrangement of pores, porous oxide layer was etched away chemically after the first step anodization. This etching process was carried out in a solution containing 6% H_3PO_4 and 1:8% H_2CrO_4 in a water bath at $60^\circ C$ for 2 h. After removing of the first oxide layer, the second step anodization was carried out with the same conditions as those used for the first step. The anodizing time was varied from 2-20 hours depending on the required thickness. Fig.2.2 shows the schematic diagram for synthesis of AAO templates.

To obtain a free-standing template, usually it takes more than 8h of anodization. Otherwise, the template would be too thin and delicate to handle. The remaining aluminium base and barrier layer is removed from the non-oxide side to get open pores. After the template preparation the templates are subjected for post treatment. In this process a mixed solution of hydrochloric acid (HCl) (99.9% , Alfa Aesar) and copper chloride ($CuCl_2$) (99.9% , Alfa Aesar) is used to dissolve the aluminium base. Afterwards the barrier layer is removed and pores were widened using 5wt% phosphoric acid (H_3PO_4) (99.9% , Alfa Aesar) solution. In general, with an increasing etching time, the pores are significantly widened because the walls get dissolved along the vertical direction.

To study the effect of anodization potential and electrolyte, anodization process was carried out in 0.3 M of oxalic, sulphuric, chromic and phosphoric acids with corresponding anodization potentials maintained at as 40 V, 20 V, 50 V and 90 V for 12 h at $8^\circ C$. to study the effect of pore widening on templates, pore widening is performed after the second step anodization using 5 Wt % of H_3PO_4 for different time durations as 0, 15, 30, 45 and 60 min at room temperature.

2.1.3 Experimental method to synthesize graphitic carbon nitride nanostructures.

Synthesis of GCN with the assistance of a hard template AAO is a simple three-step method. This includes the synthesis of AAO templates with desired pore dimensions, thermal condensation of nitrogen rich precursors into the pores of AAO templates and the removal of backing AAO template to get the GCN nanostructures.

The synthesized AAO templates were immersed in a homogeneous mixture of 10 g of cyanamide (CH_2N_2) (99.99 % Pub Chem) and 5 ml of distilled water and mixed under ultra-sonication for 10 min. The filled AAO templates were thoroughly cleaned and are dried at 120°C for 1 hr. The dried samples were heated at a temperature of 550°C for 5 h. The GCN nanostructures were produced by chemically etching the AAO templates using 2 M NaOH (99.9%, Alfa Aesar) solution. Figure 2.3 represents the schematic diagram of synthesis of GCN nanostructures using AAO templates. For comparison bulk GCN samples were prepared by polymerization of melamine at 550°C for 4 hrs. The synthesized yellow products was named as bulk GCN [Suchitra et al. 2016].

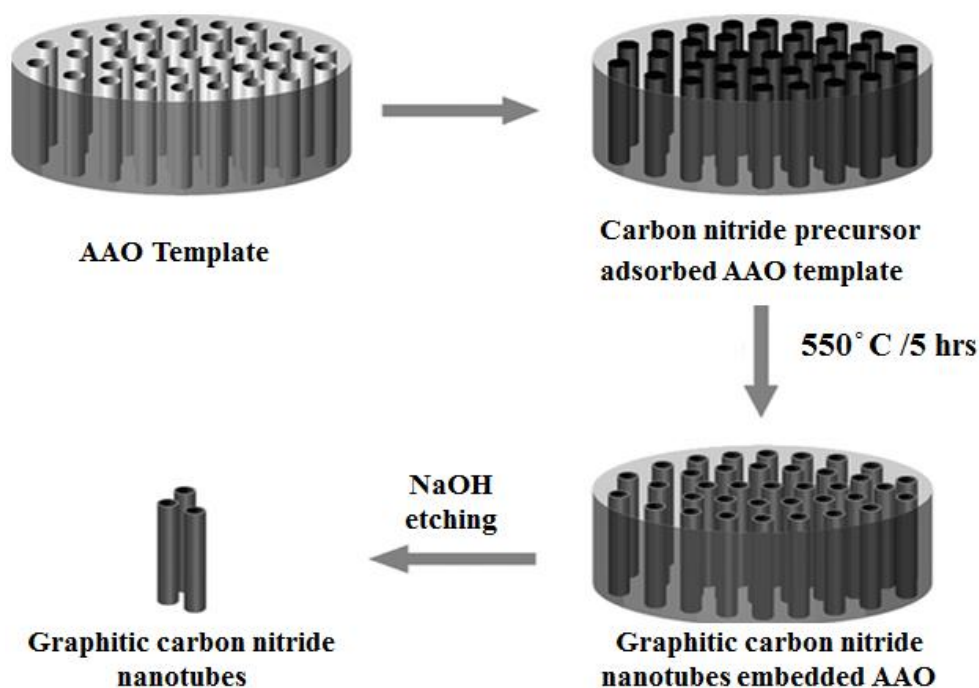


Figure 2.3: Schematic diagram of synthesis of GCN nanotubes using AAO templates.

To study the effect of temperature on synthesis of GCN nanostructures the filled AAO templates were heated to different temperatures i.e. 400°C, 450°C, 500°C, 550°C and 600°C for 4 h.

2.2 CHARACTERIZATION TECHNIQUES

Several techniques have been used to characterize AAO templates and GCN nanostructures. X-ray diffraction data were used to confirm the amorphous nature of AAO template and crystalline nature of GCN nanostructures. In addition, scanning electron microscopy (SEM) was used to characterize the surface morphology of the prepared nanostructures. Furthermore, the optical properties were recorded by the UV-Visible and photoluminescence (PL) spectra. A standard Thermo gravimetric method was used to determine the thermal properties of the nanostructures. To notice the functional groups present in GCN nanostructures fourier transform infrared spectra (FTIR) were recorded.

2.3 STRUCTURAL AND MORPHOLOGICAL ANALYSIS

2.3.1 X-ray Diffraction

X-ray diffraction (XRD) studies were carried out to study the crystallographic aspects of the prepared nanostructures. Optical and photocatalytic properties of the materials depend mainly on crystallographic nature of the nanomaterials. In crystalline solids, atoms can be imagined to be orderly arranged in different set of equidistant parallel planes denoted by miller indices (h k l). When a beam of X-ray is allowed to pass through solid material, diffraction takes place, when they satisfy Bragg's law.

Diffraction analysis is useful whenever it is necessary to know the state of chemical combination of the elements involved or the particular phase in which they are present. X-ray diffraction method is faster, requires very small sample and is non-destructive. Bragg's law is the basic law involved in the diffraction method of structural analysis.

X-ray diffraction methods have strongly demonstrated the crystallinity of solids by exploiting the fact that the spacing between atoms is comparable to the wavelength

of radiation. X-ray diffraction results easily detected by emitted beams of high intensity along certain directions when incident X-rays impinge at critical diffraction angles (θ).



Figure 2.4: X-Ray diffractometer Rigaku (Model Miniflex600).

Then Bragg's law for X-ray diffraction is given by

$$2d \sin \theta = n\lambda \quad (2.1)$$

where 'n' is the order of diffraction, ' λ ' is the wavelength of the X-rays, 'd' is the spacing between consecutive parallel planes and ' θ ' is the glancing angle. X-ray diffraction studies give a whole range of information about the crystal structure, orientation, average crystallite size and stress in the films. Experimentally obtained X-ray diffraction data of prepared sample are compared with the standard Powder Diffraction Files published by the Joint Council on Powder Diffraction Standards (JCPDS). This diffraction data are used to determine dimensions of the unit cell, crystal structure, standard deviation, and crystallinity.

In the present study, XRD pattern of AAO templates were carried out using X-ray diffractometer (Rigaku-miniflex-600: Figure 2.4) to verify the amorphous nature of the AAO templates and crystalline phases in the GCN nanostructures. Data were collected using Cu $K\alpha$ radiation ($\lambda = 1.5418\text{\AA}$) in the diffraction angle (2θ) ranging from 20° to 80° with a scanning rate of 2° per minute. The x-ray tube was operated at

40 kV and 30 mA. The XRD patterns obtained were compared with those of JCPDS data to assess the crystalline phases present.

2.3.2 Surface morphology analysis

The surface morphology of the AAO and GCN nanostructures was studied using field emission scanning electron microscopy (FE-SEM). The uniformity of the template surface plays a significant role in determining the properties of AAO templates. A number of FE-SEM micrographs was taken at a different magnification at different spots to verify surface morphology and it remains the same throughout sample prepared at constant conditions.

(a) Field Emission- Scanning Electron Microscopy

Field Emission scanning electron microscopy (FE-SEM) is one of the most widely used techniques for obtaining microstructural and surface features of nanostructures. FESEM is a microscope that works with electrons instead of light. These electrons are liberated by a field emission source. The object is scanned by electrons according to a zig-zag pattern. Field emission scanning electron microscopy (FE-SEM) provides topographical information at magnifications of 10x to 300,000x, with the virtually unlimited depth of field. Applications of FE-SEM include semiconductor device cross-section analyses for gate widths, gate oxides, film thicknesses, and construction details, advanced coating thickness and structural uniformity determination, small contamination geometry features and elemental composition information.

Electrons are liberated from a field emission source and accelerated in a high electrical field gradient. Within the high vacuum column, these so-called primary electrons are focused and deflected by electronic lenses to produce a narrow scan beam that bombards the object.

As a result, secondary electrons are emitted from each spot on the object. The angle and velocity of these secondary electrons are related to the surface structure of the object. A detector catches the secondary electrons and produces an electronic signal. This signal is amplified and transformed to a video scan-image that can be seen on a monitor and it can be processed further.



Figure 2.5: Field Emission Scanning Electron Microscopy (Carl Zeiss).

In order to avoid charging problems, a thin layer of 1.5 nm to 3 nm of gold or palladium is deposited on the specimen without altering the surface features. In the present work, the surface morphology of the nanostructures was studied using Carl Zeiss model electron microscope operated at accelerating voltage of 5 kV (figure 2.5).

(b) Image processing

The basic parameters of AAO templates have been measured using the Image-J 1.37 V software (<https://imagej.nih.gov/ij/>). This software allows extraction of the geometrical features of pores, such as the pore diameter, pore area and pore perimeter, etc. By these values it is possible to obtain the porosity, interpore distance and pore density. In order to obtain such characteristic features of the pores, a binarization of the SEM image is performed and this provides an image containing black and white zones. The black zones correspond to the pores and the white zones are associated with the alumina top surface of the AAO template.

The pore regularity and fast Fourier transform has been studied using the open software WSxM 4.0 (Horcas et al., 2007). For a quantitative analysis, the correction

aspects such as the number of pores (n), analyzed surface area (S) and porosity (a) have been considered in our analysis. The averaged regularity ratio (R), derived from the FFT radial average was calculated using the following equation (Stepniowski et al., 2014)

$$R = \frac{I}{W} \frac{\sqrt{n}}{(S)^{\frac{3}{2}}} \quad (2.2)$$

Where ‘ I ’ is the intensity of the radial average, ‘ W ’ is the width of the radial average at half of its height, ‘ n ’ is the number of pores on the analysed image and ‘ S ’ is the analysed surface area. The radial averages form soft, separate peaks which make the estimated results truthful. The physical significance of the radial average is that it exhibits the distribution of the interpore spaces in the inversed space. Hence, if the distribution of pores is not uniform, the FFT image will not be clear and the intensity of the radial average would be lower. Moreover, the abscissa of the radial average peak corresponds to the average interpore space (Stepniowski et al., 2014a) and breadth of the peak at half of its width is strongly related to the distribution of the interpore spacing values. The combination of both the software Image-J and WSxM allows the calculation of the most relevant geometrical features of the AAO templates.

2.4 Optical analyses

2.4.1 Infrared spectroscopy

The infrared region of the electromagnetic spectrum extends from the red end of the visible spectrum to microwave region, at wave numbers between 14000 and 20 cm^{-1} . The near - infrared region meets the visible region at about 12,500 cm^{-1} and extends at about 4000 cm^{-1} and there are many absorption bands resulting from harmonic overtone of fundamental and combination bands, often associated with hydrogen atom. The mid-infrared region is the most useful region, which covers frequencies from 4000-200 cm^{-1} and the fingerprint region, 300-650 cm^{-1} . In the group frequency region the principal absorption bands are due to vibrational units consisting of only two atoms of a molecule.

The major factors in the spectrum of fingerprint region are single band stretching frequencies and bending vibrations of polyatomic system. The far infrared

region $667\text{-}10\text{ cm}^{-1}$ contains the bending vibrations of carbon, nitrogen, oxygen and fluorine with heavier atoms and additional bending motions in cyclic or unsaturated systems.



Figure 2.6: Fourier transform infrared spectrometer (*Bruker Alfa FTIR spectrometer*).

Infrared spectroscopy is an important field of chemical analysis. The first task in the infrared analysis of any sample is obtaining the spectrum itself. This involves preparing the sample, placing it in an infrared spectrometer, and measuring the response of the sample to infrared light. All of the aspects of a spectrum, the position, height, width and pattern of bands carry important information about the sample.

Infrared spectroscopy has many advantages as a chemical analysis technique. Solids, liquids, gases, semi-solids, powders and polymers are all routinely analysed. Infrared spectroscopy is a relatively fast and easy technique. It is also a sensitive technique. The absorption of infrared radiation by a molecule takes place when there is a transition between the various vibrational and rotational states. In order to absorb infrared radiation, a molecule must undergo a net change in the dipole moment as a consequence of its vibrational or rotational motion. Coupling with electromagnetic radiation occurs when the vibrating molecules produce an oscillating dipole moment

that can interact with the electric field of the radiation. The transitions in vibrational energy levels result in radiation, governed by the selection rule $\Delta v = \pm 1$. Vibrations fall into basic categories of stretching and bending. A stretching vibration involves a change in the interatomic distance along the axis of the bond between two atoms. Bending vibrations are characterized by a change in the angle between two bonds and are of four types - scissoring, rocking, wagging and twisting.

In the present work, the infrared spectroscopy of the nanostructures was studied using Fourier transform infrared (*FTIR*) spectrometer were recorded with (*Bruker Alfa FTIR spectrometer*) (figure 2.6) in the range 400 to 4000 cm^{-1} .

2.4.2 UV-Vis spectroscopy (UV-Visible)

Optical characterization is one of the methods to determine different electronic and optical transitions in the material and its band gap under the illumination of light. The incident light may get reflect, some part of the incident light may get absorb and some part may get transmitted through the sample. The amount of reflection, absorption, and transmission depend on the band structure and energy of the incident light. The transmittance and absorption measurements reveal valuable information about the energy band gap (E_a) and band structure of the semiconductor material.



Figure 2.7: UV-Vis- Spectrophotometer (Model: Ocean optics USB4000-XRI-ES)

The result of band to band transition is fundamental absorption, remaining mechanisms are important if the energy of the incident light is less than the energy band gap of semiconductor material.

In the present work, optical absorption spectra of AAO templates and GCN nanostructures were obtained from UV-Vis-NIR spectrometer model Ocean optics USB4000-XRI-ES (figure 2.7). In case of direct bandgap semiconductors band gap energy is given by the equation

$$\alpha h\nu = B(h\nu - E_g)^n \quad (2.3)$$

where, $n=1/2$ for allowed direct transitions, $n=2$ for allowed indirect transitions, $n=3$ for forbidden indirect transitions and $n=3/2$ for forbidden direct transitions. 'B' is the parameter which depends on the transition probability. The plot of $(\alpha h\nu)^2$ vs photon energy ($h\nu$) is called as Tauc's plot. In the case of direct transition, $(\alpha h\nu)^2$ will show a linear dependence on the photon energy ($h\nu$). A plot of $(\alpha h\nu)^2$ against $h\nu$ will be a straight line and the intercept on energy axis at $(\alpha h\nu)^2$ equal to zero will give the bandgap energy (E_g).

2.4.3 Photoluminescence (PL)

Luminescence is the general name given to the process of spontaneous emission of light by excited atoms in a solid material. One of the ways in which the atoms can be promoted into excited states prior to spontaneous emission is by the absorption of light. Luminescence can thus accompany the propagation of light in an absorbing medium. Fluorescence and phosphorescence are two types of photoluminescence phenomena (Mendham et al., 2006).

The physical processes involved in photoluminescence are more complicated than those in absorption. This is because the generation of light by luminescence is tied up with the energy relaxation mechanism in the solid. Furthermore, the shape of the emission spectrum is affected by the distribution of electrons and holes within their bands. PL instrument used to analyse luminescent properties of AAO templates is shown in the Figure 2.8. In the present work, PL spectra were studied using FluoroMax-4 fluorescence spectrometer. Throughout PL calculations, the slit width was set as 7 nm

and each spectrum was obtained within 1 min. All the calculations were performed at room temperature with an excitation wavelength of 320 nm.



Figure 2.8: Spectrophotometer (FluoroMax-4).

2.5 THERMAL ANALYSIS

2.5.1 Thermo Gravimetric (TG) analysis

Thermal analytical methods, Thermo Gravimetric (TG) analysis and Derivative Thermo Gravimetric (DTG) analysis were done for GCN samples. The TGA is used to measure the changes of the mass of a sample that occur when the sample is heated. The DTG curve is produced electronically from the first derivative of the TG trace, and it represents change of mass as a function of time (dm/dt). The magnitude of the DTG signal is directly proportional to the rate of reaction. It separates overlapping reactions more clearly than the TGA curves. Thermo gravimetric (TGA) studies were done using (Perkin-Elmer TGA 4000) system under air atmosphere by heating the samples from room temperature to 800 °C.

These methods are used to determine thermal stability of samples and its fraction of volatile components by monitoring the weight change that occurs when a sample was heated. In this study, the sample was placed in a standard alumina crucible. The TG experiments were performed under static air atmosphere. The temperature was increased from 25°C to 1200°C with a heating rate of 10°C/min. The Derivative Thermo Gravimetric (DTG) analysis profiles, which show the rate of mass conversion from the sample versus temperature, were derived from the TGA curves. These profiles

were used to fix the temperature intervals for the pyrolysis process of samples in this study.

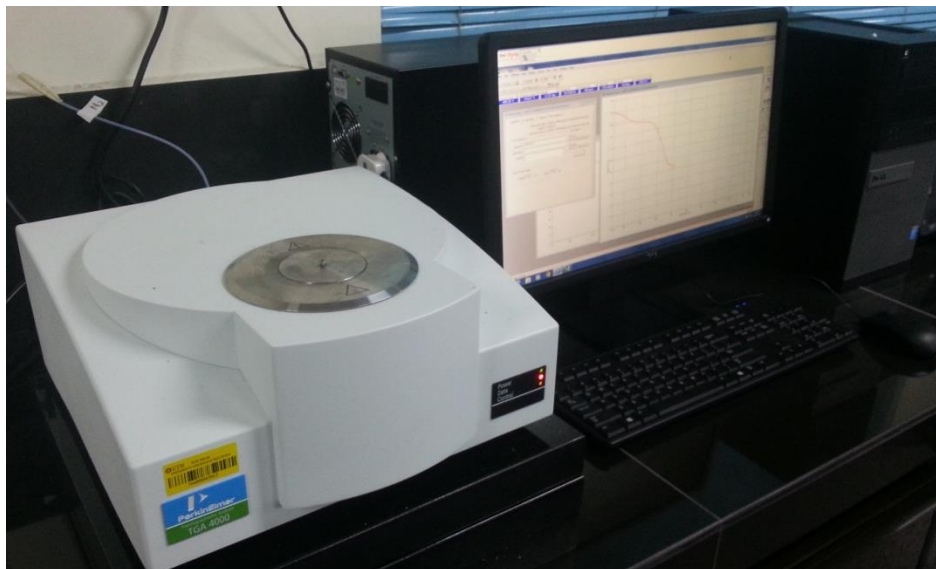


Figure 2.9: Thermogravimetric analyzer (*Perkin-Elmer TGA 4000* instrument)

2.6 PHOTOCATALYSIS

The word photocatalysis is composed of two parts: Photo and catalysis. The prefix photo is defined as “light”. Catalysis is the process where a substance participates in modifying the rate of a chemical reaction of the reactants without altering the end product. The substance is known as catalyst which increases the rate of a reaction by reducing the activation energy. Hence photocatalysis is a reaction which uses light to activate a substance which modifies the rate of a chemical reaction without involving itself. Heterogeneous photocatalysis has been used since the mid1970s to decontaminate water from harmful microorganisms. Figure 2.10 shows the schematic diagram of photocatalytic setup.

The main focus of this study is to investigate the principal applicability of photocatalysis systems for efficient treatment of water polluted with toxic dyes. In our experiments the photocatalytic activities of all catalysts were tested by studying the degradation reaction of Methylene blue (MB), Methylene orange (MO) and Rhodamine-B (RhB) dye solutions. A high pressure mercury lamp (80 W) was used as a light source placed in the photoreactor surrounded with water circulated quartz jacket to avoid thermal degradation. Solution was magnetically stirred in dark for 30 min to establish

adsorption/desorption equilibrium. The entire reactor setup is kept inside a closed chamber during catalytic experiment. For a photocatalysis experiment, 1 mg of the catalyst was dispersed in 100 ml of water and 2ml of dye is dissolved in 78 ml of water to make 80 ml of standard dye solution. Then 20 ml of catalyst solution is dispersed in 80 ml of MB solution. The above suspension was kept under constant stirring during irradiation. About 4 ml of subjected solution was sampled at regular time intervals and centrifuged to separate catalyst particles, finally analysed by recording the absorption spectra of dye solution using spectrophotometer. Figure 2.11 shows the photocatalytic reactor setup used for photocatalytic degradation process.

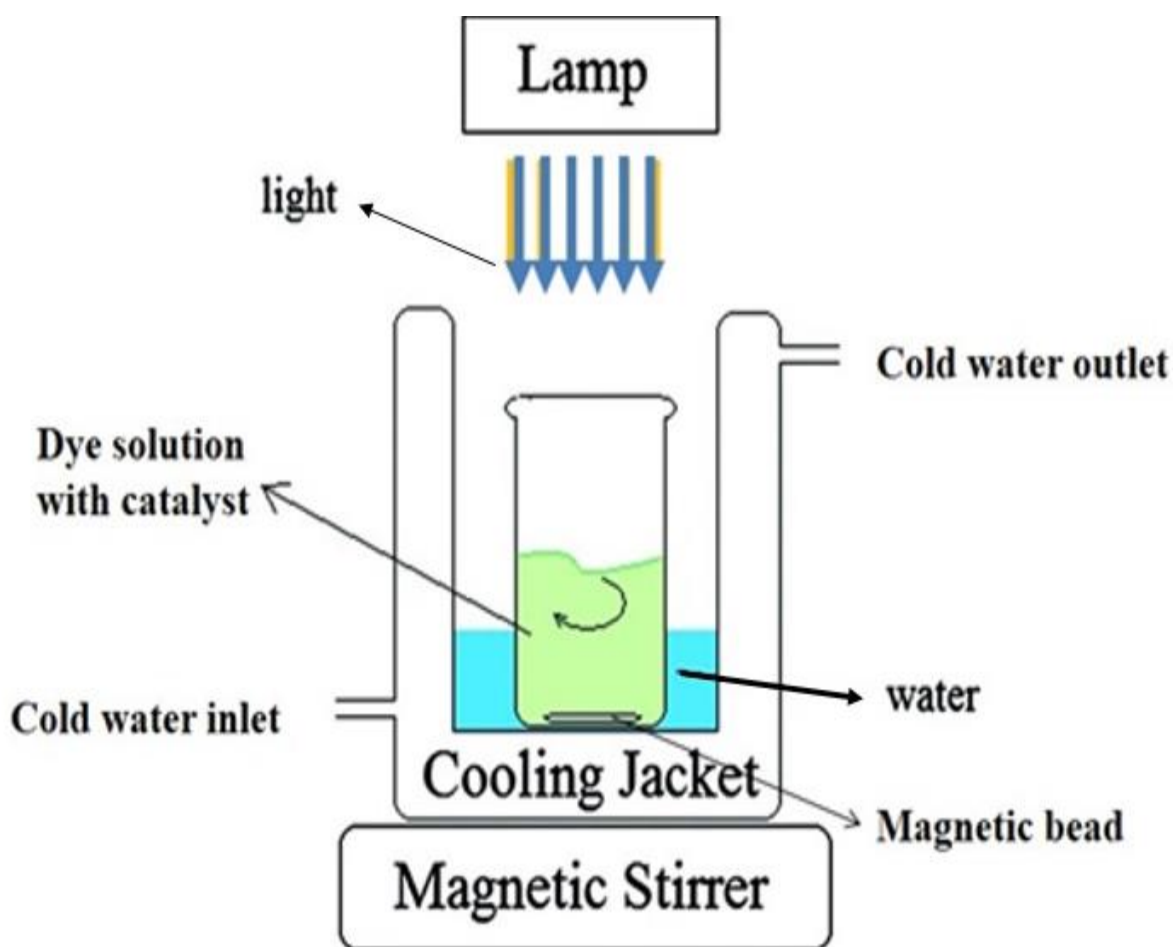


Figure 2.10: Schematic diagram of photocatalytic setup.



Figure 2.11: The experimental setup used for photocatalysis.

The absorption spectrum of dye solution after stirring the suspension in the dark for 30 min (that is, just before the visible light exposure) was recorded as a reference spectrum corresponding to the initial dye concentration (C_0). The intensity of absorbance peak (A) of dye solution after photocatalysis reaction, was taken as a measure of concentration with respect to irradiation time (C). The residual MO dye concentration was calculated using the relationship as follows.

$$\text{Percentage of degradation of dye} = \left(\frac{C_0 - C}{C_0} \right) \times 100 \quad (2.4)$$

The kinetic study of the photocatalytic degradation of dye solution by sample studied by the pseudo first order rate equation given by,

$$\ln \left(\frac{C}{C_0} \right) = -kt \quad (2.5)$$

where ' C ' is the initial concentration, ' C_0 ' is the concentration at corresponding irradiation time (t) and ' k ' is the first order rate constant and the slope of the straight line gives k value. Photocatalytic activity of MB under visible light irradiation was tested for 5 consecutive cycles.

CHAPTER 3

***FABRICATION OF POROUS ANODIC ALUMINA
TEMPLATES: OPTIMUM CONDITIONS FOR
SELF-ORDERED PORES***

CHAPTER 3

FABRICATION OF POROUS ANODIC ALUMINA TEMPLATES: OPTIMUM CONDITIONS FOR SELF-ORDERED PORES

Overview

In this chapter, fabrication of anodic Aluminum Oxide (AAO) templates using oxalic, sulfuric, phosphoric and chromic acid as electrolytes are discussed. Influence of pore widening duration on pore morphology is discussed.

3.1 Optimum conditions for self-ordered pores

In this chapter, the effect of processing parameters such as anodization voltage, type of electrolytes, concentration of electrolyte, electrolytic bath temperature, anodization time and pore widening durations on AAO templates are discussed. In particular, the concentration of electrolyte, anodization voltage, anodization duration and bath temperature are the main parameters in determining the pore parameters. Generally oxalic ($C_2H_2O_4$), sulfuric (H_2SO_4), phosphoric (H_3PO_4) and chromic (H_2CrO_4) acids are used as electrolytes to produce oxide layer. In case of oxalic acid we observed highly ordered hexagonal pore formation.

3.1.1 Effect of voltage

The self-ordered pore formation in 0.3 M oxalic acid as electrolyte was carried out at different anodization potentials in the range of 10 to 50 V while keeping the bath temperature at 18 °C. Figure.1 shows the top view SEM images of AAO templates formed at different voltages in oxalic acid.

The oxide film is formed as a result of voltage application and subsequent oxidation reaction between the metal and the electrolyte Figure.3.1 indicates that low voltages result in a set of tiny round pores with small pore diameters. Below 40V applied potential shows the randomly distributed nano pores all over the surface during anodization process. Anodization at higher voltages leads to dissolution of the oxide film and formation of less ordered porous alumina [Poinern et al. 2011]. Hence it was noticed that anodization at 40 V favored highly ordered arrangement of pores in case of oxalic acid. Anodization potential depends on the type of electrolyte which is

constant with respect to electrolyte concentrations 25 V, 195 V, and 50 V in case of sulfuric, phosphoric and chromic acid respectively.

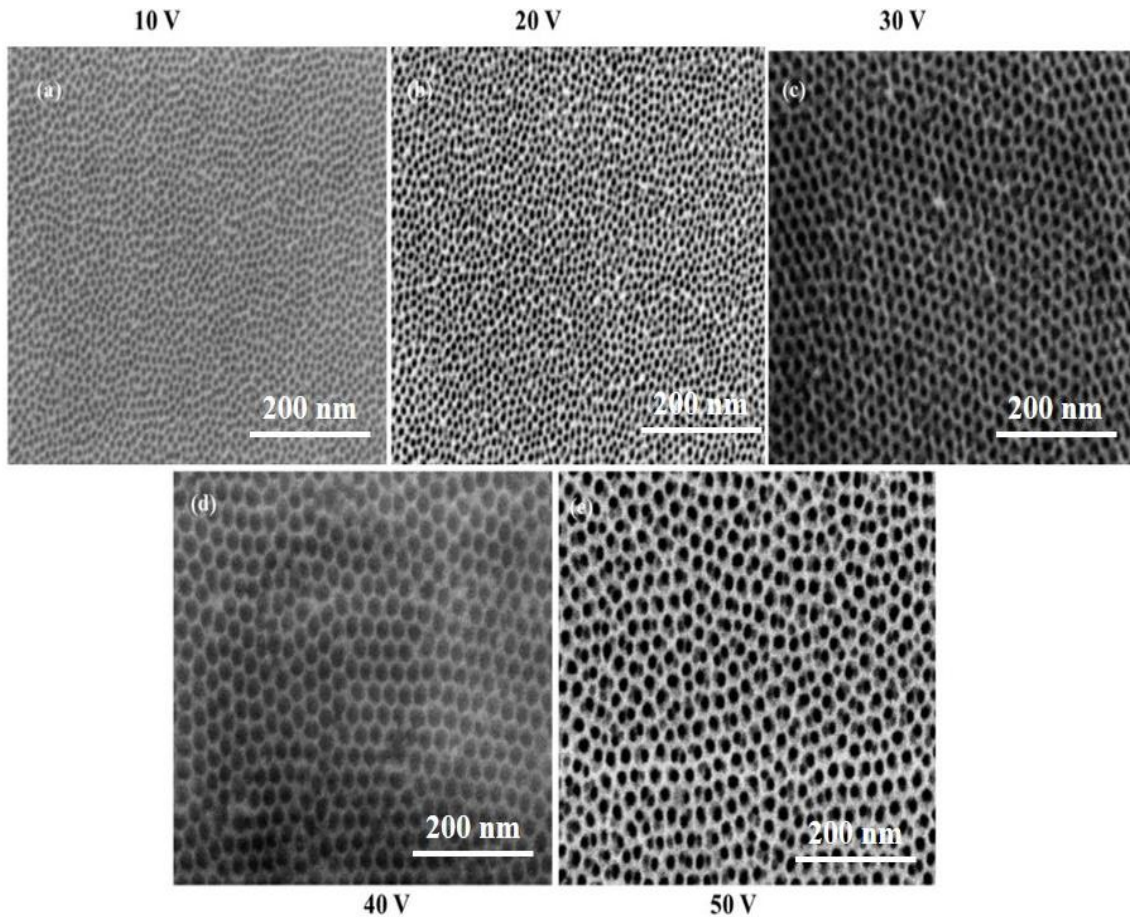


Figure 3.1: Top view SEM images of AAO templates grown at five different voltages.

3.1.2 Electrolyte concentration

Increasing the electrolyte concentration in the anodization process increases the growth in the vertical direction, which in turn increases the self-ordering configuration. Increasing the electrolyte concentration leads to rise in current density. This is attributed to the dissolution of alumina at oxide/electrolyte interface which leads to the formation of vertical pores.

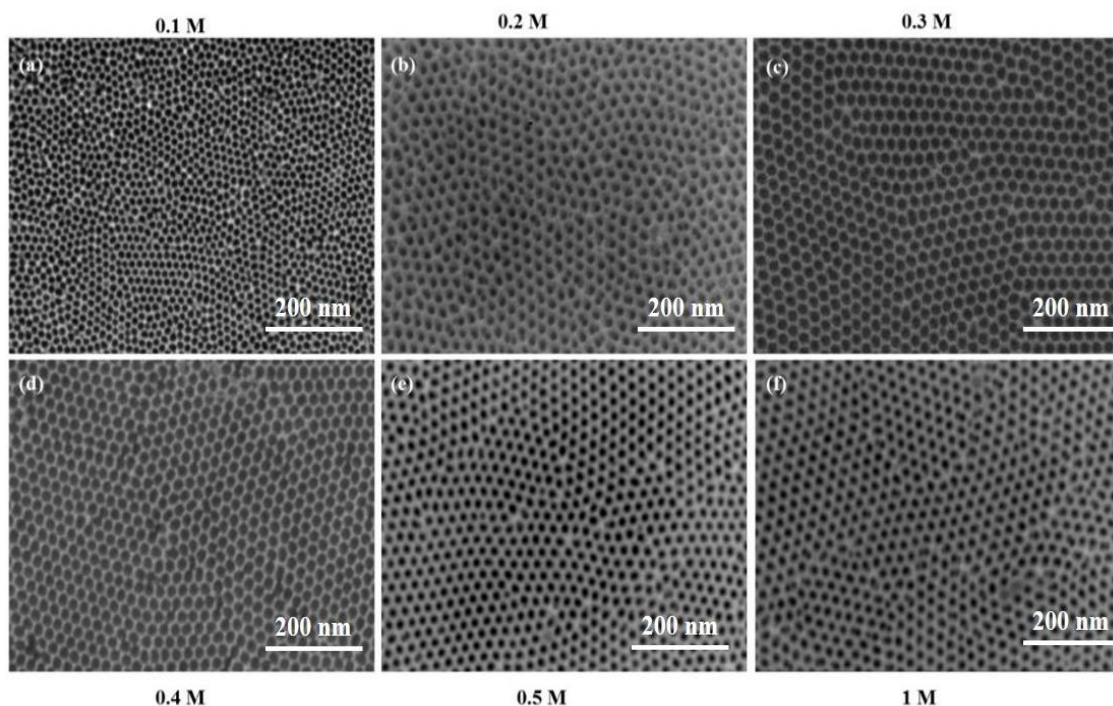


Figure 3.2: Shows the top view SEM image of pore arrays grown using oxalic acid at 18 °C and anodized at different electrolyte concentration (a) 0.1 M, (b) 0.2 M, (c) 0.3 M, (d) 0.4 M, (e) 0.5 M and (f) 1 M

3.1.3 Effect of bath temperature and different concentration of electrolyte.

The electrolyte temperature also influences the oxide dissolution during the anodization process. While doing anodization process for long time duration the etching of pore walls will take place which results in wider pores at top surface of AAO templates than that of bottom surface. Highly ordered hexagonal pore array of the template was obtained for 6 hours anodization duration at 8 °C.

This confirms that highly ordered structures are formed at low temperatures. Figure 3.3 indicates the top view SEM images of AAO templates prepared using oxalic acid as electrolyte at different anodization durations varying from 2 to 10 hours at 8 °C and 18 °C. The experimental results have shown that the electrolyte concentration has a significant effect on the quality of the nano porous arrays. Best self-organized arrays of holes were obtained using 0.3 and 0.4 M oxalic acid.

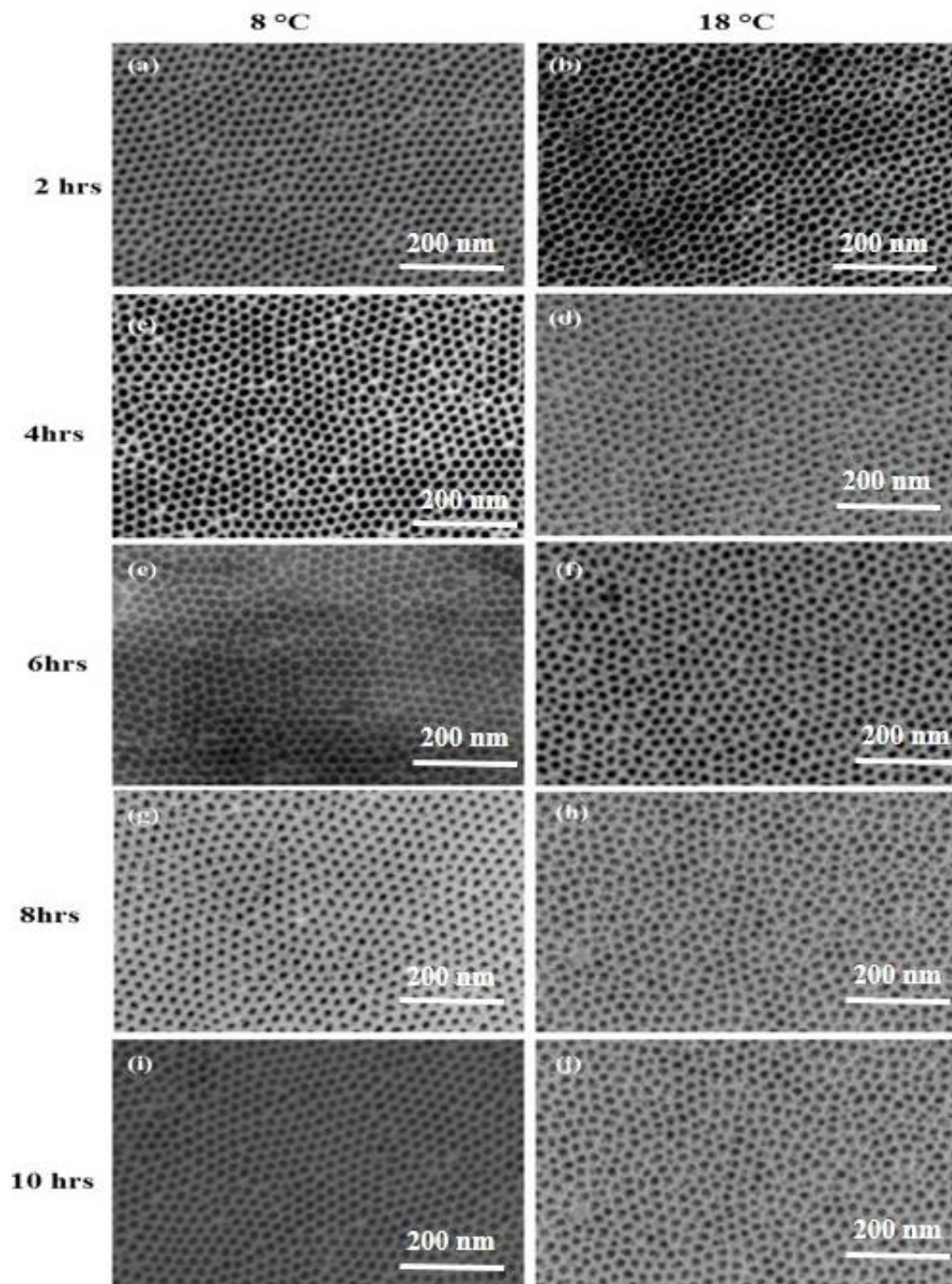


Figure 3.3: Top view SEM images of AAO templates grown at two different bath temperatures and different anodization durations.

From the above experimental results it was concluded that at high voltages and high temperatures the dissolution rate was higher due to enhanced current density. This

causes an increase of local temperature at pore bottom which leads to non-uniform pore distribution due to increased heat dissipation. Pore formation is stable at lower voltages and temperatures [Stepniowski et al. 2013].

3.1.4 Effect of pore widening duration

In order to study the effect of pore widening duration on the properties of AAO templates, AAO templates were prepared by two step anodization process using different electrolytes such as oxalic acid at 40 V, sulphuric acid at 20 V, phosphoric acid at 90 V and chromic acid at 50 V respectively. Pore widening process of AAO templates was carried out in 0.5 M of H_3PO_4 for 15, 30, 45 and 60 min respectively. For the synthesis of AAO templates, high purity aluminium foils (Alfa Aesar 99.99 %, 0.3 mm thickness) were first degreased in acetone (40 min) followed by ultra-sonication (15 min). Subsequently the aluminium foils were annealed in air atmosphere at 500 °C for 4 h and then electropolished at 10 °C in a solution containing perchloric acid and ethanol in a volume ratio of 1:4 at 200mAcm⁻². Anodization process was carried out in 0.3M of oxalic, sulphuric, chromic and phosphoric acids with corresponding anodization potentials as 40 V, 20 V, 50 V and 90 V for 6 h at 18 °C. After the first step anodization, formed aluminium oxide was removed by chemical etching in a mixture of 6 Wt % of H_3PO_4 and 1.8 Wt % of H_2CrO_4 at 60 °C. Immediately after the oxide removal, the second step anodization was done under the same anodizing conditions as those used in the first anodization. Pore widening was performed after the second step anodization using 5 Wt % of H_3PO_4 at different times as 15, 30, 45 and 60 min at room temperature.

Figure 3.4 Shows the representative XRD pattern of the AAO templates with aluminium substrate synthesized using different electrolytes pore widened at 60 min. Results show that the two diffraction peaks (1 1 1) and (3 1 1) belongs to the aluminium with JCPDS data 89 - 2769. The diffraction peak (2 2 0) belongs to Al_2O_3 with JCPDS data 01-1304 [Sulka 2008].

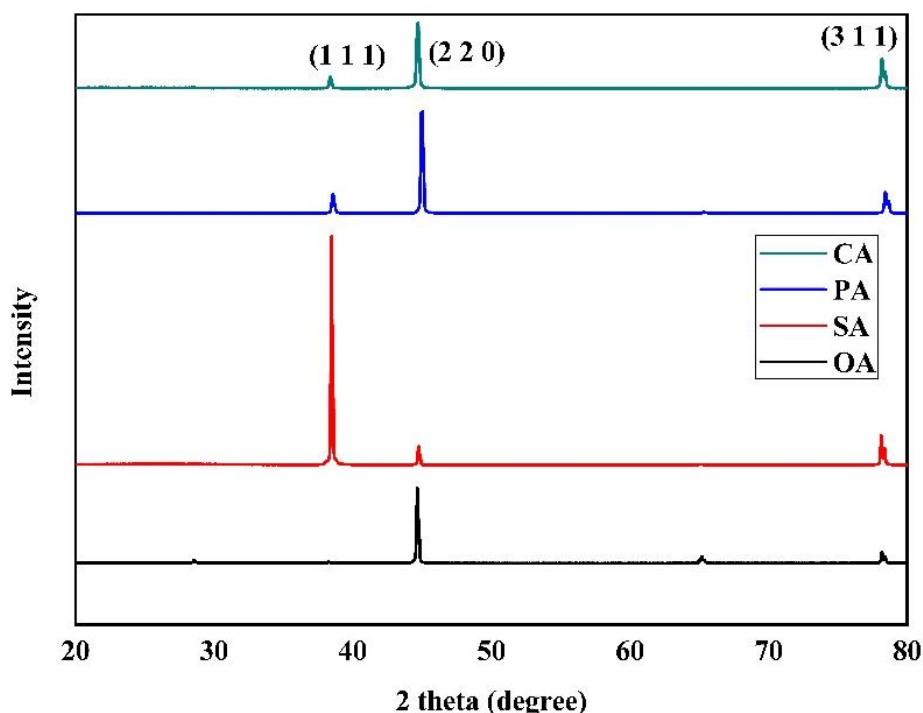


Figure 3.4: XRD pattern of the AAO templates prepared using oxalic acid, sulphuric acid, phosphoric acid and chromic acid and pore widened for 60 min respectively.

During the formation of oxide layer, the ability of electrolyte to sustain the flow of Al^{3+} ions from metal surface plays an important role. The main mechanism that is responsible for the loss of Al_3^+ ions from metal surface is the dissolution of the forming oxide layer. Here it was mentioned that all the AAO templates obtained in different electrolytes provides a similar response under the XRD measurement. But in the case of sulphuric acid the aluminium peak intensity is maximum, because the percentage of incorporation of anion content is more in case of alumina template prepared using sulphuric acid [Sulka 2008]. No sharp diffraction was observed from any particular crystallographic plane of the AAO templates in the XRD analysis. Therefore, it can be concluded that pure AAO templates were non crystalline in nature.

Morphological analysis of AAO templates formed in 0.3 M oxalic acid, sulphuric acid, phosphoric acid and chromic acid and pore widened at various different time durations were shown in Figure 5 (0 min), Figure 6 (15 min), Figure 7 (30 min), Figure 8 (45 min) and Figure 9 (60 min). It was observed that in case of all these electrolytes AAO templates formed at 60 min pore widening duration showing highly

ordered hexagonal structure, when the duration of the pore widening process is extended from 0 min to 60 min.

The analysis includes the top view FESEM images, fast Fourier transforms (FFT) and their radial averages. Firstly, all nanopores in the SEM image were identified by Image-J software to perform in depth inspection on the structural features of as synthesized AAO. Parameters such as circularity, center of mass coordinates were determined for all AAO templates in this step.

FFT analysis of AAO templates is used to obtain information about periodicity of the structure [Reddy et al. 2016]. For the ideal, hexagonal arrangement of porous structure, FFT pattern consists of six distinct points on the edges of a hexagon [Reddy and Udayashankar 2016]. But in case of poor pore arrangement; a narrow ring shape with still visible intense six dots in the FFT pattern can be observed [Sulka and Stepniowski 2009].

AAO templates formed in oxalic and sulphuric acid cases for 30, 45 and 60 min pore widening durations show six distinct points with ring shape, but in case of phosphoric and chromic acids blurred ring shapes of FFT pattern was observed. Pores on the surface formed by different electrolytes are distributed in a regular manner but ordered arrangement of nanopores are rather small and blurred ring in FFT images suggests that the short range periodicity is present in the structure [Stepniowski et al. 2013]. It was noticed from the FFT analysis that, pore widening time plays an important role on the symmetry of pore distributions.

During pore widening process the bottom surface of the template is placed downward direction in H_3PO_4 aqueous solution. Surface tension keeps the template on the top surface and only the bottom layer reacts with the etchant, as the barrier layer dissolves completely the template dips into the etchant solution. Due to this process the whole AAO template obtained with uniform nano channel.

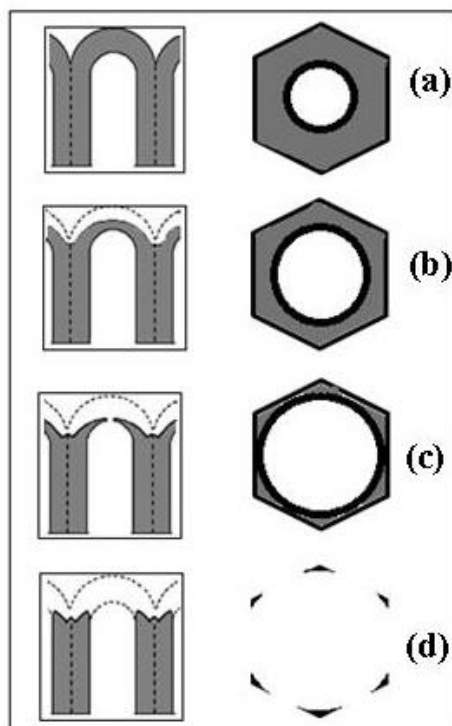


Figure 3.5. Schematic diagram of pore widening process

Based on results a schematic diagram representing oxide layer dissolution and corresponding pore widening curves are presented in Figure 3.5. At beginning of the dissolution process slow thinning of the alumina layer is observed, which is represented as small dots. As the porewidening time increases the oxide layer dissolution also increases [Zhang et al. 2010]. By further increasing pore widening duration the walls of the cell become thinner and the size of the pore enlarges until the walls begin to break at certain locations.

To get a better insight into the pore arrangement, the regularity ratio of nanopore array in AAO templates was quantitatively investigated by using 2D FFT pattern of the FESEM images. FFT images were generated using WSxM software. Regularity ratio was measured as a maximum of the intensity of the radial average profile to the width at the half of the height. Figure(3.6) to figure (3.10) shows the FESEM micrographs (a,d,g,j) together with FFT images (b,e,h,k) and radial average (c,f,i,l) of AAO templates prepared using Oxalic, Sulphuric, Phosphoric and Chromic acids at different pore widening durations.

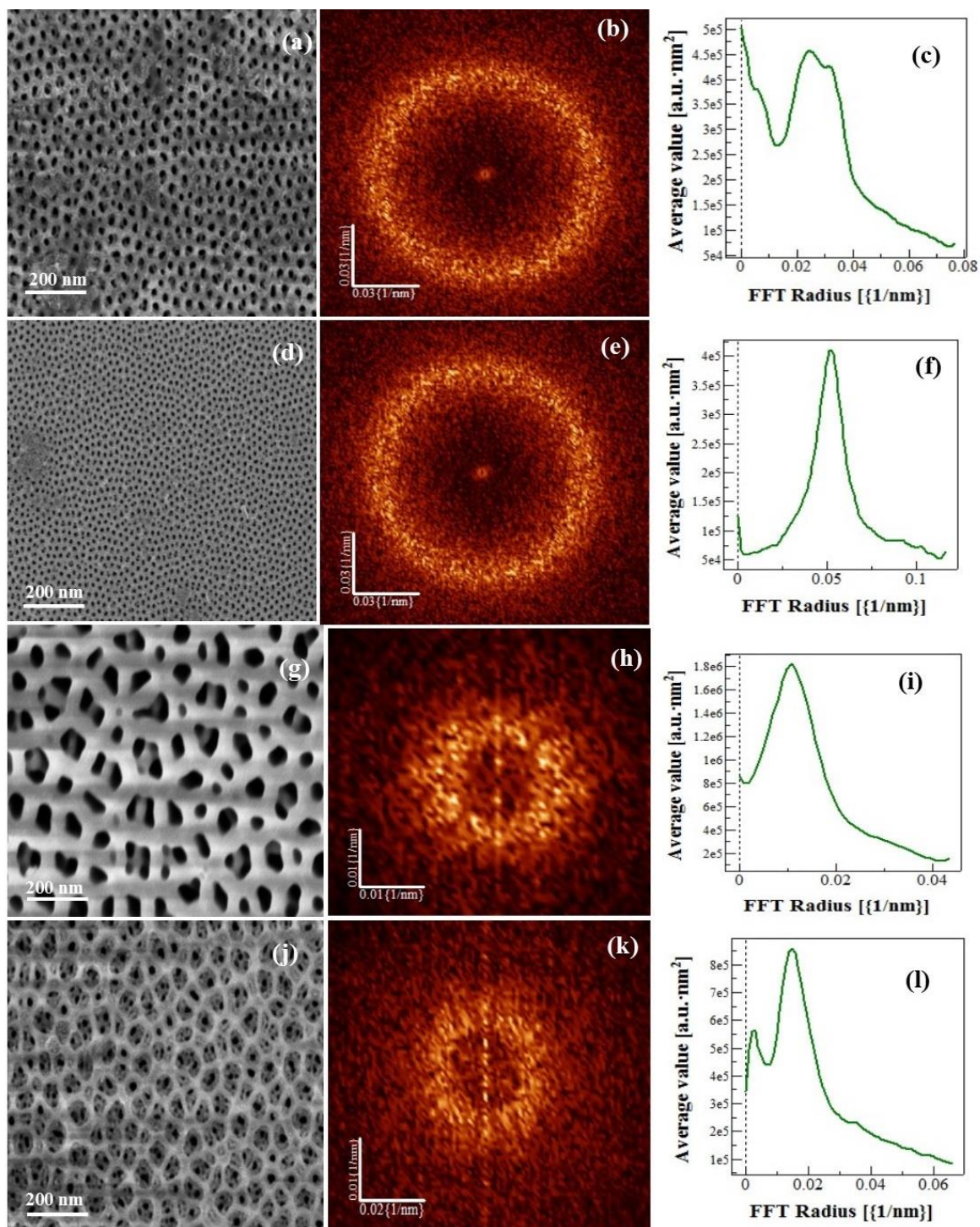


Figure 3.6. FESEM micrographs (a,d,g,j) together with FFT images (b,e,h,k) and radial average (c,f,i,l) of AAO templates prepared using Oxalic, Sulphuric, Phosphoric and Chromic acids and without pore widening.

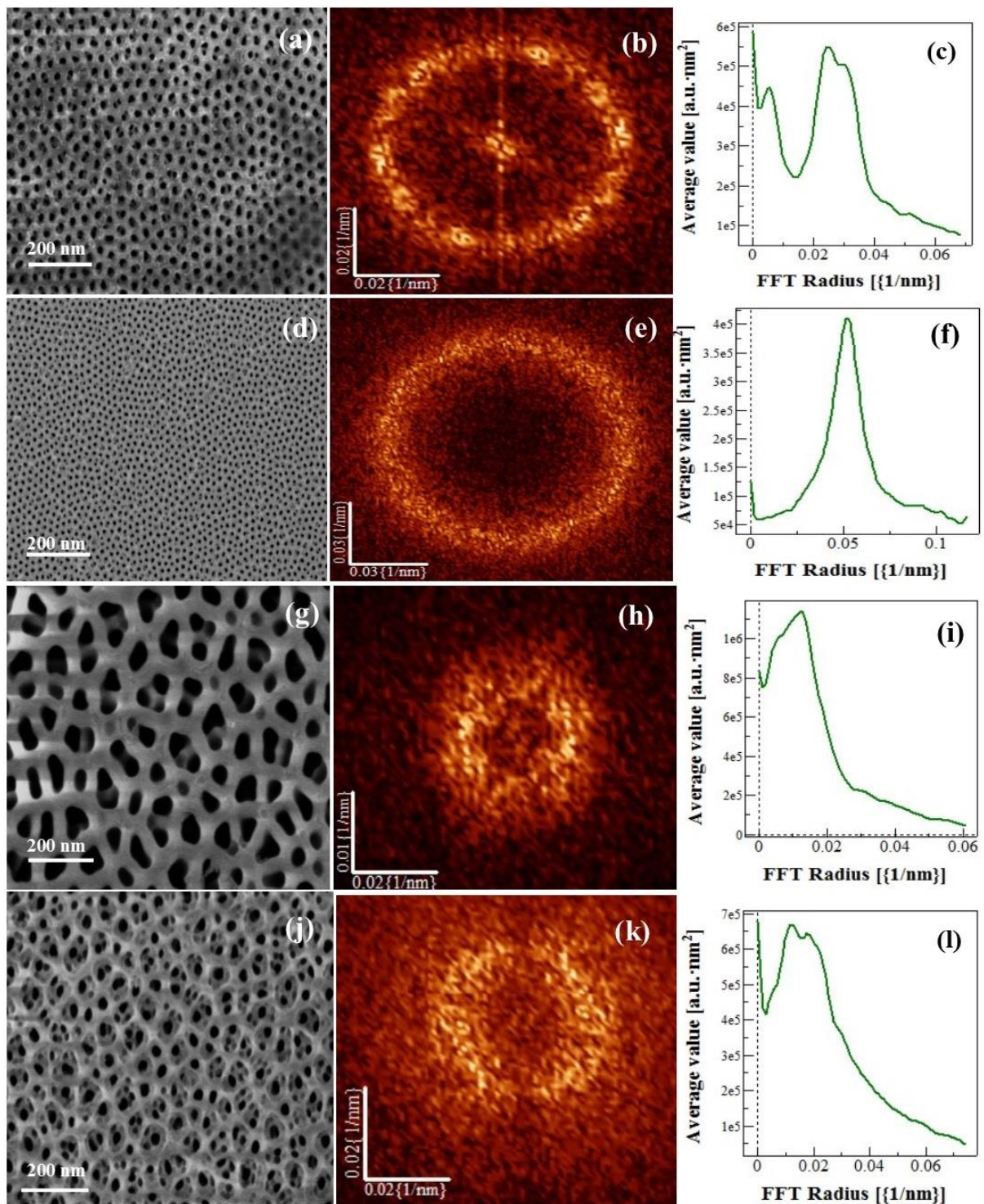


Figure 3.7: FESEM micrographs (a,d,g,j) together with FFT images (b,e,h,k) and radial average (c,f,i,l) of AAO templates prepared using Oxalic, Sulphuric, Phosphoric and Chromic acids and pore widened for 15 min respectively.

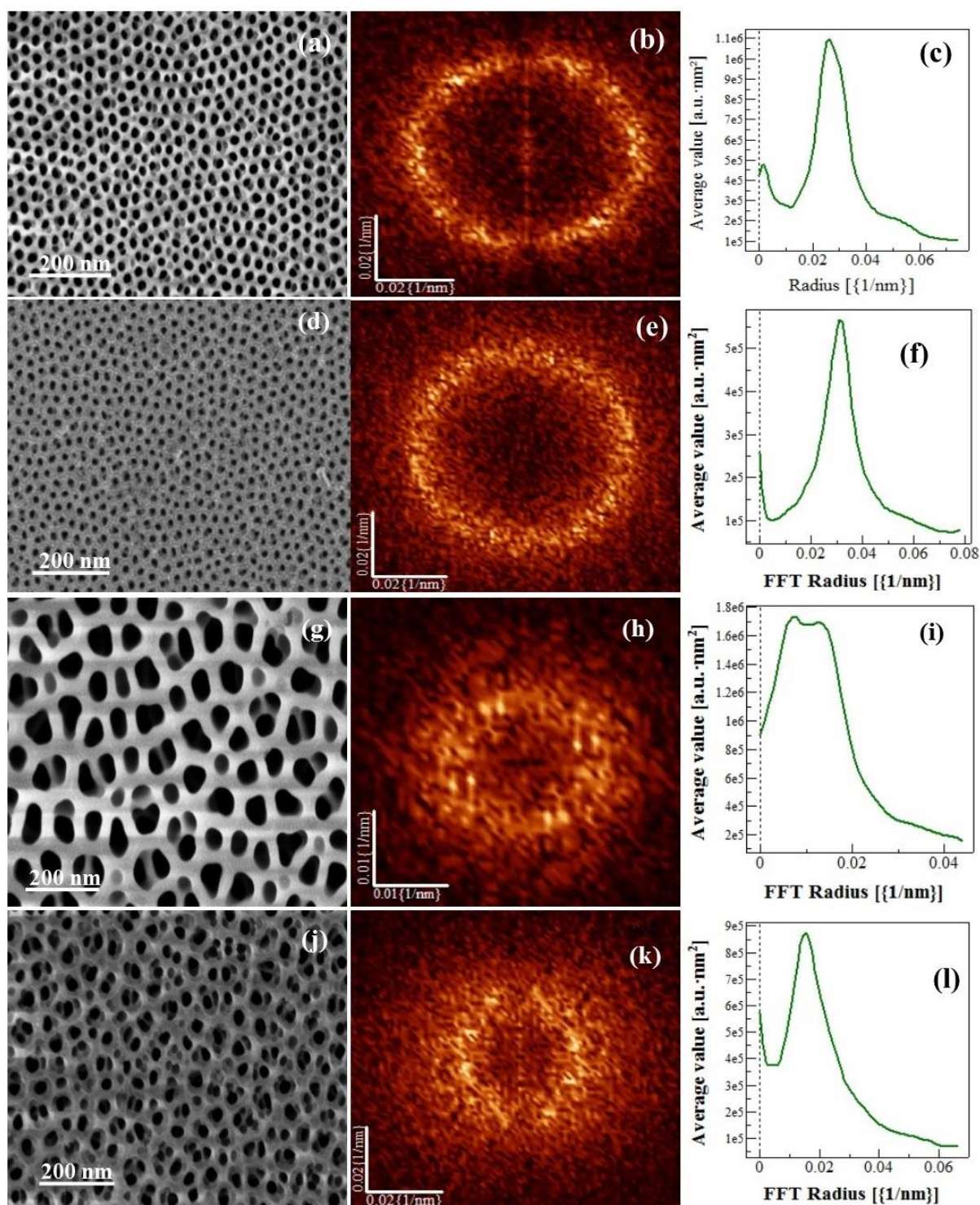


Figure 3.8: FESEM micrographs (a,d,g,j) together with FFT images (b,e,h,k) and radial average (c,f,i,l) of AAO templates prepared using Oxalic, Sulphuric, Phosphoric and Chromic acids and pore widened for 30 min respectively.

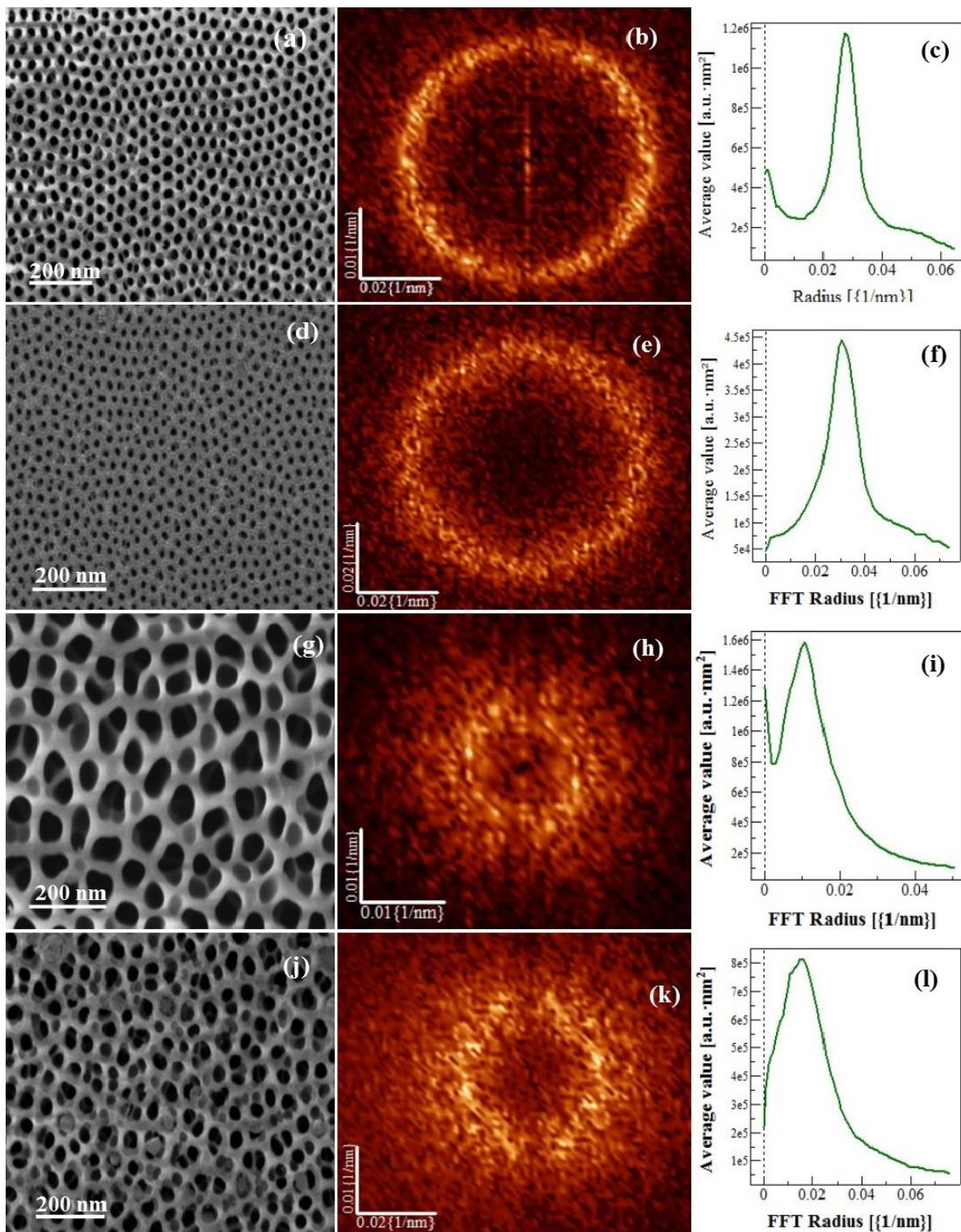


Figure 3.9: FESEM micrographs (a,d,g,j) together with FFT images (b,e,h,k) and radial average (c,f,i,l) of AAO templates prepared using Oxalic, Sulphuric, Phosphoric and Chromic acids and pore widened for 45 min respectively.

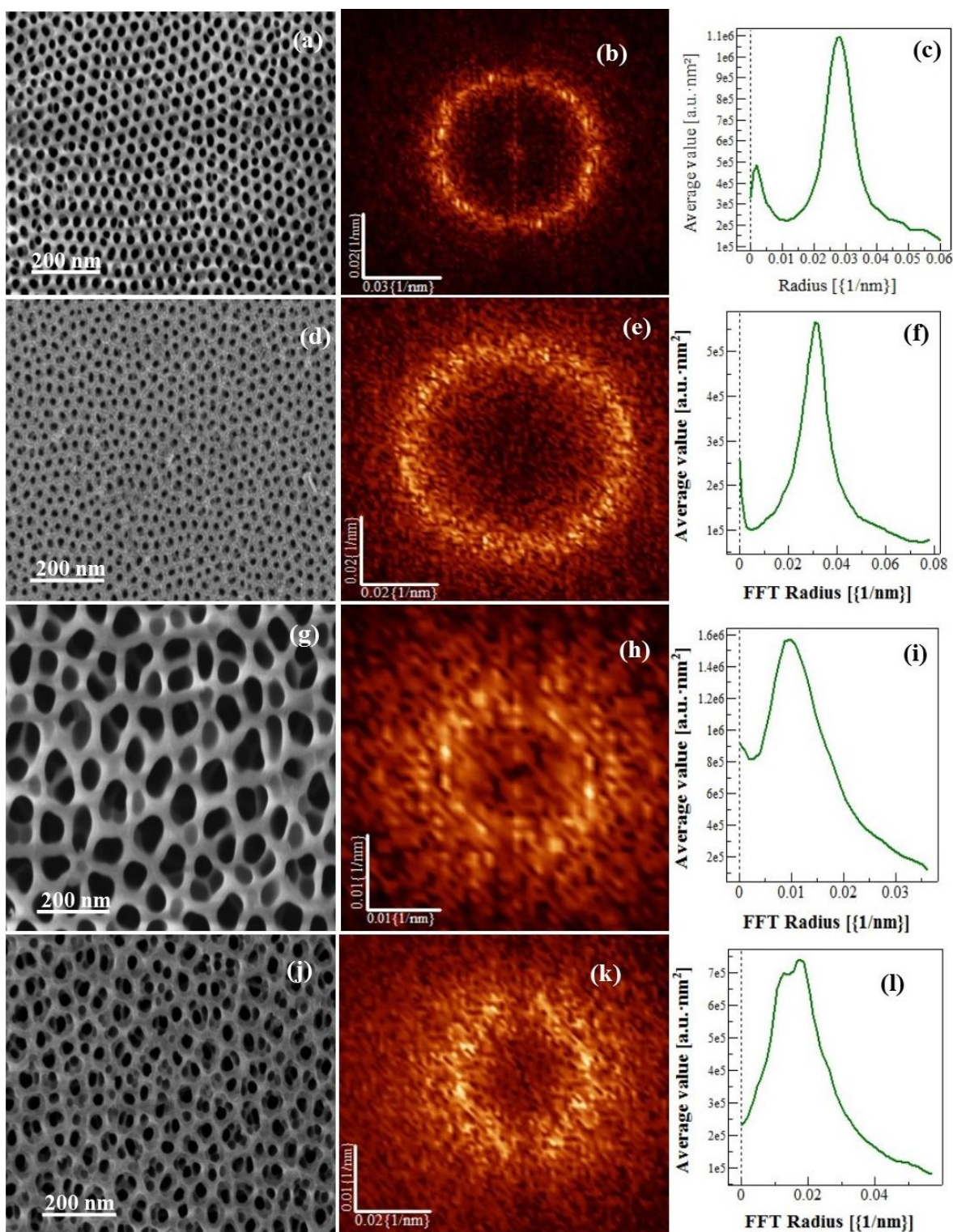


Figure 3.10: FESEM micrographs (a,d,g,j) together with FFT images (b,e,h,k) and radial average (c,f,i,l) of AAO templates prepared using Oxalic, Sulphuric, Phosphoric and Chromic acids and pore widened for 60 min respectively

The periodic arrangement of nanopores in the AAO structure are studied quantitatively by calculating the averaged regularity ratio (R), obtained from the FFT and was measured from the following expression [Stępniewski et al. 2014b].

$$R = \frac{I \sqrt{n}}{W (S)^{\frac{3}{2}}} \quad (3.1)$$

Where I is intensity of the radial average, W is the width of the radial average at half of its height, n is the number of pores on the analyzed image and S is analyzed surface area. The highest value of regularity ratio measured for the AAO structures prepared using oxalic acid as electrolyte was in the range of 1.09-3.02 and the lowest value of regularity ratio was observed in case of chromic acid was in the range 0.31-0.44. In the case of sulphuric acid regularity ratio was in the range of 1.63 to 2.11 and for phosphoric acid case it was 0.85 to 1.35. For all the electrolytes, the lowest values of regularity ratio were for alumina pore widened at 0 min. The regularity ratio increases with pore widening time up to 60 min. The regularity ratios of oxalic, sulphuric, chromic and phosphoric at different pore widening durations were calculated as shown in Figure. 3.11.

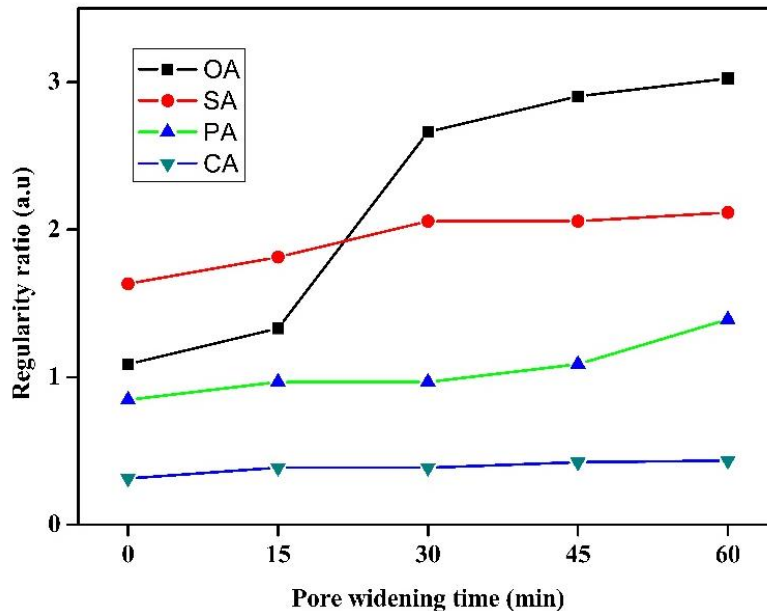


Figure 3.11: Regularity ratio vs. pore widening time for of AAO templates prepared using Oxalic, Sulphuric, phosphoric and Chromic acids and pore widened for 0 min, 15 min, 30 min, 45 min and 60 min.

The highest regularity ratio has been obtained for anodic alumina structures formed at 60 min pore widening time in all electrolytes. It was observed that in case of all the electrolytes AAO structures formed at 60 min pore widening duration showing highly ordered hexagonal structure, when the duration of the pore widening process was extended from 0 min to 60 min.

Structural parameters are calculated using following formulas.

$$\text{Pore Diameter (D}_P\text{)} = k \cdot U \quad (3.2)$$

$$\text{Interpore Distance (D}_i\text{)} = \frac{\sqrt{2\sqrt{3}}}{\pi} D_p \quad (3.3)$$

Where U is applied potential, and k is proportionality constant equal to $k=0.9$ nm/v.

Structural features such as pore diameter (D_p), interpore distance (D_i), porosity (P) and pore density of the samples were calculated for different pore widening durations with respect to different electrolytes and shown in the Figure 3.12 a, b, c, d. The pore parameters are tabulated in table-3.1 (oxalic acid), table-3.2 (sulphuric acid), table-3.3 (phosphoric acid) and table-3.4 (chromic acid) respectively.

From Figure 3.12, it is evident that average size of the pores increases linearly with pore widening time for all electrolytes. Average pore diameter varies with pore widening time (Figure. 3.12a) in oxalic, sulphuric, phosphoric and chromic acid. They are in the range of 30-84 nm, 26-40 nm, 180-195 nm and 287-365 nm respectively. It is evident that average pore diameter of AAO structures varies with the type of electrolyte [Sulka 2008]. The increase in pore diameter is due to dissolution of alumina occurring in the vertical direction during pore widening process. Further the interpore distance was almost constant with pore widening time for different electrolytes (Figure. 3.12b).

The pore wall thinning does not affect the distance between the pores. The measured interpore distances for oxalic, sulfuric, phosphoric and chromic acids were in the range of 92-95 nm, 58-62nm, 359-361 nm and 490-495 nm respectively. Porosity (P) of AAO structures calculated with the following expression [Stępniewski et al. 2014c].

$$P = \frac{\pi D_p^2}{2\sqrt{3} D_i^2} \quad (3.4)$$

Table 31: Structural parameters of AAO templates prepared by oxalic acid with respect to different pore widening time.

Pore widening time (min)	Oxalic acid(0.3 M)					
	Pore diameter (D_P) (nm)	Inter pore distance (D_i) (nm)	Porosity (P) (%)	Pore density (n)	Circularity (C)	Regularity ratio (R)
0	30.68	92.48	25	18.1	0.94	1.09
15	34.56	96.95	39	16.5	0.94	1.33
30	51.66	97.51	41	16.3	0.98	2.66
45	68.42	98.22	44	16.2	1	2.90
60	84.65	103.41	60	14.5	1	3.02

Table 3.2: Structural parameters of AAO templates prepared by sulfuric acid with respect to different pore widening time.

Pore widening time (min)	Sulfuric acid (0.3 M)					
	Pore diameter (D_P) (nm)	Inter pore distance (D_i)(nm)	Porosity (P) (%)	Pore density (n)	Circularity (C)	Regularity ratio (R)
0	26.33	58.34	18	33.9	0.88	1.63
15	32.56	65.44	22	27	0.89	1.81
30	34.37	68.33	23	24.7	0.9	2.05
45	38.33	70.11	27	23.5	0.92	2.05
60	40.3	72.33	28	22.1	0.94	2.11

Table 3.3: Structural parameters of AAO templates prepared by phosphoric acid with respect to different pore widening time.

Pore widening time (min)	Phosphoric acid (0.3 M)					
	Pore diameter (D_p) (nm)	Inter pore distance (D_i) (nm)	Porosity (P) (%)	Pore density (n)	Circularity (C)	Regularity ratio (R)
0	180.44	359.72	21	8.90	0.84	0.85
15	184.43	381.08	21	7.90	0.86	0.97
30	192.11	385.57	22	7.70	0.87	0.97
45	193.68	396.70	22	7.30	0.88	1.09
60	195.59	400.73	22	7.10	0.89	1.39

Table 3.4: Structural parameters of AAO templates prepared by chromic acid with respect to different pore widening time.

Pore widening time (min)	Chromic acid (0.3 M)					
	Pore diameter (D_p) (nm)	Inter pore distance (D_i)(nm)	Porosity (P) (%)	Pore density (n)	Circularity (C)	Regularity ratio (R)
0	287.25	490.16	30	4.8	0.83	0.31
15	306.47	530.42	30	4.1	0.84	0.39
30	327	560.01	31	3.6	0.85	0.39
45	351.62	608.63	31	3.1	0.86	0.42
60	365.35	623.33	31	2.9	0.87	0.44

By increasing the pore widening time the porosity of the AAO structures also increased in case of all electrolytes (Figure. 3.12c). For AAO structures prepared with oxalic acid and sulfuric acid as electrolytes the porosity increased from 2.5 to 6% and 1.8 to 2.8% with pore widening time respectively. But in phosphoric 2.0 to 2.1% acid and chromic acid 3.0 to 3.15% porosity is almost constant because inter pore distance is high in these cases.

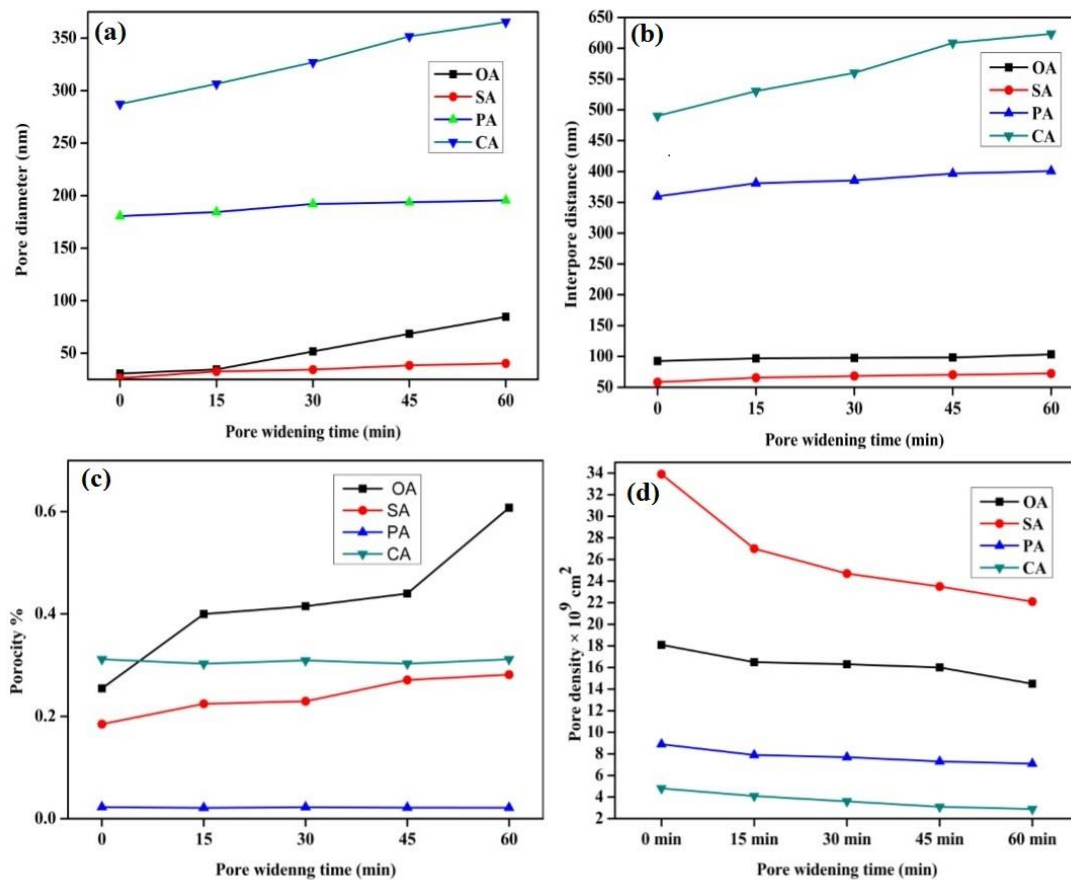


Figure 3.12: Variation of (a) pore diameter, (b) Inter pore distance, (c) Porosity and (d) Pore density with respect to different pore widening time of AAO templates prepared using Oxalic, Sulphuric, phosphoric and Chromic acids.

It may be noted that for perfect honey comb structure of pore arrangement in AAO structures have porosity of about 10% [Gopal Khan et al. 2013] was observed. Hence in case of template prepared by oxalic acid ordered pore structure with high porosity was observed. The pore density is defined as the number of pores occupied in

the unit surface area and is calculated by the following equation [Routkevitch et al. 1996].

$$n = \frac{2 \times 10^{14}}{\sqrt{3} \times Di^2} \quad (3.5)$$

From Figure. 3.12d, it was noticed that pore density is almost constant with increase in pore widening time. Since the variation of interpore distance is stable corresponding pore density is also constant with respect to pore widening duration for all electrolytes [Stepniowski and Bojar 2011]. The estimated values of pore density for different pore widening process in oxalic, sulphuric, Phosphoric and chromic acid are in the range of $18.1-17.2 \times 10^9 \text{cm}^{-2}$, $33.9-31.1 \times 10^9 \text{cm}^{-2}$, $8.9-7.2 \times 10^9 \text{cm}^{-2}$ and $4.8-2.9 \times 10^9 \text{cm}^{-2}$ respectively. Pore shape was analyzed by calculating a circularity coefficient and is defined as [Stepniowski et al. 2013].

$$\text{Circularity} = 4\pi \frac{S}{\text{Perimeter}^2} \quad (3.6)$$

Where S is the surface area occupied by the pore. The circularity value near to 0 indicates that the pore is similar to polygon shape, and the value 1 indicates pore is ideally circular. The average circularity coefficients calculated for AAO structures were shown in Figure 3.13.

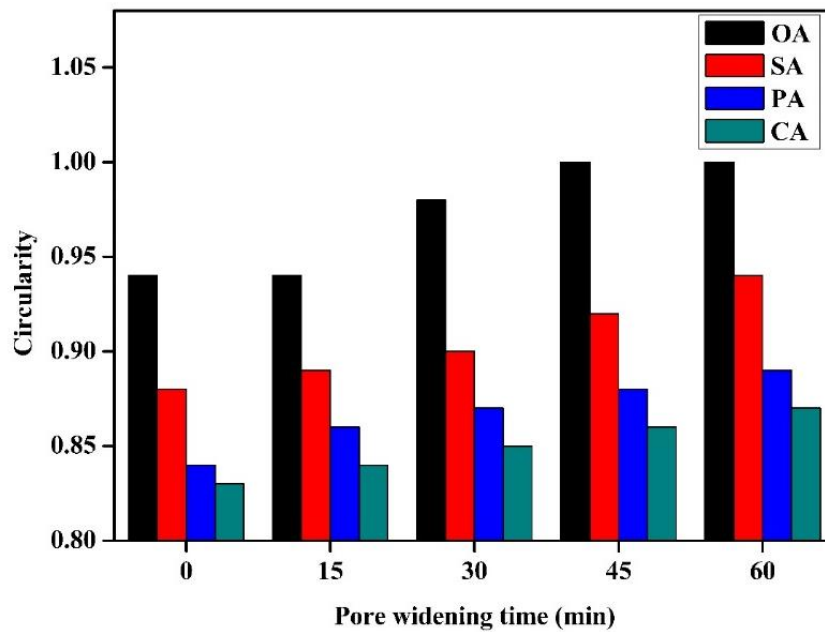


Figure 3.13: Circularity vs. pore widening time for of AAO templates prepared using Oxalic, Sulphuric, phosphoric and Chromic acids and pore widened for 0 min, 15 min, 30 min, 45 min and 60 min.

The uniformity of the surface pore structure can be investigated by the analysis of pore circularity [Li et al. 2005]. As can be seen in Figure 3.13, circularity coefficients increase with pore widening duration in case of all electrolytes. In oxalic acid, the maximum pore circularity was observed for pore widening carried out at 60 min compared with other electrolytes. Moreover, on increasing the pore widening time from 0 min to 60 min, the pore circularity increases because the amount of etching of aluminum oxide at the oxide-electrolyte interface was increased [Stepniowski et al. 2014c].

3.2 Optimum conditions for template preparation

Porous anodic alumina templates with hexagonally ordered nanopore arrays was prepared using a two-step anodization of Al in an electrolyte using 0.3 M oxalic acid. Figure 15 and figure 16 show the surface morphology of the porous template with top and cross-sectional view.

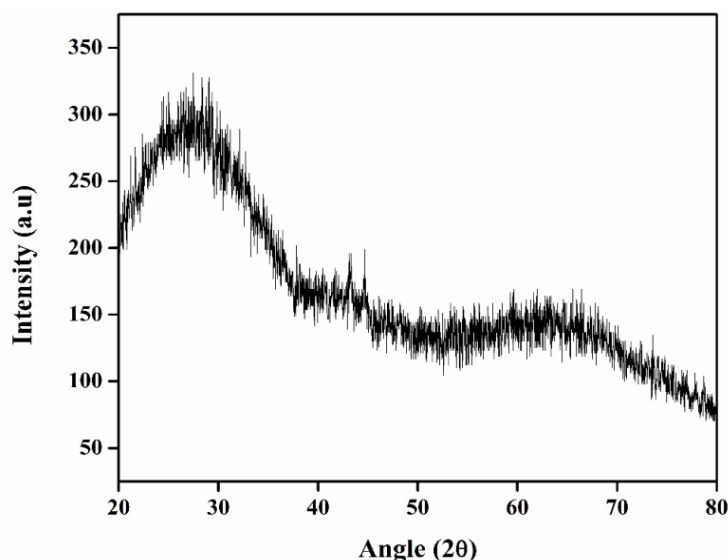


Figure 3.14. XRD pattern of the AAO template prepared using 0.3 M oxalic acid.

XRD pattern of the AAO template prepared using 0.3 M oxalic acid is shown in figure 3.14. Cross sectional image of the AAO template was shown in Figure 16. From Figure 16, it was observed that AAO layer thickness~ 100 nm.

For oxalic acid electrolyte, the pore diameter was around 40 nm when anodized at 40 V, and then it can be tuned to till 80 nm by the pore widening process as described in section 3.2.4, Figure 3.5 show the process of pore wall layer removal at different etching time. Moreover, while comparing the pore geometry with the samples prepared using oxalic acid electrolyte, we observed that the highly ordered structures were observed.

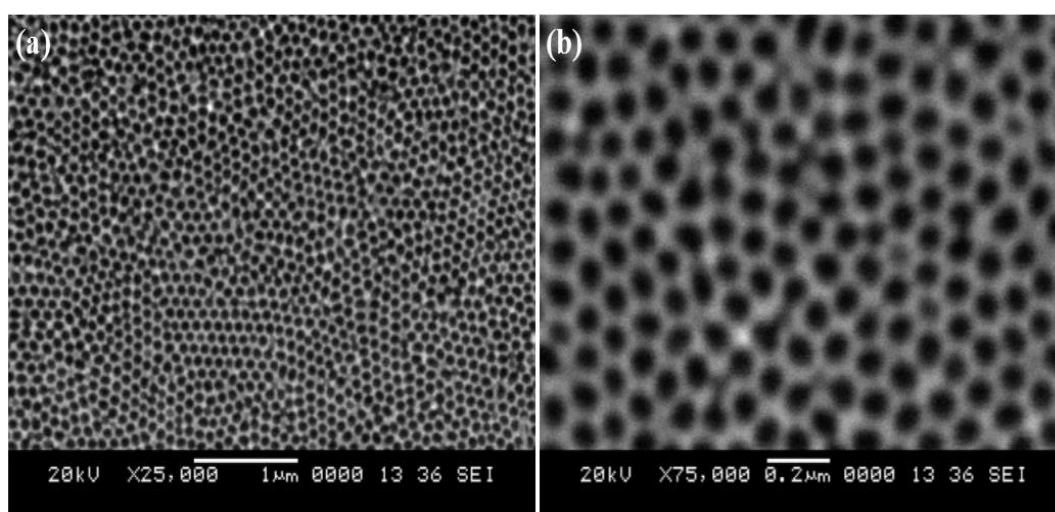


Figure 3.15. SEM images of AAO templates fabricated using 0.3 M oxalic acid

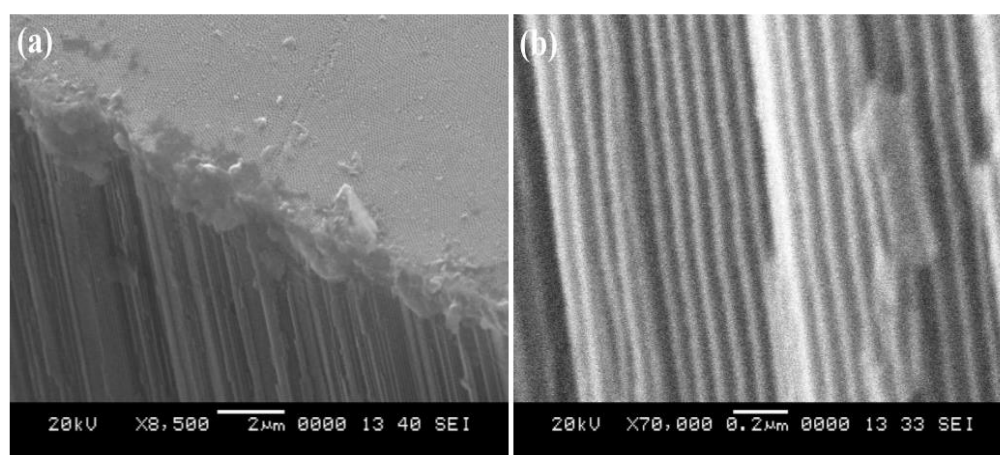


Figure 3.16: Cross sectional view of AAO templates fabricated using 0.3 M oxalic acid

Table 3.5 shows the optimum conditions for the growth of anodic aluminium oxide templates using different electrolytes and they are pore widened for 60 min pore

widening duration. Structural studies show that AAO templates were amorphous in nature which confirmed that the prepared templates are purely aluminium oxide templates.

Table 3.5: Optimum conditions for self-ordered AAO template.

	Electrolyte			
	Oxalic acid	Sulfuric acid	Phosphoric acid	Chromic acid
Applied voltage	40 V	20 V	90 V	60 V
Bath temperature	8 °C	8 °C	8 °C	8 °C
Electrolyte concentration	0.3M	0.3M	0.3M	0.3M
Pre cleaning 1 st step	30 min	30 min	30 min	30 min
Chemical etching 2 nd step	12 hrs	12 hrs	12 hrs	12 hrs
Al Removal	60 min at 60 °C	30 min at 60 °C	60 min at 60 °C	60 min at 60 °C
	6 hrs	6 hrs	6 hrs	6 hrs
	45 min at RT	45 min at RT	45 min at RT	45 min at RT
Porewidening duration	60 min	60 min.	60 min	60 min
Pore Diameter	80-85 nm	25-35 nm	190-1950 nm	360-366 nm
Interpore distance	94-95 nm	60-62 nm	360-361 nm	492-495 nm

Conclusions

From above results it could be inferred that, the anodization of aluminium is one of the inexpensive electro-chemical self-assembly processes to develop highly ordered nanoporous templates. These templates with their cylindrical pore geometry can be used for the fabrication of nanostructures and nano-scale devices. Increasing electrolyte concentration also shows the changes in pore dimensions from 0.1 to 0.3 M in oxalic acid. This can be attributed to growth rate and volume expansion of aluminium oxide that increases with increasing electrolyte concentration. The nanopore regularity was assessed based on the FFT images using WSxM software. From the FFT analysis, it

was revealed that the better nanopore arrangement was possible for optimal anodization duration of 6h and electrolyte concentration of 0.3 M in oxalic acid.

Further AAO templates might be used for different applications including synthesis of nanostructures such as nanotubes, nanofibers, nanorods and nanowires with distinct sizes. It was shown that the conditions for the growth of porous anodic aluminium oxide templates for the synthesis of nanostructures were optimized. Templating using porous anodic alumina is the efficient approach for ordered array of nanostructures with high surface area. The high surface area of these nanostructures has well-known optical and photocatalytic applications.

CHAPTER 4

***SYNTHESIS AND CHARACTERIZATION OF
GRAPHITIC CARBON NITRIDE
NANOSTRUCTURES USING POROUS ANODIC
ALUMINA TEMPLATES***

Chapter 4

SYNTHESIS AND CHARACTERIZATION OF GRAPHITIC CARBON NITRIDE NANOSTRUCTURES USING POROUS ANODIC ALUMINA TEMPLATES

Overview

In the present chapter, we discussed the preparation of Graphitic carbon nitride (GCN) nanostructures using porous anodic aluminium oxide membranes as templates through thermal condensation process. The structural, morphological, thermal and optical properties of the prepared nanostructures were investigated. Further the properties of these nanostructures were compared with the corresponding bulk samples.

It was well known that nanostructured materials possess unique structural, optical, electronic and chemical properties. These properties are different from those of bulk structures. The physical properties of these nanostructures are influenced by their morphology and dimensions like diameter and length of the nanostructures [Huang and Lin 2012] [Wang et al. 2012]. One dimensional nanostructures such as nanowires, nanotubes were quite routinely synthesized using templates [Li et al. 2011]. Nano tube-like materials have attracted extensive consideration because of their specific properties and promising applications in opto-electronic devices, photo catalysis, electro catalysis, separation, and electrochemical sensors. In recent times, a number of methods have been established to synthesize new tube-like materials such as hydrothermal, solvothermal, self-organisation, surfactant-based synthesis, and template assisted synthesis. Compared to all other methods, template-assisted synthesis is most widely used for preparing a variety of nanomaterials[Wang et al. 2015].

Porous anodic aluminum oxide (AAO) templates are widely used as hard templates for the preparation of nanostructures because templates have a well-ordered closely packed group of hexagonal cells with circular pores [Chen and Chen 2012]. They are well organised systems for the synthesis of high surface area nanostructures (nanotubes and nanowires). The nano tube and nano wire length and diameter can be

changed by varying the thickness and diameter of the AAO templates [Lillo and Losic 2009]. In case of template assisted synthesis of nano materials the structure of the synthesized nanomaterials can be easily tailored by varying the processing parameters hence we can prepare the desired nanostructures [Che et al. 1998]. However the removal of alumina backing is difficult task and also chemical etchants used for the removal of alumina can cause minor damages to the synthesized nanostructures.

GCN nanostructures are widely used in case of metal free visible light driven photocatalysis, photodegradation of organic pollutants, electrocatalysis, photo electric conversion, CO₂ activation [Huang et al. 2002], water splitting [Wang et al. 2012]. In this paper, we used AAO membranes as templates to synthesis of Graphitic carbon nitride nanotubes by thermal condensation of cyanamide into the nanopores of AAO templates. One dimensional nanostructures such as nanowires nanotubes nanorods nanobelts nanofibers etc have gathered massive attention due to their applications in many fields [Kolmakov et al. 2005] [Wang et al. 2008].

GCN is an excellent material with major application as a catalyst for degradation of organic pollutants, hydrogen storage material, and electrode for fuel cells [Algara-Siller et al. 2014] [Barton et al. 1999]. There are many methods to prepare GCN like sol-gel, solvothermal method, thermal condensation of nitrogen rich precursors and pyrolysis. [Cheng et al. 2013] [Kiskan et al. 2012] [Mousavi and Habibi-Yangjeh 2016] [Shi et al. 2014]. Fabrication of one dimensional graphitic carbon nitride is still a challenging task because its self-assembly is difficult [Xiong et al. 2015]. There are comparatively less reports on the synthesis of one dimensional nanostructures like fibers, rods tubes and wires using thermal condensation method. Some of the research groups used soft or hard templates to synthesize one dimensional Graphitic carbon nitride nanostructures [Cao and Liu 2008].

The good catalyst must have low electron-hole pair recombination rate [Zhu et al. 2014] maximum surface to volume ratio and high mass diffusion properties [Jiang et al. 2015]. In this respect nanostructured materials show good photocatalytic performance compared to bulk materials. There are different methods to synthesize nanostructured materials and among them template based synthesis of GCN nanostructures seems to be very versatile method [Martin 1995]. Templating is

alternative method to increase the crystallinity [Martin 1996] which results in good photocatalytic performance of the material. Therefore, we synthesized graphitic carbon nitride nanofibers by making use of advantage of the AAO template for size dependent photocatalyst [Yan et al. 2010] [Zhou et al. 2011].

4.1 Results and discussion

4.1.1 Structural analysis

X-ray diffraction (XRD) was conducted to identify phase and structural characterizations of bulk GCN and GCNNF as shown in Figure 4.1 (a) and Figure 4.1 (b) respectively.

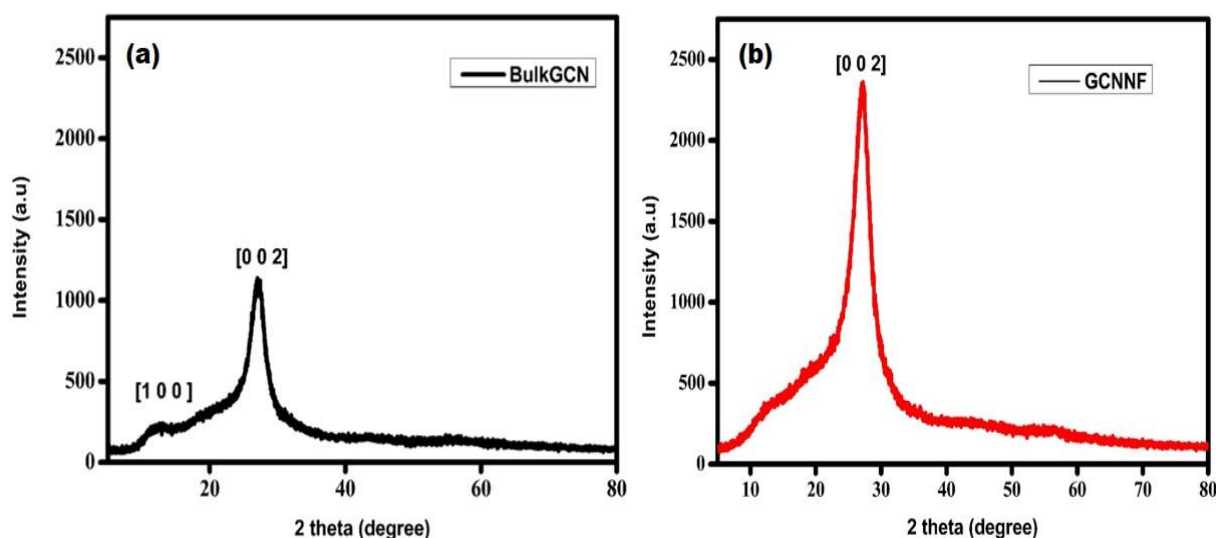


Figure 4.1: XRD pattern of (a) bulk GCN and (b) GCN nanofibers.

There are two distinct diffraction peaks for GCN at 13.1° and 27.3° . The low-angle reflection peak at 13.1° was identified as (100) corresponding to $d = 0.676$ nm resulting from the nitrogen linkage of tri-s-triazine units. A strong peak at 27.3° corresponds to $d = 0.326$ nm [Tahir et al. 2013] due to long range interplanar stacking of aromatic systems recognized as (002). These two XRD peaks are in good agreement with reported GCN. There is only one peak for GCNNF at 27.3° that corresponds to a distance $d = 0.326$ nm due to long-range interplanar stacking of aromatic systems recognized as the (002) [Gao et al. 2012].

4.1.2 Morphological analysis

A Fast Fourier scanning electron microscope (FESEM) is used to investigate the textural structure and morphology of GCN nanostructures and is shown in Figure 4.2. Figure 4.2(a) shows the typical FESEM images of the bulk GCN sample. From these SEM images it is clear that bulk GCN sample shows quite irregular morphology with small flakes and large agglomerations.

From Figure 4.2 (b) we can observe that GCNNF grow in fibrous morphology having very dense and uniform structure with an average diameter of 100 nm and 20 μm in length. The length and diameter of the grown GCNNF are almost same as that of the AAO template.

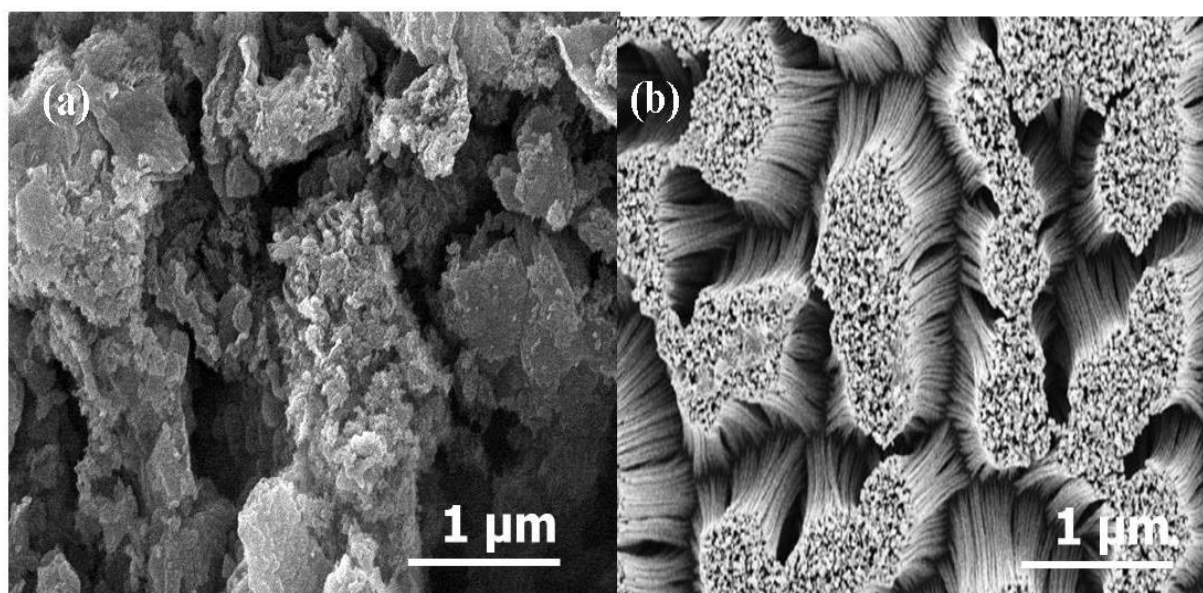


Figure 4.2: SEM images of (a) bulk GCN and (b) GCN nanofibers.

4.1.3 Optical properties

(i) UV-Visible Spectroscopy

The optical properties of bulk GCN and GCNNF were studied using UV-Visible spectrophotometer measurements at room temperature as a function of wavelength.

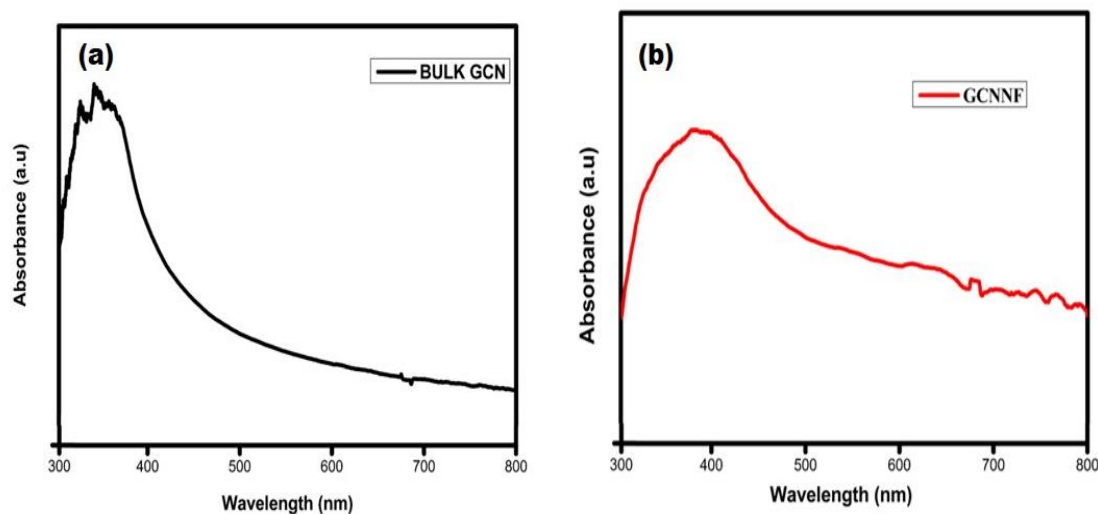


Figure 4.3: UV-Visible spectra of (a) bulk GCN and (b) GCN nanofibers.

The optical characteristics like absorption coefficient and bandgap are important parameters for photocatalysts. So, we measured the optical bandgap and absorption coefficient using the absorbance data.

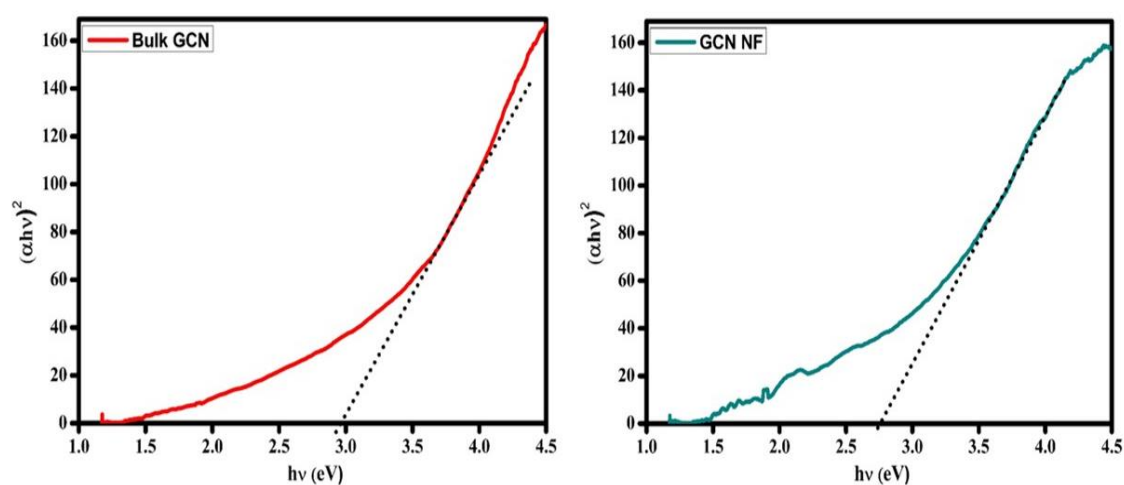


Figure 4.4: Tauc's plot of (a) bulk GCN and (b) GCN nanofibers.

The UV-vis diffuse reflectance spectrum of bulk GCN and GCNNF features typical semiconductor like absorption which can be seen in Figure 4.3 and corresponding Tauc's plot is shown in figure 4.4. From these results it was noticed that Bulk GCN has a band edge at 385 nm corresponding to 2.97 eV, while GCNNF has a band edge at 400 nm corresponding to a bandgap at 2.40 eV indicating a slight blue shift by 0.57 eV compared to bulk GCN. This is due to a more perfect packing,

electronic coupling, and quantum confinement effect that shifts conduction and valence band edges.

(ii) Photoluminescence properties

Figure 4.5 shows the photoluminescence emission spectra for bulk GCN and GCNNF. The PL emission peak for bulk GCN shows a strong peak at 430 nm, whereas for GCNNF an emission peak is observed at 380 nm as shown in Figure 4.5(b). Both peaks are coherent with their bandgap measurements of the respective GCN and GCNNF products. It belongs to a blue-violet light band that indicates the existence of the π state in GCNNF [Ong et al. 2015]. The larger bandgap by 0.57 eV of the GCNNF is also confirmed by PL. From Figure 4.5(a,b) it is also proved that PL intensity of bulk GCN is high in comparison to that of GCNNF which indicates the slow recombination rate of photogenerated electrons and holes. The decrease of PL intensity is because of the defects in crystal structure which reduce the strength of fluorescence peaks. These defects are the recombination centres for electrons and holes generated during photocatalysis. Therefore, a decrease in the number of defects in GCNNF ultimately increases its photocatalytic performance[Yuan et al. 2015].

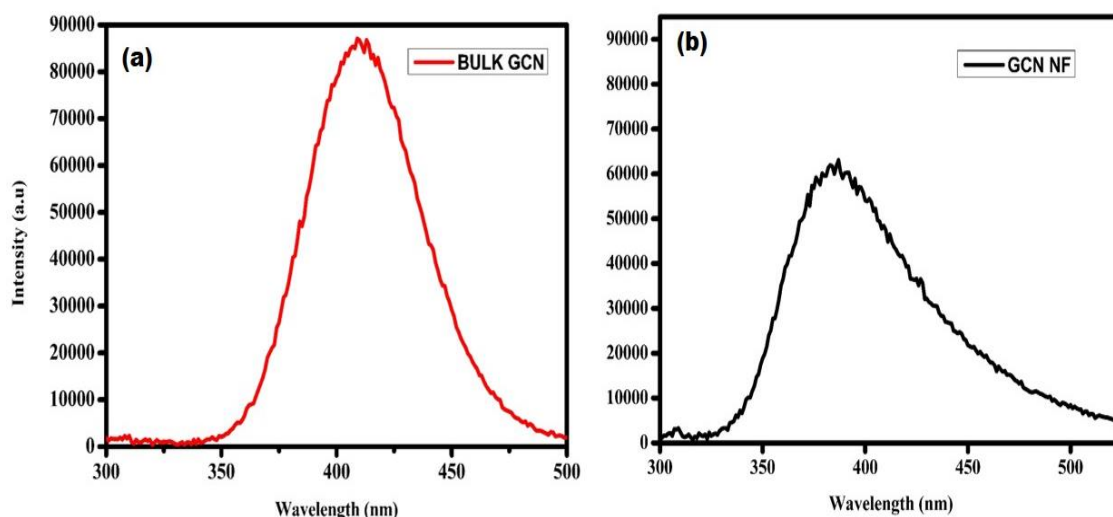


Figure 4.5: Photoluminescence spectra of (a) bulk GCN and (b) GCN nanofibers.

4.1.4 FTIR Spectroscopy

Fourier transform infrared spectroscopy (FTIR) was utilized to characterize the chemical bonds present in bulk GCN and GCNNF.

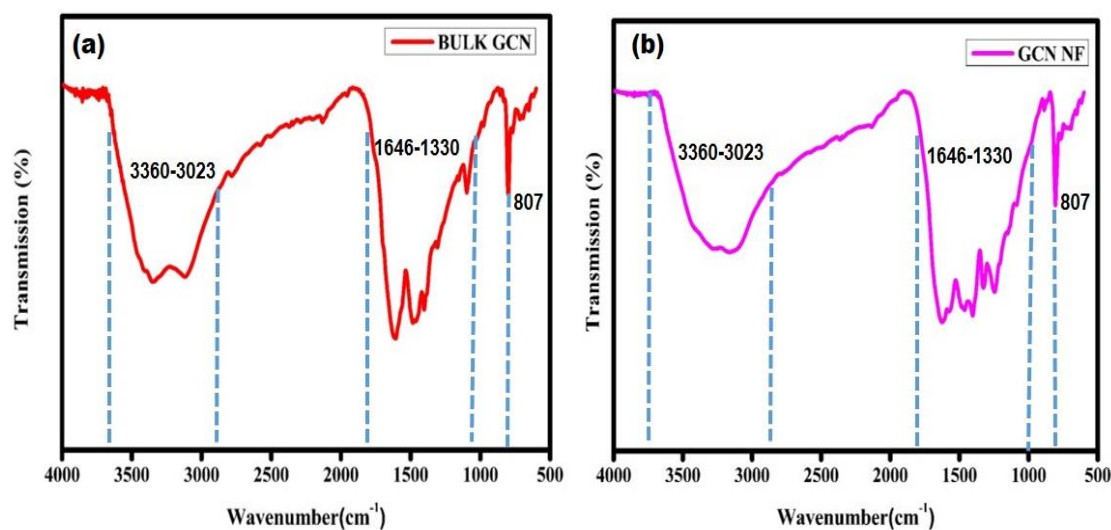


Figure 4.6: FTIR spectra of (a) bulk GCN and (b) GCN nanofibers.

Figure 4.6 shows the FTIR spectra of bulk GCN and GCNNF which confirm the presence of two main bands in the products. The absorption peaks which range from 800 to 1670 cm^{-1} are strong indications of the heterocycles present in GCN, and these peaks are due to the breathing mode of striazine, sp^3 C-N bonds, and sp^2 C=N.

Furthermore, these results are consistent with XRD results of GCNNF. The peaks arising from the stretching vibration modes of NH and NH_2 groups are observed in the range of 3000–3300 cm^{-1} in both samples. In fact, a small difference in the intensity of the peaks can be observed between bulk GCN and GCNNF samples, as the NH_2 groups of nitrogen rich precursors actually decompose toward the formation of g- C_3N_4 networks.

4.1.5 Thermal Properties

It is known that upon heating, nitrogen rich precursors undergo condensation reactions with elimination of ammonia (deamination). Therefore, a thermal analysis of GCN samples was necessary in order to investigate the changes in physical and chemical state in relation to the rising temperature. The results of TGA measurements were shown in Figure 4.7.

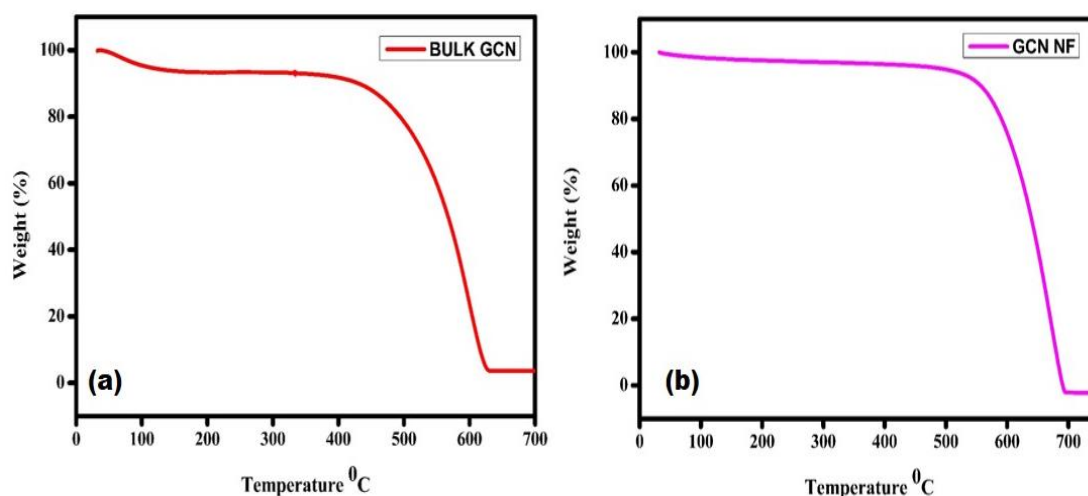


Figure 4.7: TGA curve of (a) bulk GCN and (b) GCN nanofibers.

Thermo gravimetric analysis (TGA) in general measures the changes in mass of a substance as function of temperature. In our experiment, the TG curve shows a large step from 400 °C to 590 °C and from 500 °C to 700°C in case of bulk GCN and GCNNF respectively. This step represent the volatilization of ammonia and consequently the loss of total mass. The results shows that the mass yield of bulk GCN sample is lower than GCNNF. Comparatively GCNNF sample is thermally more stable than the bulk GCN. The photocatalytic properties of bulk GCN and GCNNF samples for the degradation of different dyes using visible light are discussed in chapter 6.

Conclusions

From the above studies it was concluded that GCN nanostructures are crystalline in nature. SEM morphology reveals that sample is made up of array of nanofibers aligned nearly parallel to each other. The nanofibers were 60-80 nm in diameter and 50-70 μm in length. The optical absorption band was observed in the range 230-630 nm, which is typically observed for nitrogen rich carbon nitride material based systems. From absorption studies, we noticed that Bulk GCN has a band edge at 385 nm corresponding to 2.97 eV, while GCNNF has a band edge at 400 nm corresponding to a bandgap at 2.40 eV indicating a slight blue shift by 0.57 eV compared to bulk GCN. PL intensity of bulk GCN is high in comparison to that of GCNNF which indicates the slow recombination rate of photogenerated electrons and holes in case of GCNNF. Difference in the intensity of the FTIR peaks can be observed between bulk GCN and

GCNNF samples, as the NH_2 groups of nitrogen rich precursors actually decompose toward the formation of g- C_3N_4 networks in case of GCNNF samples. TGA results shows that the mass yield of bulk GCN sample is lower than that of GCNNF. In addition to these GCNNF sample is thermally more stable as compared to the bulk GCN.

CHAPTER 5

***TEMPERATURE DEPENDENT STUDIES ON
TAILORED GRAPHITIC CARBON NITRIDE
NANOSTRUCTURES***

CHAPTER 5

TEMPERATURE DEPENDENT STUDIES ON TAILORED GRAPHITIC CARBON NITRIDE NANOSTRUCTURES

Overview

In the present chapter we discuss in detail the synthesis and characterization of a series of GCN nanostructures prepared by changing the temperature through thermal condensation of cyanamide using porous anodic aluminium oxide (AAO) templates.

In recent years, many researchers have focused their attention on developing highly-efficient photocatalysts due to their solar energy utilization and environmental applications. To date, the majority of research is in the domain of photocatalysts containing metals such as metal oxide, metal sulfide, tungstates, niobates and tantalates [Liu et al. 2015]. However, the development of efficient, sustainable and environmental-friendly photocatalysts remains a formidable challenge. GCN has graphite like structure with band gap of 2.7 eV. GCN exhibits excellent photocatalytic activity in many photo chemical reactions, including water splitting using visible light, hydrogen production, CO₂ activation photo degradation of dyes etc. GCN has good chemical and thermal stability, and it is nontoxic[Yan et al. 2010].

However its wide range of application as a visible-light photocatalyst is limited due to its small specific surface area. Therefore, the preparation of GCN nanostructures with high surface area by a simple method is an attractive scheme and worthy of detailed investigation [Li et al. 2016]. From previous results we observed that hard template method is flexible, cost effective to fabricate geometrically different GCN nano materials. A large number of nanostructured GCN, including helical GCN nanorods [Li et al. 2015b], nanospheres [He et al. 2013] nanospherical GCN [Giannakoudakis et al. 2017], GCN nanosheets [Liang et al. 2015] have been prepared using templates. [Yang et al. 2015]. There exists sufficient literature on efforts made to obtain high quality one dimensional GCN nanostructures like nanotubes [Guo et al. 2004], nanowires [Wang et al. 2015], nanobelts [Thomas et al. 2008], nanofibers [Cao et al. 2015], and nanorods [Wang et al. 2012b]. The thermal condensation of nitrogen

rich precursors inside the empty AAO templates resulting into the highly condensed and ordered array of GCN nanostructures.

The fabrication of GCN nanostructures using templates offers good controllability to their physical dimensions. To solve the problem on purity, crystallinity and regularity, we synthesized GCN using AAO templates under controlled conditions. In this work the precursors were taken inside the nano channels of AAO templates with pore diameter of about 60 nm and then heated at different temperatures. With XRD, SEM and TGA, the structure and composition of the synthesized samples were examined that confirmed high quality GCN produced through this approach. Optical properties of GCN nanostructures play an important role in photocatalytic reactions. We carried out optical characterizations including FTIR, UV-visible spectroscopy and Photoluminescence spectroscopy (PL).

5.1 Template assisted synthesis and characterization of nanostructures

Synthesis of GCN samples at different processing temperatures is discussed in chapter 2. In the following sections, the effect of processing temperature on the properties of physically confined GCN nanostructures is discussed in detail.

5.2 Structural and morphological studies

5.2.1 X-ray diffraction studies

Figure.5.1. shows the X-ray diffraction spectra of GCN samples prepared under different processing temperatures in air atmosphere from 400-600°C. The highly intense diffraction peak is observed around 2θ value 27.42° representing (002) direction for all samples, corresponding to the interplanar stacking of conjugated planes [Wang et al. 2012b] [Maeda et al. 2014]. This indicates that the polymerization reaction of cyanamide occur at 400°C to form GCN. Generally during synthesis of GCN nanostructures using templates, highly crystalline products are obtained by self-condensation of nitrogen rich precursors such as urea, thiourea, melamine, cyanamide dicyandiamide etc. The peak experiences a right shift from 27.42 - 27.76° with gradual increase in processing temperature from 400 to 600°C. The enhancement in crystallinity and orientation of nanostructures confirmed the confinement effect of AAO templates.

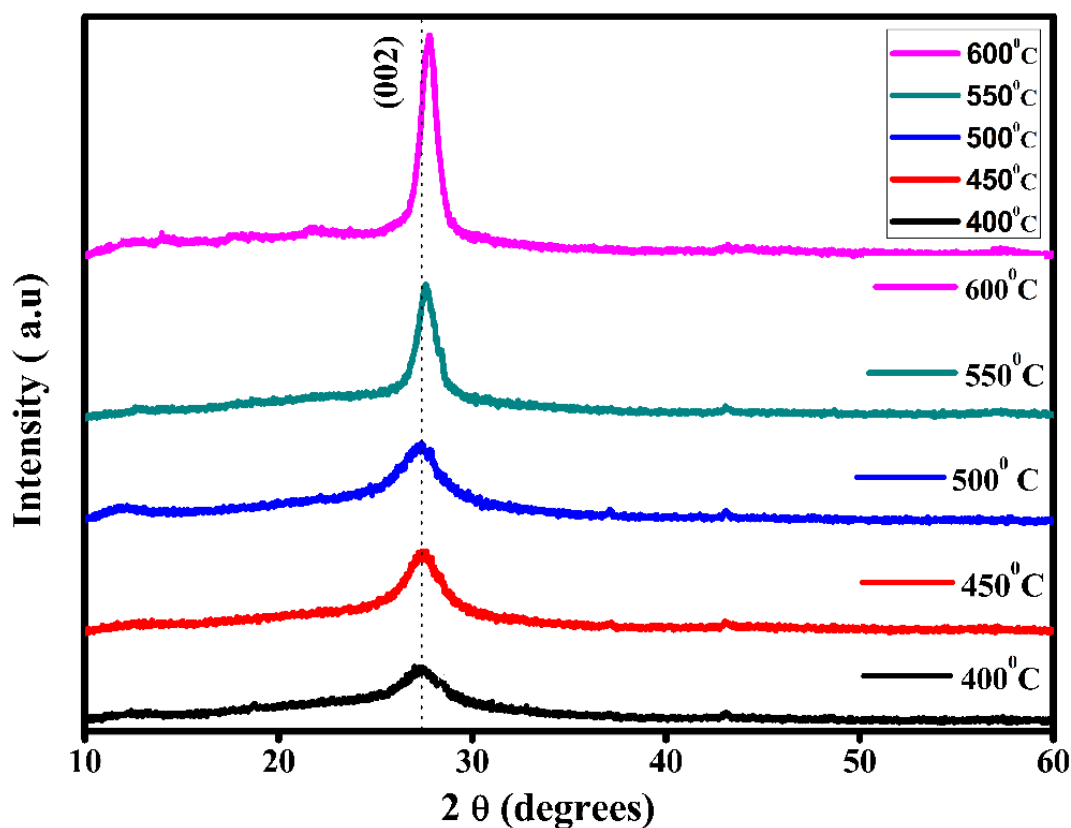


Figure: 5.1 The XRD spectra of the GCN nanostructures obtained at different temperatures.

5.2.2 Morphological studies

Figure.5.2 shows the FESEM images of the GCN products synthesized at different temperatures. It is seen from figure that when processing temperature is kept as low as 400 °C the GCN sample consists of small nano wire like structures with some nanoparticles providing cyanamide impurities. The FESEM images for 450°C shows the formation of complete wire like structures. The wires at 500°C are more prominent(Figure.5.2(d)), The FESEM image of GCN sample prepared at 600 °C shows the presence of both wires and flake kind of structures (Figure.5.2(e)). From surface morphology studies of the GCN samples it can be noticed that after thermal treatment of cyanamide using of AAO templates wire like structures with same dimensions as that of the templates used were obtained.

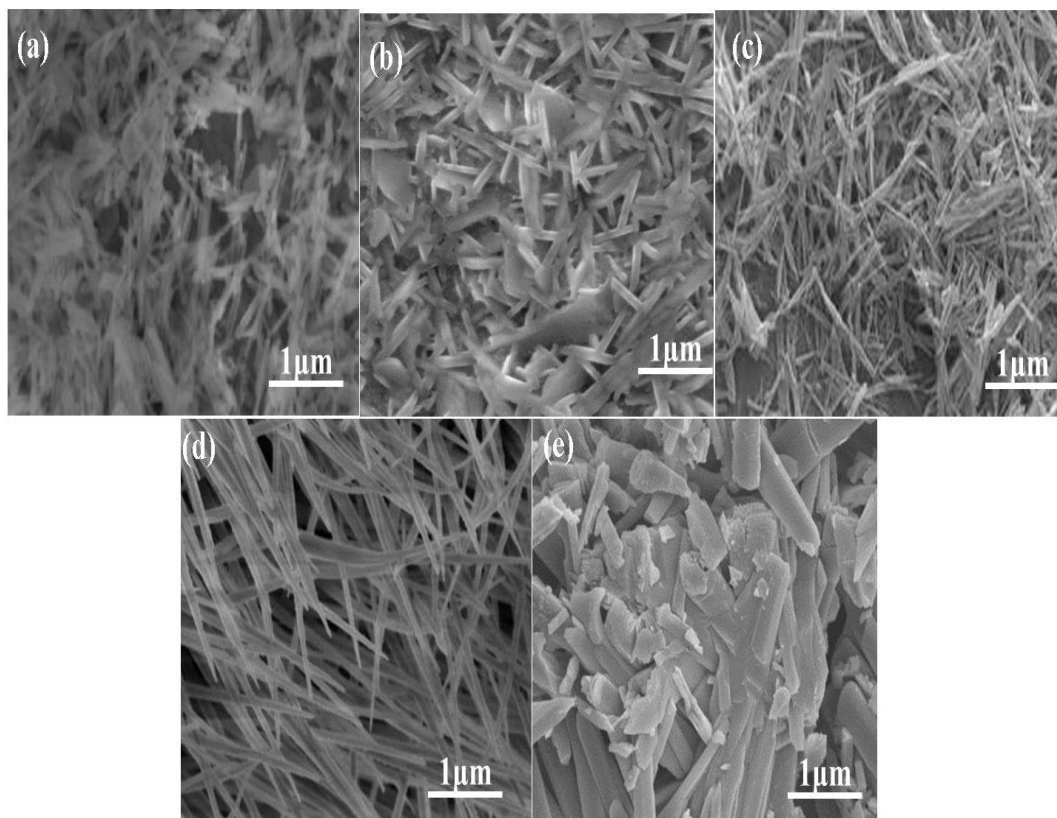


Figure: 5.2 The FESEM images of GCN nanostructures obtained at different temperatures (a) 400 °C, (b) 450 °C, (c) 500 °C, (d) 550 °C, (e) 600 °C.

At lower temperature there are some intermediate products like dicyandiamide and melamine [Das et al. 2017]. These impurities are present in particulate form since they are crystalline in nature. With increase in temperature, gradual wire formation shows up. But when temperature increases to 600°C the wire like structures modify into small flaky chips like structures. Since the structural parameters of AAO templates also change with temperature and the template loses its porous structure and degradation of the pores starts on annealing through higher temperatures. Thus it can be noted that the gradual increase in the synthesis temperature results in the formation of GCN nanowires leading to flake kind of GCN structures on AAO templates.

5.3 Thermo gravimetric analysis

The Thermo gravimetric analysis (TGA) was performed to measure thermal stability of the GCN samples. All samples were subjected to heat treatment from room temperature to 800°C at the ramping rate of 10 °C min⁻¹ in air. TGA curves are shown

in figure.5.3. From this figure, it was observed that, there are three major steps, firstly the samples prepared at 400°C, 450°C and 500°C, have weight loss for water at 100 °C. Second step corresponds to the thermal degradation of the precursor forming intermediate but poor crystalline compounds at 450°C [Li et al. 2009] [Xu et al. 2013].

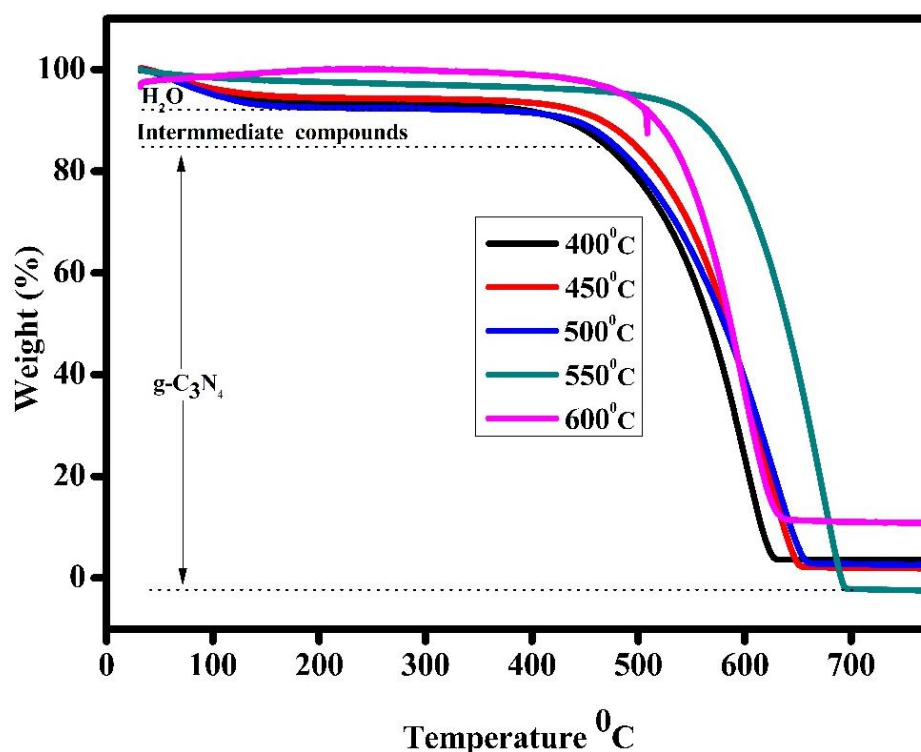


Figure: 5.3 TGA results of the GCN nanostructures synthesized at different temperatures.

Third step begins at 540°C, and the prominent weight loss is observed at this step. The samples lose weight and completely decompose when temperature reaches 620 °C. In case of sample prepared at 550°C, the complete thermal decomposition was observed around 700 °C. This suggests that up to this temperature (~ 700 °C) pure GCN nanostructures are stable. At higher temperature there will be a rapid decomposition which leads to the weight loss in the sample [Long et al. 2014]. Increasing the temperature leads to the instability of the GCN samples and nanowires will break down and modify into flake kind of structures. This is consistent with FESEM results also. On the other hand, thermo gravimetric data can be presented as a derivative thermo gravimetric (DTG) curve, which is a plot of first derivative of the TGA data against temperature [Yang et al. 2001]. The peak of the first derivative indicates the point of

greatest rate of change on the weight loss curve [Kim et al. 2004]. Figure.5.4 shows the DTG curves for the samples prepared at different temperatures. From figure.5.4 it was observed that for sample prepared at 550°C the first derivative peak temperature is occurring at 700°C and for other samples the peak is around 600-620°C which can be attributed to the thermal decomposition and complete vaporization of the sample. By the absorption of heat energy the pure GCN sample will oxidize into carbon dioxide[Li et al. 2009].

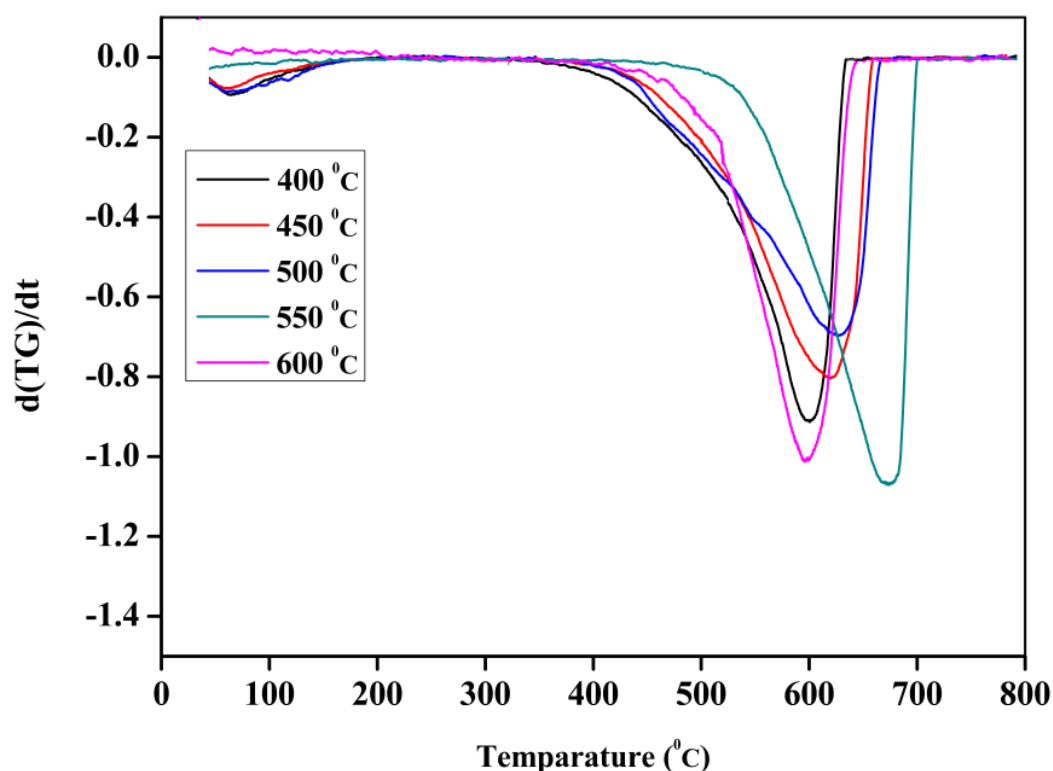


Figure: 5.4 DTG plots of the GCN nanostructures synthesized at different temperatures.

5.4 Fourier transform infrared spectroscopy (FTIR) and Raman studies of GCN nanostructures

To study the chemical structure of the samples during thermal condensation of Cyanamide inside the channels of the AAO templates Fourier transform infrared spectroscopy (FTIR) were conducted on the GCN samples. Figure. 5.5 shows the FTIR spectra of GCN samples. All synthesized samples showed similar characteristics confirming pure phase formation of GCN nanostructures using AAO templates. There

are a set of peaks appearing in the range of 1200-1700 cm^{-1} [Livneh et al. 2002] corresponding to stretching vibrational modes of C=N [Wang et al. 2005] [Jorge et al. 2013] and C–N heterostructures [Kang et al. 2015]. The peak at 807 cm^{-1} corresponds to the breathing mode of triazine ring [Li et al. 2015a] [McMillan et al. 2009].

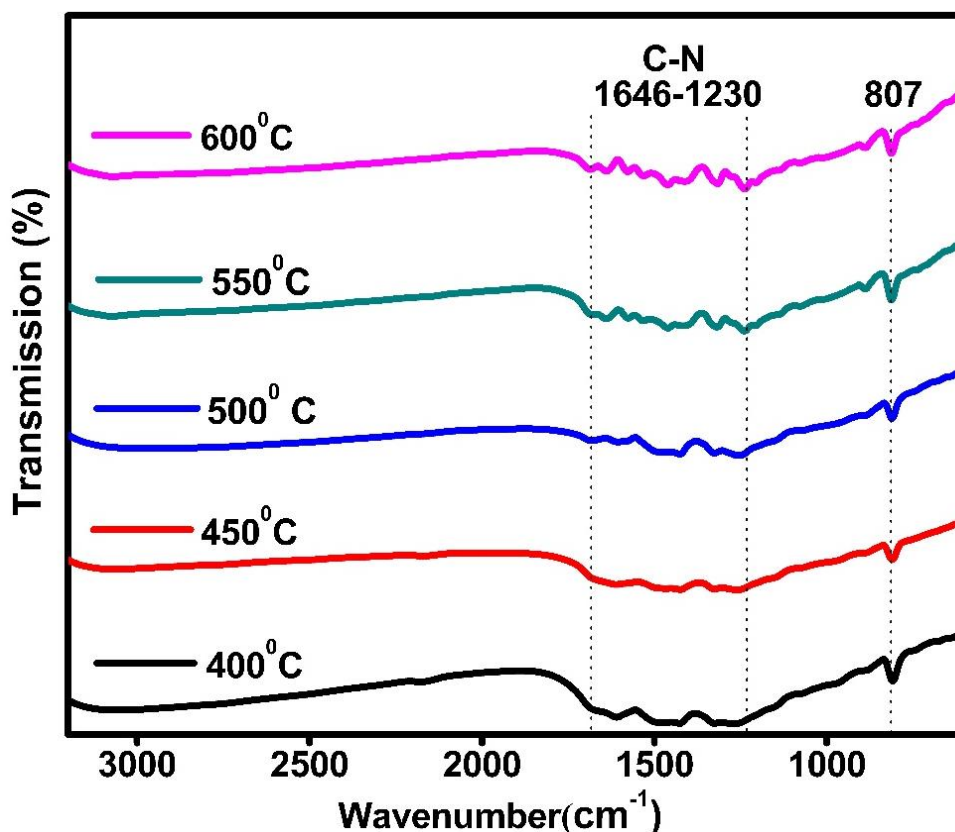


Figure: 5.5 The FTIR spectra of the GCN nanostructures obtained at different temperatures.

5.5 Absorption properties of GCN nanostructures

Optical absorption properties of GCN samples were studied using UV-Vis absorption spectroscopy. Figure 5.6 shows typical absorption pattern of GCN nanostructures prepared at different temperatures. In figure, it was noticed that the strong absorption is in the range of 350 to 470 nm due to electron excitation from valance band to conduction band of GCN sample [Tahir et al. 2013].

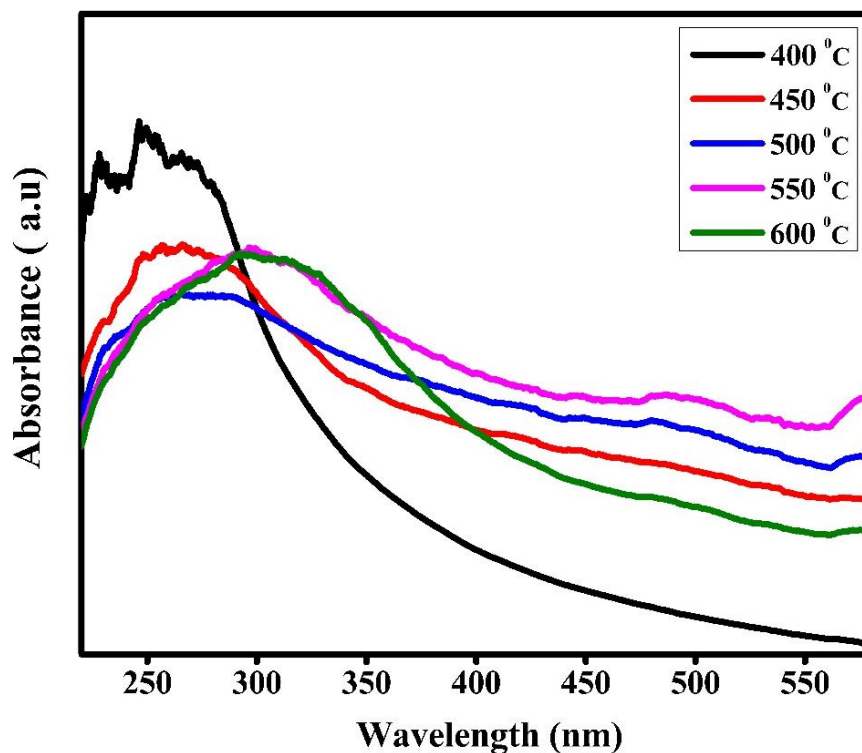


Figure: 5.6 The Uv-Vis spectra of the GCN nanostructures obtained at different temperatures.

For sample prepared at 400 °C the absorption peak is at 400 nm. This might be due to less thermal condensation [Lee et al. 2010]. As the temperature increases the degree of condensation also increases, the enhancement in the condensation temperature represents the wider absorption spectra. Sample prepared at 550 °C presents longer absorption at 451 nm. The sample synthesized at 550 and 600 °C had broad absorption that was assigned to $n-\pi^*$ electronic transitions involving N lone pair electron [Jorge et al. 2013].

By changing the processing temperature the band gap also changed slightly as shown in the figure.5.7. As the temperature increased from 400°C to 600 °C, the band gap energy decreases from 3.3eV to 2.7eV. This is due to smaller and thinner nanostructure formation at higher temperatures because of nano confinement effect. This size dependent change in band gap is mainly due to structural changes and is confirmed by FESEM images also.

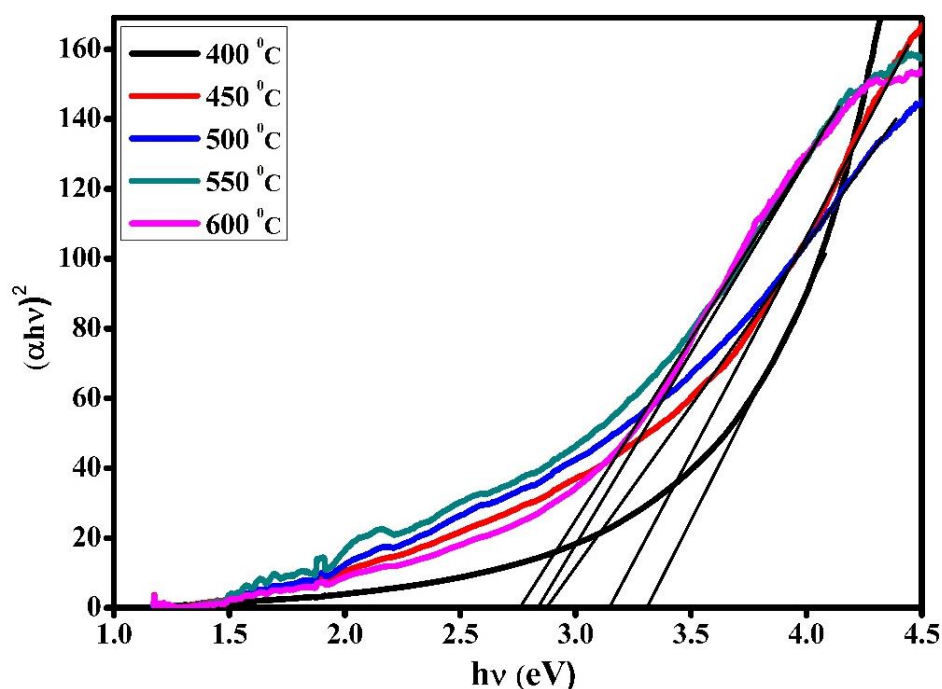


Figure: 5.7 The Tauc's plot of the UV-Visible spectra of GCN nanostructures obtained at different temperatures.

5.6 Emission properties of GCN nanostructures

Photoluminescence studies of prepared GCN samples were carried out to understand the emission properties. Figure. 8 shows the photoluminescence (PL) spectra of the GCN samples. From PL analysis, we notice that as the processing temperature increases there is a shift in luminescence centre. For the sample prepared at 400°C, centre of the PL spectra is at 420 nm, and for GCN rich sample 550°C, centre of the PL spectra is at 435nm, for sample prepared at 600°C centre of the PL spectra is at 454 nm. However broad peak is due to impurities [Wang et al. 2012a]. To understand the origin and nature of the excitons in GCN sample, Gaussian fitting is done for luminescence spectra for all the samples and presented in the figure 5.8.

For the emission spectrum of GCN samples three main emission centers have been validated. The peak position of the luminescent centres is displayed in Figure.5.9. According to the previous reports the band gap states of GCN consists of lone pair nitride atom, sp^2 C–N π band and sp^3 C–N σ band [Wang et al. 2012a]. For sample prepared at 550°C, the emission centers are at R1 (431 nm), R2 (452 nm) and R3 (497 nm).

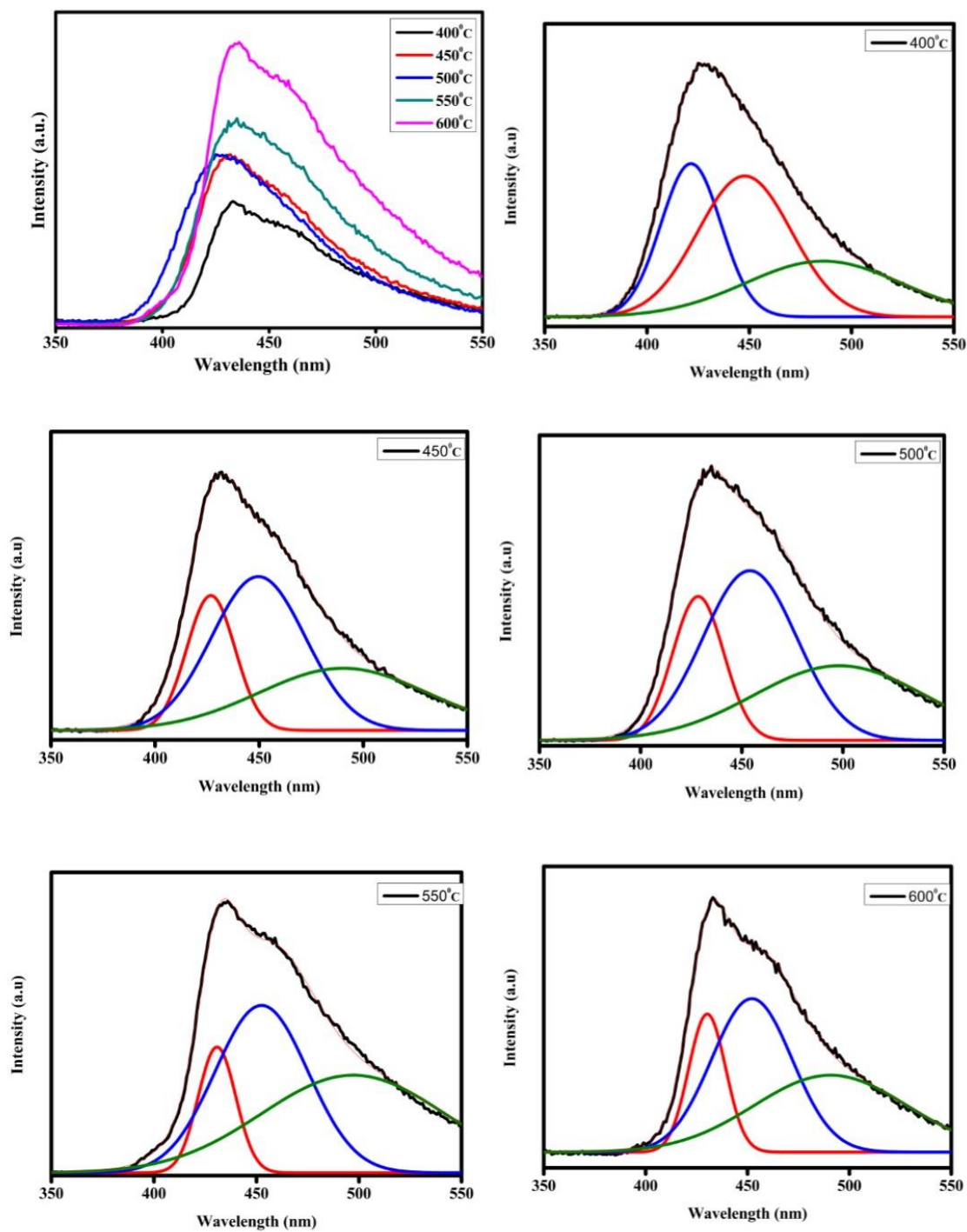


Figure: 5.8 (a) The normalized PL emission spectra of the GCN nanostructures prepared at different temperatures. (b),(c),(d),(e) and (f) the Gaussian fitting of PL emission spectra of the 400,450,500,550 and 600 °C samples respectively.

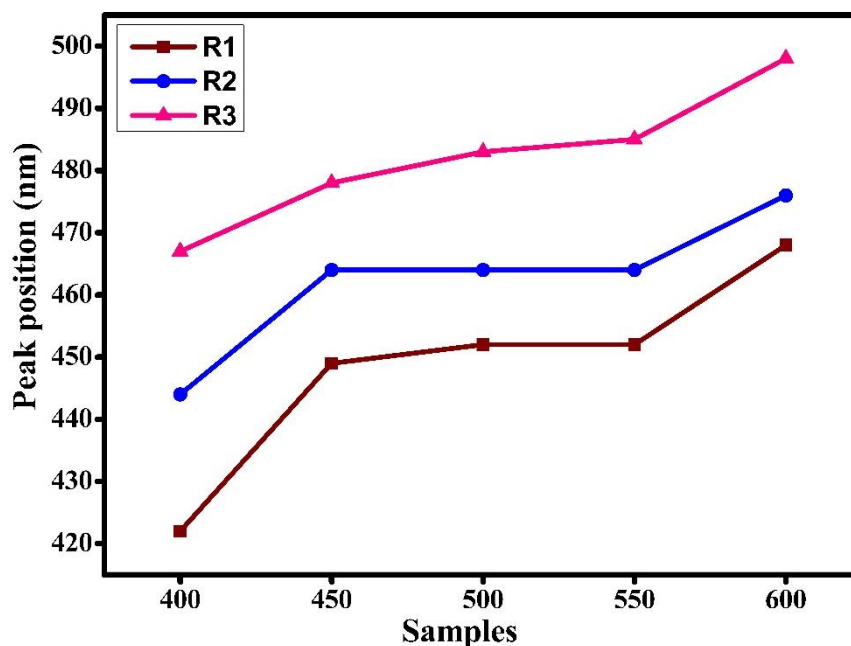


Figure: 5.9 The peak position of R1, R2 and R3 of the GCN nanostructures obtained at different temperatures.

These luminescent centres are originated from the transitions of $\pi^*-\pi$ [Wang et al. 2011] σ^* -lone pair and π^* -lone pair states [Fanchini et al. 2002]. As the processing temperature increases red shift of luminescent centres is observed [Das et al. 2017].

From the above results it was noticed that synthesis of GCN nanostructures by thermal condensation of cyanamide using AAO templates at different processing temperatures leads to the change in structural, optical and morphological properties. GCN samples exhibited tuneable luminescence properties with the increase of processing temperature. The photocatalytic degradation of methylene blue dye using GCN samples is discussed in the chapter 6.

Conclusions

Synthesis of GCN nanostructures using AAO templates with respect to variation of temperature proves the enhancement in crystallinity and orientation of nanostructures which confirmed the confinement effect of AAO templates.

It can be noted that the gradual increase in the synthesis temperature results in the formation of GCN nanowires leading to flake kind of GCN structures. As the

processing temperature increases the position of these peaks also slightly shifts. This shift indicate the structural changes during thermal condensation process. These characteristics are observed for all the samples but better features are observed at higher temperatures. The FTIR analysis of samples shows the compositional change of the GCN products during thermal condensation of cyanamide inside the nano channels of AAO templates. The luminescent properties of GCN samples at different processing temperatures have been studied. GCN samples exhibited tuneable luminescence properties with the increase of processing temperature.

CHAPTER 6

APPLICATIONS TOWARDS PHOTOCATALYTIC PROPERTIES OF GRAPHITIC CARBON NITRIDE NANOSTRUCTURES

CHAPTER 6

APPLICATIONS TOWARDS PHOTOCATALYTIC PROPERTIES OF GRAPHITIC CARBON NITRIDE NANOSTRUCTURES

6.1 PHOTOCATALYSIS

Photocatalysis is the process where a substance participates in modifying the rate of a chemical transformation of the reactants without being altered in the end. The substance is known as catalyst which increases the rate of a reaction by reducing the activation energy.

In photocatalytic process the acceleration of a chemical reaction is either by direct irradiation or by the irradiation of a catalyst that in turn lowers the activation energy for the primary reaction to occur. In a photocatalytic process, photo induced chemical reactions or molecular transformations occur at the surface of a catalyst. This general process can be further divided into catalysed or sensitized photoreactions based upon whether the initial excitation occurs at the surface of the adsorbate molecule or the catalyst. A catalysed photoreaction occurs when the initial photo excitation occurs in an adsorbate molecule, which then reacts with a catalyst substrate [Linsebigler et al. 1995]. A sensitized photoreaction occurs when the initial photo excitation occurs in the catalyst substrate and then energy transfer, which is often in the form of electron transfer, from a ground state molecule.

6.1.1 Principles of Photocatalytic Reactions

In general, a sensitized photocatalytic oxidation process is one in which a semiconductor upon absorption of a photon of suitable energy can act as a photocatalytic substrate by producing highly reactive radicals that can oxidize organic compounds. Photoactive semiconductor surfaces can attract electron donors and acceptors through both chemical and electrostatic forces including van der Waals forces. When a photocatalyst is irradiated with photons with energies greater than that

of the semiconductor's band gap, E_g (eV), an electron is transferred to the conduction band, leaving behind a positive hole in the valence band. The pair of photo excited charges that occurs within a material is called an electron-hole pair. The energy required by a photon to generate an electron-hole pair in a photocatalyst is related to the wavelength of the incident radiation.

The efficiency of a photocatalyst is measured in terms of the number of reactions occurring per photon absorbed. This depends on various facts like, the rate of the generation, fate of migration, and energy levels of the photo excited electron-hole pairs. The rate that electron-hole pairs generated is determined first by irradiation conditions such as photon energies and fluxes, and secondly by optical absorption characteristics of the photocatalytic particles such as their band gap, size and surface area.

Dye degradation: It is a process in which the large dye molecules are chemically cut down into smaller products like carbon dioxide, water and other by products which are used in the process of dye preparation. In everyday life synthetic dyes are commonly used in variety of products like furniture's, leather accessories, artificial flowers, clothes etc. However, a side effect of their widespread use is that up to 12% of these dyes are wasted during the dying process and about 20% of this wastage enters the clean water supply. Commonly used dyes are methylene blue ($C_{16}H_{18}ClN_3S$), Methylene orange ($C_{14}H_{14}N_3NaO_3S$), Rhodamine B ($C_{28}H_{31}ClN_2O_3$) etc. In this work we used GCN nanostructures as catalysts to study degradation of different dyes using visible light.

6.2 Photocatalytic properties of Bulk and AAO assisted GCN nanostructures

6.2.1 Photocatalytic activity of nanostructures for the degradation of Methylene blue dye

The Photocatalytic activity of the prepared samples was studied for the degradation of methylene blue (MB) dye under visible light. The adsorption of MB dye solution was carried out for 60 min in the dark. Then the solution is placed in the

photocatalytic reactor chamber. The degradation of MB dye using bulk GCN and GCN nanofibers are shown in figure (4). GCNNF was able to degrade MB completely in 40 min, whereas bulk GCN will degrade it completely in 180 min.

Figure (6.2a) shows the relationship between the irradiation time and C/C_0 of blank sample without any catalyst, with bulk GCN and with GCNNF. The blank sample shows that there is no degradation with the use of visible light. This result suggests that the self-degradation of dye is negligible.

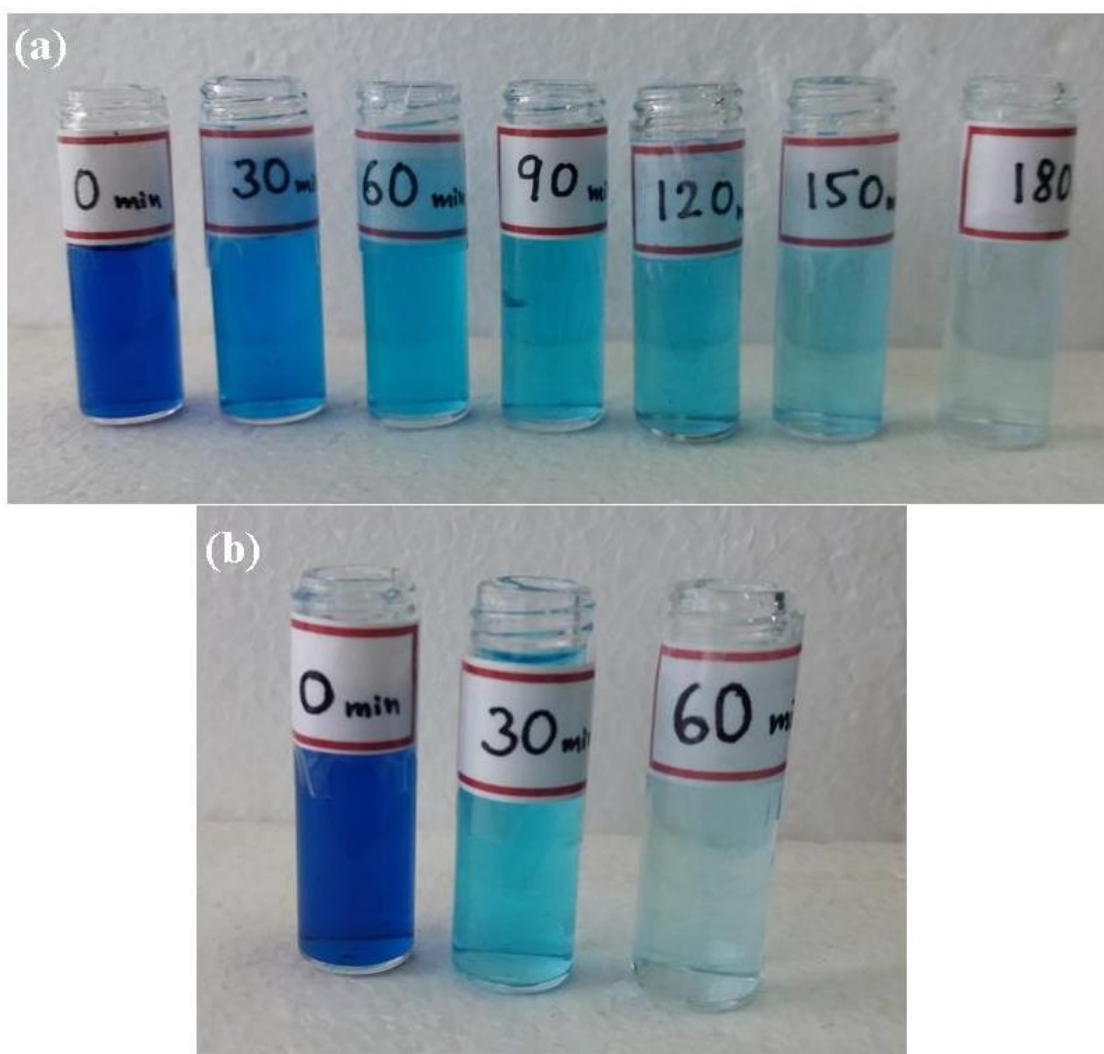


Figure 6.1: Photodegradation of MB solution for (a) bulk GCN and (b) GCN nanofibers.

Figure 6.2: Absorption spectra of degradation of methylene blue dye using bulk and GCNNF nanostructures

The kinetics of photo degradation of MB dye by the synthesized bulk GCN and GCNNF corresponds to the pseudo first-order rate equation as shown in equation (1), where C is the initial concentration, C_0 is the concentration at corresponding irradiation time (t) and k is the first order rate constant [Sadiq et al. 2016].

$$\ln(C/C_0) = -kt \quad (6.1)$$

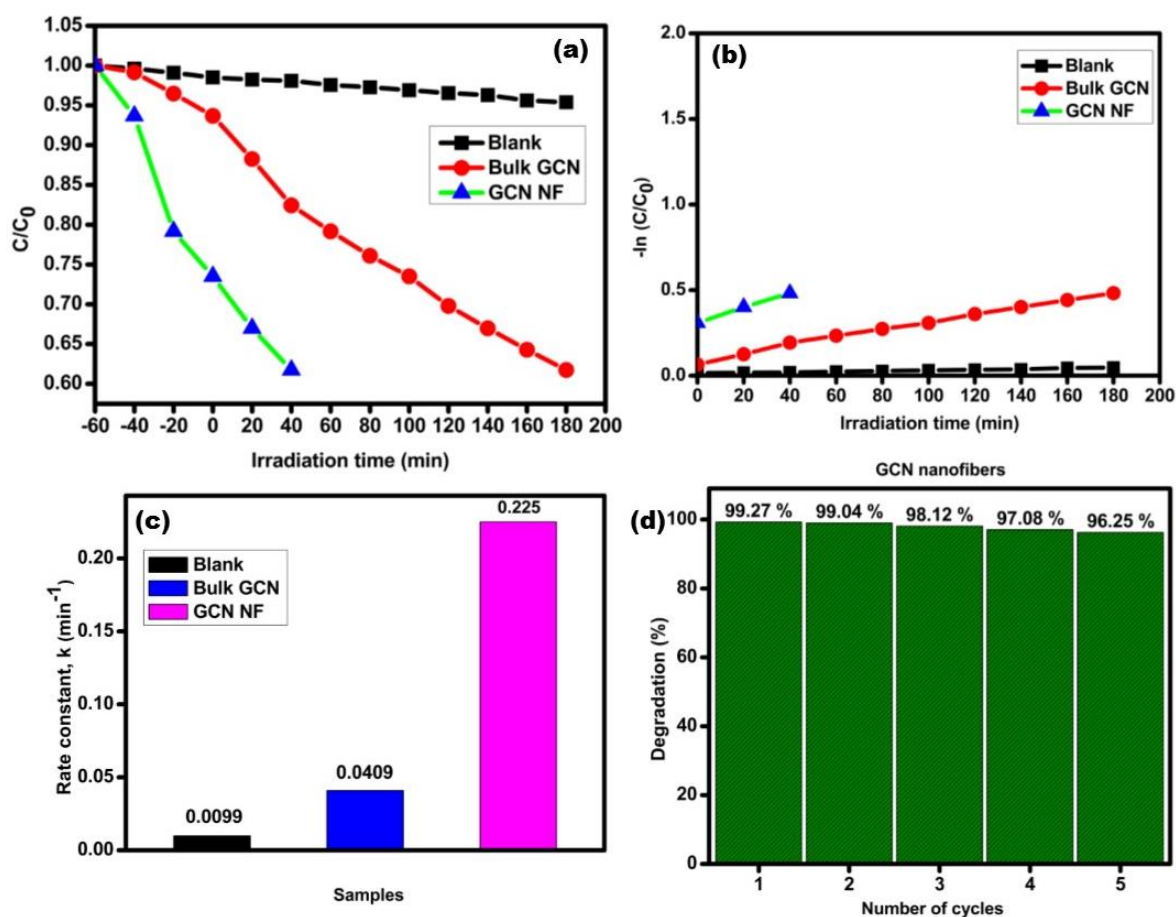


Figure: 6.2 (a) Dye relative concentration (b) Dye kinetics (c) Dye rate constant and (d) Dye stability of bulk and GCN nanofibers for MB dye.

Figure 6.2(c) corresponds to the rate constant of different samples with respect to degradation of MB. The values of k were measured from the slope of the straight line. The measured k value for bulk GCN is 0.0409 min^{-1} and for GCNNF is 0.225 min^{-1} which is almost 5 times greater than bulk GCN. To study the reusability and stability of GCNNF the photodegradation experiment is repeated for several times as shown in figure 6.2(d).

The photo degradation capacity of GCNNF has decreased only 3% after five continuous cycles. This elucidates excellent stability and reusability of GCNNF. The maximum photocatalytic activity of GCNNF relates to its less number of structural defects and higher surface area. It is important to draw attention that during photocatalytic reaction the stability of a catalyst is a major factor for its practical application.

6.2.2 Photocatalytic activity of nanostructures for the degradation of Rhodamine-B dye

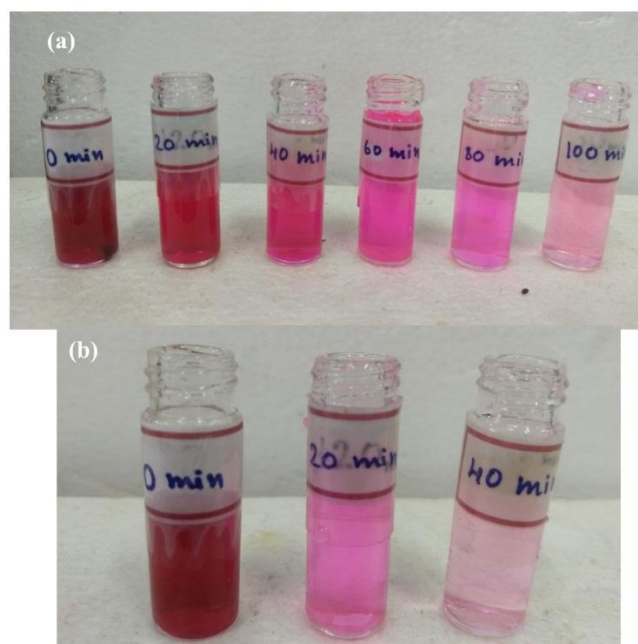


Figure 6.3: Photodegradation of Rh-B dye solution for (a) bulk GCN and (b) GCN nanofibers.

Photocatalytic activity of prepared GCN nanofibers was evaluated by degradation of Rhodamine-B (RhB) under visible light irradiation. The line noted as blank in figure was obtained without light illumination showing the self-degradation capacity of the dye.

To notice the absorption-desorption equilibrium the solution is subjected for degradation in dark chamber. It was half an hour for the system to achieve the adsorption-desorption equilibrium. Self-degradation is almost negligible. Then solution is placed inside the photocatalytic reactor chamber and is allowed for degradation under visible light irradiation. Figure shows that GCNNF was able to degrade RhB solution completely in 40 min, whereas bulk GCN degrades completely in 100 min.

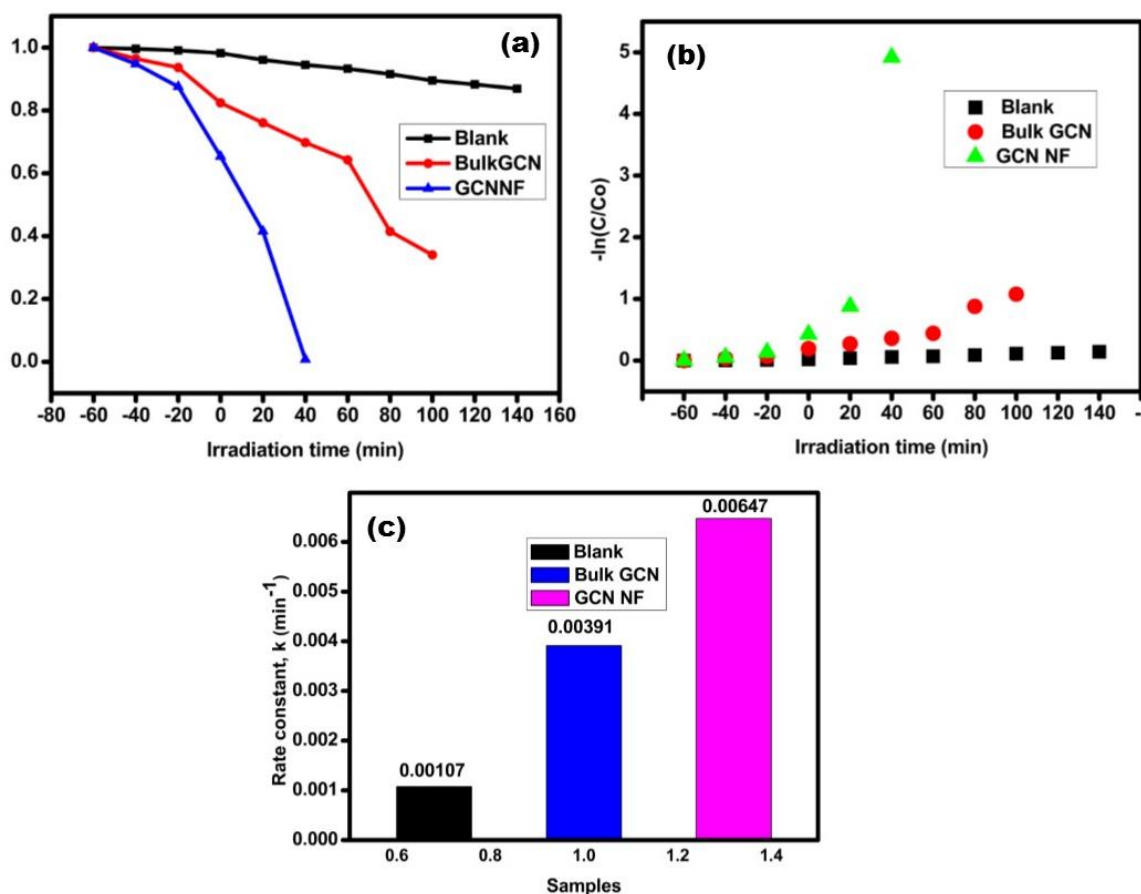


Figure: 6.4 (a) Dye relative concentration (b) Dye kinetics (c) Dye rate constant and of bulk and GCN nanofibers for photodegradation of RhB dye.

Results show that the use of GCN nanofibers leads to almost 90% degradation of RhB in 40 min which is much better than the degradation efficiency of bulk GCN sample. The studies on kinetics of the degradation indicates that GCN nanofibers exhibits 2.5 times higher photodegradation rate than that of bulk GCN samples. Figure 6.3 shows the relative concentration of dye with respect to time. Figure 6.4 shows the dye kinetics and rate constant of the samples for degradation of RhB dye using visible light.

6.2.3 Photocatalytic activity of nanostructures for the degradation of Methylene orange dye

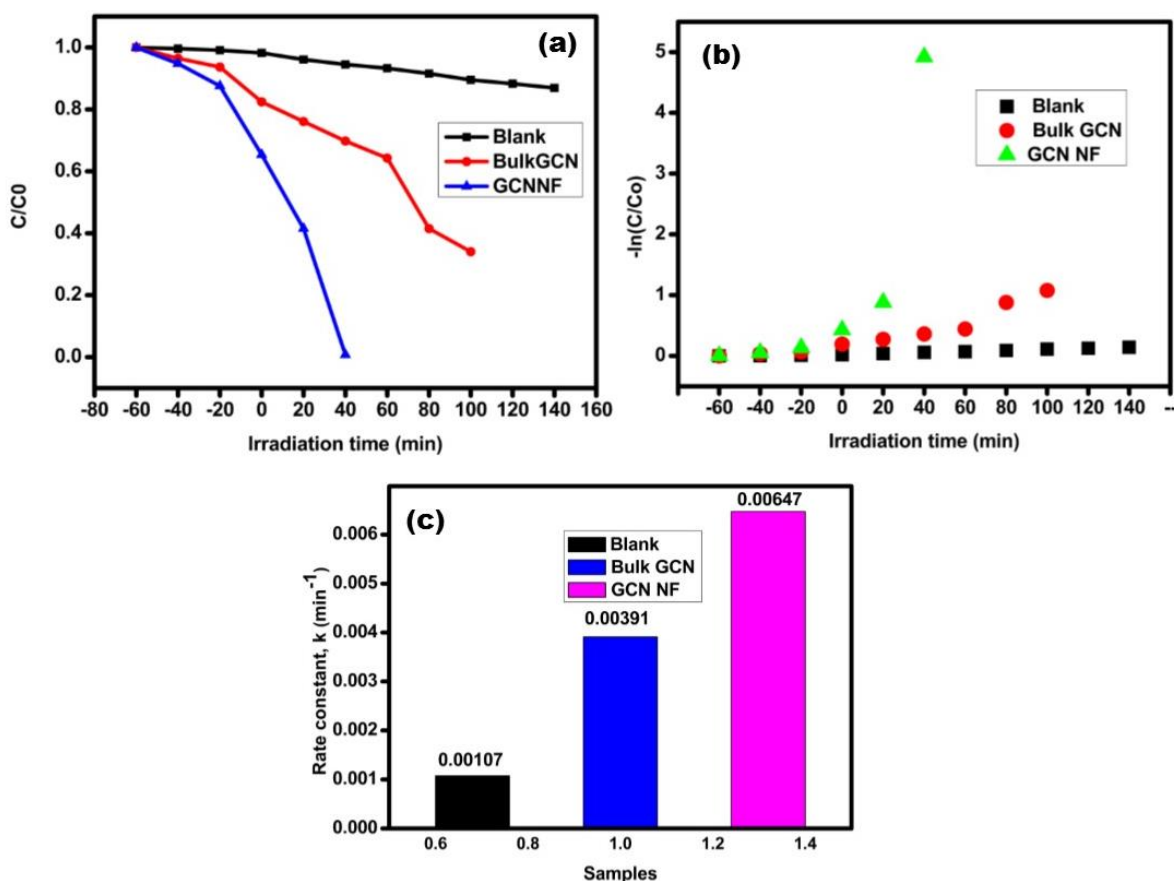


Figure: 6.5 (a) Dye relative concentration (b) Dye kinetics (c) Dye rate constant and of bulk and GCN nanofibers for photodegradation of MO dye.

The visible light photocatalytic activity of GCN nanofibers was evaluated for the photo degradation of methyle orange (MO) under visible light irradiation. Figure shows the photocatalytic activity of GCN nanostructures using Methyle orange (MO) dye using visible light.

As shown in figure 6.6, GCN nanofibers exhibited better efficient photocatalytic activity than bulk GCN sample. After 140 min visible light irradiation, almost 95% MO was degraded by GCN nanofibers, while only 42% MO was degraded by Bulk GCN under same conditions. The excellent photocatalytic activity of GCN nanofibers compared with Bulk GCN samples may be attributed to the strong absorption of radiation in the visible region and due to larger surface area. Figure 6.5 shows the photocatalytic degradation activity of GCN nanostructures and related kinetic studies.

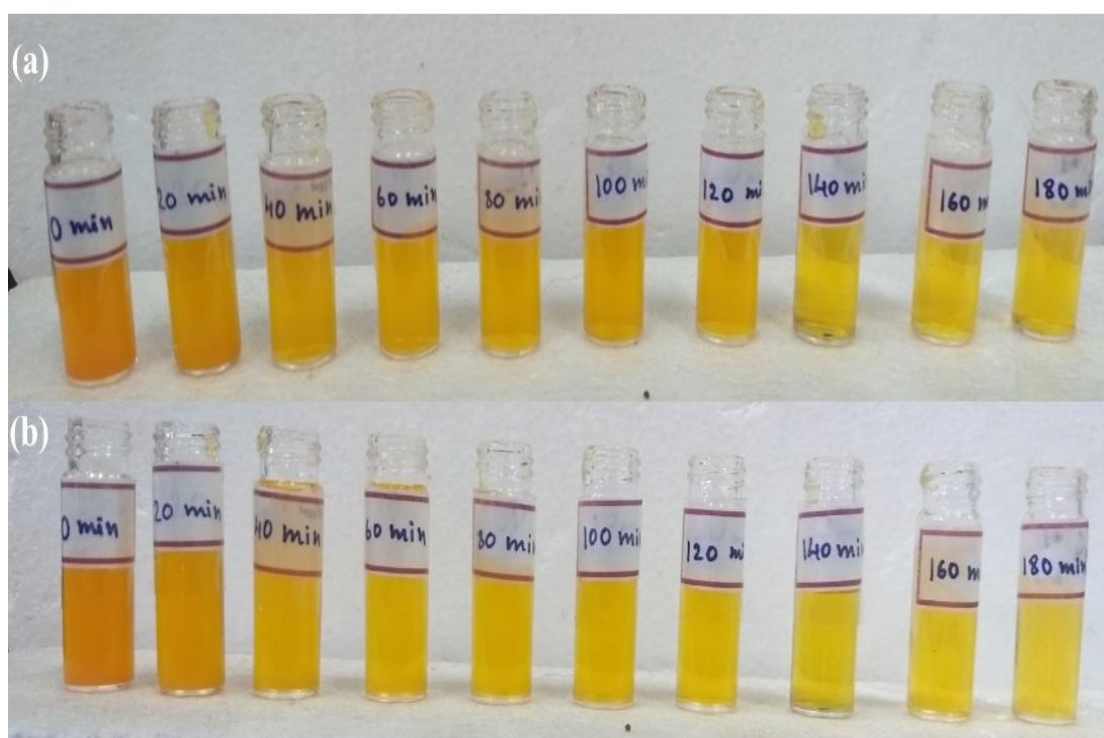


Figure 6.6: Photodegradation of MO dye solution for (a) bulk GCN and (b) GCN nanofibers.

6.3 Photocatalytic properties of GCN nanostructures synthesized at different temperatures

The adsorption property of the MB solution was carried out for 60 min in the dark chamber to achieve adsorption–desorption equilibrium of the GCN samples before subjecting it to the visible light. To check the self-degradation of MB, dye solution was taken without GCN samples in the photocatalytic reactor. There was very much less degradation of dye solution which suggest that self-degradation of the dye solution is negligible.

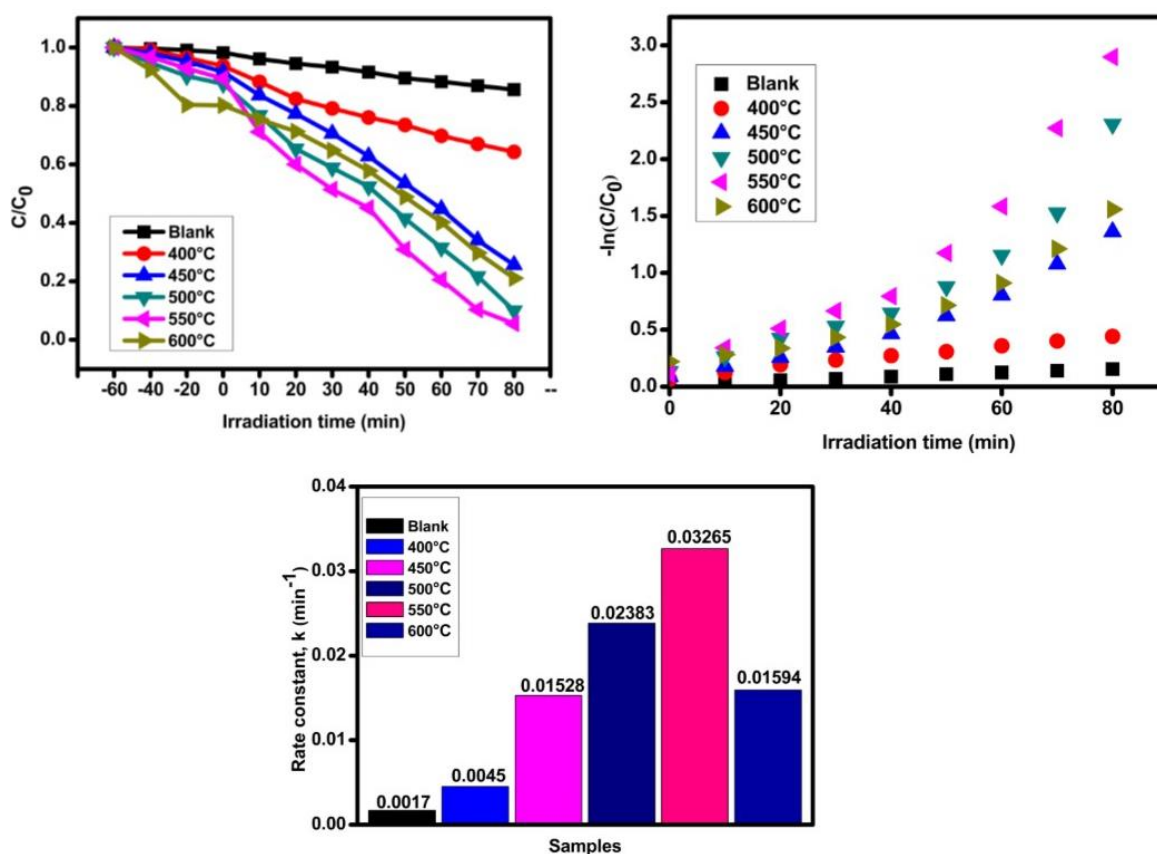


Figure: 6.7 (a) Dye relative concentration (b) Dye kinetics (c) Dye rate constant of GCN nanostructures obtained at different temperatures.

Figure 6.7 (a) shows the relative dye concentration of MB after photocatalytic degradation by GCN samples under visible light irradiation. As the processing

temperature was increased from 400°C to 550°C the degradation rate also increased. The different structural changes resulted in the different optical properties such as UV-Vis absorption, photoluminescence (PL). Light absorption is one of the major factors affecting photocatalytic activity. In general, broad absorption of light by the samples leads to the enhancement in photocatalytic activity. In case of sample prepared at 550°C, the photocatalytic degradation of MB dye is more pronounced. For sample prepared at 600°C the degradation rate was less and this was due to production of too many surface defects.

To compare the rate constants of different GCN samples the bar diagram is shown in Figure 6.6(c). As can be seen from the figure the sample prepared at 550°C shows higher efficiency than the other samples. Moreover, it has been found that template assisted GCN samples shows a better photocatalytic performance compared to the normally heat treated GCN samples.

Conclusions

The best degradation efficiency was observed for AAO assisted GCN samples for RhB dye degradation. It was observed that GCNNF exhibits an excellent photocatalytic degradation rate four times higher than that of bulk GCN samples. The photocatalytic degradation of GCN samples shows that the maximum photocatalytic efficiency was achieved for the sample prepared at 550°C. All these studies prove that the structural, optical and catalytic properties can be conveniently tuned by using the template assisted growth of GCN products.

CHAPTER 7
Summary and conclusions

Chapter 7

Summary and conclusions

The conclusions of the thesis are given below. Further a few directions for future work are also indicated in this chapter.

7.1 Summary and conclusions

The work presented in the thesis provides a detailed investigation of the synthesis, characterization and performance determination of the novel photocatalyst GCN synthesized using porous anodic aluminium oxide templates. The synthesized GCN nanostructures have potential applications in a number of direct energy conversion as well as environmental applications of solar energy. In a very systematic manner it handles the above mentioned issues; reports a number of strategies, duly supported by experimental results, to improve the performance; and in the process fills some gaps found in the literature.

In present study we discussed the effect of processing parameters such as anodization duration, anodization potential, electrolyte type, electrolytic bath temperature and electrolyte concentration on pore parameters of AAO templates were investigated in detail. It was found that increasing anodization duration causes the changes in pore dimensions and uniformity of pore structure. In order to study the effect of pore widening duration on AAO templates pore widening duration was increased, the inner pore wall will dissolve vertically so that pore will open completely and highly ordered hexagonal cells with circular pores will be observed at 60 min pore widening duration.

GCN nanostructures were grown using optimized AAO templates by thermal condensation method. It was shown that the synthesis of GCN nanofibers using porous anodic alumina template is the efficient approach for increasing crystallinity and surface area. The high surface area of GCN nanofibers has a good impact on novel photocatalytic and optical properties of the bulk GCN. It was observed that GCN NF demonstrates better photocatalytic activity in the photodegradation of Methylene blue which is almost 5 times higher than that of bulk GCN. This work is throws light on GCN nanostructures with high surface area for different applications. Also GCN nanostructures hold great potential for synthesizing efficient photocatalysts.

7.2 Directions for future work

Well-ordered GCN nanostructures with desired dimensions can be prepared using AAO templates to improve photocatalytic efficiency further. These GCN nanostructures can be utilised for the sensing applications. Metals, metal oxide compositions may be added to improve the efficiency of photocatalytic degradation of the dyes by various GCN nanostructures. Degradation experiment can also be extended for some other dyes and various industrial wastes etc, so as to shift the work from laboratory scale to industrial levels.

REFERENCES

- Arico, A.S., Bruce, P., Scrosati, B., Tarascon, J.-M. and Van Schalkwijk, W. (2011). Nanostructured materials for advanced energy conversion and storage devices. In *Materials For Sustainable Energy: A Collection of Peer-Reviewed Research and Review Articles from Nature Publishing Group*, (World Scientific), pp 148–159.
- Aruna, S.T. and Mukasyan, A.S. (2008). "Combustion synthesis and nanomaterials." *Curr. Opin. Solid State Mater. Sci.*, 12 (3–4), 44–50.
- Baker, S.N. and Baker, G.A. (2010). "Luminescent carbon nanodots: emergent nanolights." *Angew. Chem. Int. Ed.*, 49 (38), 6726–6744.
- Bell, A.T. (2003). "The impact of nanoscience on heterogeneous catalysis." *Science*, 299 (5613), 1688–1691.
- Belwalkar, A., Grasing, E., Van Geertruyden, W., Huang, Z. and Misiolek, W.Z. (2008). "Effect of processing parameters on pore structure and thickness of anodic aluminum oxide (AAO) tubular membranes." *J. Membr. Sci.*, 319 (1), 192–198.
- Brumlik, C.J., Menon, V.P. and Martin, C.R. (1994). "Template synthesis of metal microtubule ensembles utilizing chemical, electrochemical, and vacuum deposition techniques." *J. Mater. Res.*, 9 (5), 1174–1183.
- Bryant, G.W. (1989). "Resonant tunneling in zero-dimensional nanostructures." *Phys. Rev. B*, 39 (5), 3145.
- Cao, G. and Wang, Y. (2004). "Zero-dimensional nanostructures: nanoparticles." *Nanostructures Nanomater. Synth. Prop. Appl. Ed. G Cao Ed Imp. Coll. Press Lond.*, 51–109.
- Chen, X. and Mao, S.S. (2007). "Titanium dioxide nanomaterials: synthesis, properties, modifications, and applications." *Chem. Rev.*, 107 (7), 2891–2959.
- Chik, H. and Xu, J.M. (2004). "Nanometric superlattices: non-lithographic fabrication, materials, and prospects." *Mater. Sci. Eng. R Rep.*, 43 (4), 103–138.
- Curulli, A., Valentini, F., Padeletti, G., Viticoli, M., Caschera, D. and Palleschi, G. (2005). "Smart (Nano) materials: TiO₂ nanostructured films to modify electrodes for assembling of new electrochemical probes." *Sens. Actuators B Chem.*, 111 441–449.
- De Vito, S. and Martin, C.R. (1998). "Toward colloidal dispersions of template-synthesized polypyrrole nanotubules." *Chem. Mater.*, 10 (7), 1738–1741.

Dignam, M.J. (1962). "Oxide films on aluminum I. Ionic conduction and structure." *J. Electrochem. Soc.*, 109 (3), 184–191.

Dong, G., Zhang, Y., Pan, Q. and Qiu, J. (2014). "A fantastic graphitic carbon nitride (gC₃N₄) material: Electronic structure, photocatalytic and photoelectronic properties." *J. Photochem. Photobiol. C Photochem. Rev.*, 20 33–50.

Fujita, S., Habuchi, H., Takagi, S. and Takikawa, H. (2016). "Optical properties of graphitic carbon nitride films prepared by evaporation." *Diam. Relat. Mater.*, 65 83–86.

Heath, J.R. (1999). "Nanoscale materials (ACS Publications).

Holmes, J.D., Lyons, D.M. and Ziegler, K.J. (2003). "Supercritical fluid synthesis of metal and semiconductor nanomaterials." *Chem. Eur. J.*, 9 (10), 2144–2150.

Huang, Y., Duan, X., Wei, Q. and Lieber, C.M. (2001). "Directed assembly of one-dimensional nanostructures into functional networks." *Science*, 291 (5504), 630–633.

Huczko, A. (2000). "Template-based synthesis of nanomaterials." *Appl. Phys. A*, 70 (4), 365–376.

Hulteen, J.C. and Martin, C.R. (1997). "A general template-based method for the preparation of nanomaterials." *J. Mater. Chem.*, 7 (7), 1075–1087.

Khan, A.H., Ghosh, S., Pradhan, B., Dalui, A., Shrestha, L.K., Acharya, S. and Ariga, K. (2017). "Two-dimensional (2D) nanomaterials towards electrochemical nanoarchitectonics in energy-related applications." *Bull. Chem. Soc. Jpn.*, 90 (6), 627–648.

Kuchibhatla, S.V., Karakoti, A.S., Bera, D. and Seal, S. (2007). "One dimensional nanostructured materials." *Prog. Mater. Sci.*, 52 (5), 699–913.

Kwon, C.-W., Son, J.-W., Lee, J.-H., Kim, H.-M., Lee, H.-W. and Kim, K.-B. (2011). "High-Performance Micro-Solid Oxide Fuel Cells Fabricated on Nanoporous Anodic Aluminum Oxide Templates." *Adv. Funct. Mater.*, 21 (6), 1154–1159.

Lakshmi, B.B., Patrissi, C.J. and Martin, C.R. (1997). "Sol-gel template synthesis of semiconductor oxide micro- and nanostructures." *Chem. Mater.*, 9 (11), 2544–2550.

Li, D., Zhao, L., Jiang, C. and Lu, J.G. (2010). "Formation of anodic aluminum oxide with serrated nanochannels." *Nano Lett.*, 10 (8), 2766–2771.

Li, H., Kang, Z., Liu, Y. and Lee, S.-T. (2012). "Carbon nanodots: synthesis, properties and applications." *J. Mater. Chem.*, 22 (46), 24230–24253.

- Li, H., Wang, X., Xu, J., Zhang, Q., Bando, Y., Golberg, D., Ma, Y. and Zhai, T. (2013). "One-Dimensional CdS Nanostructures: A Promising Candidate for Optoelectronics." *Adv. Mater.*, 25 (22), 3017–3037.
- Li, L., Fan, M., Brown, R.C., Leeuwen, J. (Hans) V., Wang, J., Wang, W., Song, Y. and Zhang, P. (2006). "Synthesis, Properties, and Environmental Applications of Nanoscale Iron-Based Materials: A Review." *Crit. Rev. Environ. Sci. Technol.*, 36 (5), 405–431.
- Li, X., Ruzic, D.N., Chun, I.S., Chow, E.K. and Flauta, R.E. (2013). "Method of forming nanoscale three-dimensional patterns in a porous material.
- Li, X.-H., Zhang, J., Chen, X., Fischer, A., Thomas, A., Antonietti, M. and Wang, X. (2011). "Condensed graphitic carbon nitride nanorods by nanoconfinement: promotion of crystallinity on photocatalytic conversion." *Chem. Mater.*, 23 (19), 4344–4348.
- Liu, J., Wang, H. and Antonietti, M. (2016). "Graphitic carbon nitride “reloaded”: emerging applications beyond (photo)catalysis." *Chem. Soc. Rev.*, 45 (8), 2308–2326.
- Masuda, H., Yada, K. and Osaka, A. (1998). "Self-ordering of cell configuration of anodic porous alumina with large-size pores in phosphoric acid solution." *Jpn. J. Appl. Phys.*, 37 (11A), L1340.
- Marsal, L., Besombes, L., Tinjod, F., Kheng, K., Wasiela, A., Gilles, B., Rouvière, J.-L. and Mariette, H. (2002). "Zero-dimensional excitons in CdTe/ZnTe nanostructures." *J. Appl. Phys.*, 91 (8), 4936–4943.
- Mattevi, C., Kim, H. and Chhowalla, M. (2011). "A review of chemical vapour deposition of graphene on copper." *J Mater Chem*, 21 (10), 3324–3334.
- Mousavi, M., Habibi-Yangjeh, A. and Pouran, S.R. (2018). "Review on magnetically separable graphitic carbon nitride-based nanocomposites as promising visible-light-driven photocatalysts." *J. Mater. Sci. Mater. Electron.*, 29 (3), 1719–1747.
- Muller, G.A., Cook, J.B., Kim, H.-S., Tolbert, S.H. and Dunn, B. (2015). "High performance pseudocapacitor based on 2D layered metal chalcogenide nanocrystals." *Nano Lett.*, 15 (3), 1911–1917.
- Naseri, A., Samadi, M., Pourjavadi, A., Moshfegh, A.Z. and Ramakrishna, S. (2017). "Graphitic carbon nitride (g-C₃N₄)-based photocatalysts for solar hydrogen generation: recent advances and future development directions." *J. Mater. Chem. A*, 5 (45), 23406–23433.

- Pacholski, C., Kornowski, A. and Weller, H. (2002). "Self-assembly of ZnO: from nanodots to nanorods." *Angew. Chem. Int. Ed.*, 41 (7), 1188–1191.
- Sanguansri, P. and Augustin, M.A. (2006). "Nanoscale materials development—a food industry perspective." *Trends Food Sci. Technol.*, 17 (10), 547–556.
- Šepelák, V., Baabe, D., Mienert, D., Schultze, D., Krumeich, F., Litterst, F.J. and Becker, K.D. (2003). "Evolution of structure and magnetic properties with annealing temperature in nanoscale high-energy-milled nickel ferrite." *J. Magn. Magn. Mater.*, 257 (2–3), 377–386.
- Šepelák, V., Baabe, D., Mienert, D., Schultze, D., Krumeich, F., Litterst, F.J. and Becker, K.D. (2003). "Evolution of structure and magnetic properties with annealing temperature in nanoscale high-energy-milled nickel ferrite." *J. Magn. Magn. Mater.*, 257 (2–3), 377–386.
- Shah, K.A. and Tali, B.A. (2016). "Synthesis of carbon nanotubes by catalytic chemical vapour deposition: A review on carbon sources, catalysts and substrates." *Mater. Sci. Semicond. Process.*, 41 67–82.
- Shingubara, S. (2003). "Fabrication of nanomaterials using porous alumina templates." *J. Nanoparticle Res.*, 5 (1–2), 17–30.
- Simon, P. and Gogotsi, Y. (2010). Materials for electrochemical capacitors. In *Nanoscience And Technology: A Collection of Reviews from Nature Journals*, (World Scientific), pp 320–329.
- Smith, J.F., Knowles, T.P.J., Dobson, C.M., MacPhee, C.E. and Welland, M.E. (2006). "Characterization of the nanoscale properties of individual amyloid fibrils." *Proc. Natl. Acad. Sci.*, 103 (43), 15806–15811.
- Stępniewski, W.J. and Bojar, Z. (2011). "Synthesis of anodic aluminum oxide (AAO) at relatively high temperatures. Study of the influence of anodization conditions on the alumina structural features." *Surf. Coat. Technol.*, 206 (2), 265–272.
- Stępniewski, W.J., Michalska-Domańska, M., Norek, M. and Czujko, T. (2014a). "Fast Fourier transform based arrangement analysis of poorly organized alumina nanopores formed via self-organized anodization in chromic acid." *Mater. Lett.*, 117 69–73.
- Stępniewski, W.J., Nowak-Stępniewska, A., Presz, A., Czujko, T. and Varin, R.A. (2014b). "The effects of time and temperature on the arrangement of anodic aluminum oxide nanopores." *Mater. Charact.*, 91 1–9.
- Sun, H.-L., Shi, H., Zhao, F., Qi, L. and Gao, S. (2005). "Shape-dependent magnetic properties of low-dimensional nanoscale Prussian blue (PB) analogue $\text{SmFe}(\text{CN})_6 \cdot 4\text{H}_2\text{O}$." *Chem. Commun.*, 0 (34), 4339–4341.

Sun, Y., Ha, W., Chen, J., Qi, H. and Shi, Y. (2016). "Advances and applications of graphitic carbon nitride as sorbent in analytical chemistry for sample pretreatment: A review." *TrAC Trends Anal. Chem.*, 84 12–21.

Takei, K., Fang, H., Kumar, S.B., Kapadia, R., Gao, Q., Madsen, M., Kim, H.S., Liu, C.-H., Chueh, Y.-L. and Plis, E. (2011). "Quantum confinement effects in nanoscale-thickness InAs membranes." *Nano Lett.*, 11 (11), 5008–5012.

Tian, J., Zhao, Z., Kumar, A., Boughton, R.I. and Liu, H. (2014). "Recent progress in design, synthesis, and applications of one-dimensional TiO₂ nanostructured surface heterostructures: a review." *Chem. Soc. Rev.*, 43 (20), 6920–6937.

Tiwari, J.N., Tiwari, R.N. and Kim, K.S. (2012). "Zero-dimensional, one-dimensional, two-dimensional and three-dimensional nanostructured materials for advanced electrochemical energy devices." *Prog. Mater. Sci.*, 57 (4), 724–803.

Uchi, H., Kanno, T. and Alwitt, R.S. (2001). "Structural features of crystalline anodic alumina films." *J. Electrochem. Soc.*, 148 (1), B17–B23.

Utamapanya, S., Klabunde, K.J. and Schlup, J.R. (1991). "Nanoscale metal oxide particles/clusters as chemical reagents. Synthesis and properties of ultrahigh surface area magnesium hydroxide and magnesium oxide." *Chem. Mater.*, 3 (1), 175–181.

Verwey, I.E.J.W. (1935). "Electrolytic conduction of a solid insulator at high fields The formation of the anodic oxide film on aluminium." *Physica*, 2 (1–12), 1059–1063.

Wang, N., Zhang, W., Xu, J., Ma, B., Zhang, Z., Jin, Q., Bunte, E., Hüpkes, J. and Bochem, H.P. (2010). "Initial stage of pore formation process in anodic aluminum oxide template." *J. Solid State Electrochem.*, 14 (8), 1377–1382.

Wang, P. (2006). "Nanoscale biocatalyst systems." *Curr. Opin. Biotechnol.*, 17 (6), 574–579.

Wang, Y., Bansal, V., Zelikin, A.N. and Caruso, F. (2008). "Templated synthesis of single-component polymer capsules and their application in drug delivery." *Nano Lett.*, 8 (6), 1741–1745.

Weintraub, B., Zhou, Z., Li, Y. and Deng, Y. (2010). "Solution synthesis of one-dimensional ZnO nanomaterials and their applications." *Nanoscale*, 2 (9), 1573–1587.

Wiesner, M.R., Lowry, G.V., Alvarez, P., Dionysiou, D. and Biswas, P. (2006). "Assessing the risks of manufactured nanomaterials (ACS Publications).

Xie, X.N., Chung, H.J., Sow, C.H. and Wee, A.T.S. (2006). "Nanoscale materials patterning and engineering by atomic force microscopy nanolithography." *Mater. Sci. Eng. R Rep.*, 54 (1–2), 1–48.

Xia, Y., Yang, P., Sun, Y., Wu, Y., Mayers, B., Gates, B., Yin, Y., Kim, F. and Yan, H. (2003). "One-dimensional nanostructures: synthesis, characterization, and applications." *Adv. Mater.*, 15 (5), 353–389.

Yang, R.S.H., Chang, L.W., Yang, C.S. and Lin, P. (2010). "Pharmacokinetics and Physiologically-Based Pharmacokinetic Modeling of Nanoparticles.

Yang, Z., Zhang, Y. and Schnepf, Z. (2015). "Soft and hard templating of graphitic carbon nitride." *J. Mater. Chem. A*,

Ye, J., Zhang, H., Yang, R., Li, X. and Qi, L. (2010). "Morphology-Controlled Synthesis of SnO₂ Nanotubes by Using 1D Silica Mesostructures as Sacrificial Templates and Their Applications in Lithium-Ion Batteries." *Small*, 6 (2), 296–306.

Yu, Z., Tetard, L., Zhai, L. and Thomas, J. (2015). "Supercapacitor electrode materials: nanostructures from 0 to 3 dimensions." *Energy Environ. Sci.*, 8 (3), 702–730.

Zaraska, L., Stępniewski, W.J., Ciepiela, E. and Sulka, G.D. (2013). "The effect of anodizing temperature on structural features and hexagonal arrangement of nanopores in alumina synthesized by two-step anodizing in oxalic acid." *Thin Solid Films*, 534 155–161.

Zhang, H. (2015). "Ultrathin two-dimensional nanomaterials." *ACS Nano*, 9 (10), 9451–9469.

Zhang, H., Lamb, R. and Lewis, J. (2005). "Engineering nanoscale roughness on hydrophobic surface—preliminary assessment of fouling behaviour." *Sci. Technol. Adv. Mater.*, 6 (3–4), 236.

Zhu, Y.-P., Li, M., Liu, Y.-L., Ren, T.-Z. and Yuan, Z.-Y. (2014). "Carbon-Doped ZnO Hybridized Homogeneously with Graphitic Carbon Nitride Nanocomposites for Photocatalysis." *J. Phys. Chem. C*, 118 (20), 10963–10971.

Curriculum Vitae

Address for Correspondence:

Suchitra S.M

#1782/29

Shiva Sankalpa 6th Cross

Vinayaka Badavane

Vidyanagara

Davanagere 577 001

Karnataka, India

Mobile No.:+91-9008554148

Email: suchitra.123sm@gmail.com



Academic Qualification:

2011-2012 M.Sc. (Condensed Matter Physics)
PG centre, Davanagere University
Davanagere, Karnataka, India

2014-2018 **Ph.D.**,
Department of Physics
National Institute of Technology Karnataka,
Mangalore-575025, Karnataka, India

Skills & Activities:

Skills: Electrodeposition, Anodization, Material Characterization, X-ray Diffraction, Optical properties, Electrical properties, SEM. Origin, particle analysis using Image-J and WSxM software's

Languages: Kannada, English, and Hindi.

Work Experience

Lecturer 2012-2014

Department of physics

GM Institute of technology, Davanagere

Teaching Assistant, 2014-2018

M.Sc & B.Tech Department: Physics

NITK Surathkal, Karnataka

List of Journal Publications:

- 1) **Suchitra S.M** , Udayashankar N.K “Synthesis and photocatalytic properties of graphitic carbon nitride nanofibers using porous anodic alumina templates” (Material research express DOI: 10.1088/2053-1591/aa9b20)(IOP)
- 2) **Suchitra S.M**, Udayashankar N.K, “Influence of porewidening duration on the template assisted growth of graphitic carbon nitride nanostructures ” Material Research Express. Doi:10.1088/2053-1591/aaa808,(2018),(015056)(IOP)
- 3) **Suchitra S.M**, Ramana reddy P, Udayashankar N.K, “Synthesis and characterization of graphitic carbon nitride Nanotubes using Porous Anodic Alumina templates” Advance science letters. Adv. Sci. Lett. 24, 5673–5676 (2018) (AIP)
- 4) **Suchitra S.M** , Ramana reddy P, Aswathi P, Udayashankar N.K, “ structural and photoluminescence studies of porous anodic alumina templates prepared using different electrolyts”, (Journal of NanoScience, Nano Engineering & applications ISSN: 2231-1777, Volume 6, Issue 2)
- 5) **Suchitra S.M** , Ramana reddy P, Udayashankar N.K, “Effect of pore widening time on the structural aspects of self-organized nanopore arrays formed by anodization of aluminum in chromic acid” (Materials today proceedings, 2042–2051 (2016); doi:10.1016/j.matpr.2016.04.107)
- 6) **Suchitra S.M**, Ramana reddy P, Udayashankar N.K, “Structural and wetting properties of porous anodic alumina templates prepared by different electrolytes” (AIP proceedings, 1728, 020407 (2016); doi: 10.1063/1.4946458)34
- 7) Ramana reddy P, **Suchitra S.M**, Devika M, Udayashankar N.K “ structural and optical properties of porous anodic alumina annealed at different temperatures” (Journal of Nanotechnology and Its Applications ISSN: 0973-418X Volume 18,Issue(2)

PAPERS PRESENTED IN NATIONAL/INTERNATIONAL CONFERENCES:

- 1) International Conference on Recent advances in Condensed Matter and Applied Physics; 30-31st October 2015. (Oral presentation)
- 2) International conference on Condensed Matter and Applied Physics; 30- 31st October 2015 (Poster presentation)
- 3) International conference on nonnanoscience and Nanotechnology (ICNAN’16)’ at VIT University, Vellore on 19th-21st October, 2016. (Poster presentation).

- 4) International conference on nanoscience and nanotechnology (ICONN-17) at SRM university, Chennai on August 9th-11th August, 2017.(Poster presentation) and got (*Best poster presentation award*)

WORKSHOPS ATTENDED

1. INUP- workshop on synthesis and characterization of nano materials held at IISc Bangalore, during 18-20 may 2015.
2. TEQIP-II sponsored workshop on “Nano structured materials and their applications in catalysis and fuel cells” held at department of chemical engineering, NITK, Suratkal, during Sep 29 to Oct 1, 2016.
3. GIAN sponsored program on “Novel functional materials for energy conversion” conducted Chemistry department, NITK, Suratkal, Mangalore, during Oct 04- 07th, 2016.
4. Participated in the Global Initiative for Academic Networks course on “Novel Functional materials for Energy Conversion” October-2016 at National Institute of Technology Karnataka (NITK), Surathkal.

Awards

1. Best paper award in International conference on nanoscience and nanotechnology at SRM university, Chennai.

REFERENCES:

1. Dr. N. K Udayashankar
Professor, Department of Physics
National Institute of Technology Karnataka, Srinivasnagar (P.O.)
Surathkal, Mangalore-575025, India
Email: nkuday_01@yahoo.co.in
2. Dr. Madhu B J
Professor, Department of Physics
Government Science collage
Chitradurga
Karnataka, India
Email: madhybj@gmail.com

Permanent Address

Suchitra S.M
D/O Maheswarappa S H
#1782/29
Shiva Sankalpa 6th Cross
Vinayaka Badavane, Vidyanagara
Davanagere 577 001
Karnataka, India

APPENDIX- I

Publications

Journal publications

Suchitra S.M and Udayashankar N.K “Synthesis and photocatalytic properties of graphitic carbon nitride nanofibers using porous anodic alumina templates” (**IOP: Material research express** DOI: 10.1088/2053-1591/aa9b20)

Suchitra S.M and Udayashankar N.K, “Influence of porewidening duration on the template assisted growth of graphitic carbon nitride nanostructures” (**IOP: Material research express** DOI: 10.1088/2053-1591/aaa808)

Suchitra S.M, Ramana reddy P and Udayashankar N.K, “Synthesis and characterization of graphitic carbon nitride Nanotubes using Porous Anodic Alumina templates” **AIP: Advance science letters** Volume 24, Number 8 (2018).

Suchitra S.M , Ramana reddy P, Aswathi P and Udayashankar N.K, “ structural and photoluminescence studies of porous anodic alumina templates prepared using different electrolytes”, (**Journal of NanoScience, Nano Engineering & applications** ISSN: 2231-1777, Volume 6, Issue 2)

Ramana reddy P, Suchitra S.M, Devika M and Udayashankar N.K “ structural and optical properties of porous anodic alumina annealed at different temperatures” (**Journal of Nanotechnology and Its Applications** ISSN: 0973-418X Volume 18, Issue(2)

Suchitra S.M and Udayashankar N.K, “Temperature dependent studies on tailored graphitic carbon nitride nanostructures” **Journal of nanotechnology** (Under review)

Conference Proceedings

Suchitra S.M , Ramana reddy P and Udayashankar N.K, “Effect of pore widening time on the structural aspects of self-organized nanopore arrays formed by anodization of aluminum in chromic acid” (**Elsevier : Materials today proceedings**, 2042–2051 (2016); DOI:10.1016/j.matpr.2016.04.107)

Suchitra S.M, Ramana reddy P and Udayashankar N.K, “Structural and wetting properties of porous anodic alumina templates prepared by different electrolytes” (**AIP proceedings,1728, 020407 (2016)**; DOI: 10.1063/1.4946458) 34

Workshop attended

- INUP- workshop on synthesis and characterization of nano materials held at IISc Bangalore, during 18-20 may 2015.
- TEQIP-II sponsored workshop on “Nano structured materials and their applications in catalysis and fuel cells” held at department of chemical engineering, NITK, Suratkal, during Sep 29 to Oct 1, 2016.
- GIAN sponsored program on “Novel functional materials for energy conversion” conducted Chemistry department, NITK, Suratkal, , during Oct 04- 07th, 2016.

International conference:

International Conference on Recent advances in Condensed Matter and Applied Physics; 30-31st October 2015. (**Oral presentation**)

International conference on Condensed Matter and Applied Physics; 30- 31st October 2015 (**Poster presentation**)

International conference on nonnanoscience and Nanotechnology (ICNAN'16)' at VIT University, Vellore on 19th-21st October, 2016. (**Poster presentation**).

International conference on nanoscience and nanotechnology (ICONN-17) at SRM university, Chennai on August 9th-11th August, 2017.(**Poster presentation**) and got (**Best poster presentation award**)